Design of Lightweight Web Core Sandwich Panels and Application to Residential Roofs

A DISSERTATION
SUBMITTED TO THE FACULTY OF THE GRADUATE SCHOOL
OF THE UNIVERSITY OF MINNESOTA
BY

Casey R. Briscoe

IN PARTIAL FULFILLMENT OF THE REQUIREMENTS
FOR THE DEGREE OF
DOCTOR OF PHILOSOPHY

Susan C. Mantell and Jane H. Davidson, Co-Advisers

May 2010

Acknowledgments

The work described in this thesis was funded by the United States Department of Energy National Energy Technology Laboratory, grant #DE-FC26-04NT42114, and by the Initiative for Renewable Energy and the Environment at the University of Minnesota. In addition, the Minnesota Supercomputing Institute allowed me to perform the finite element analysis described here by providing access to the necessary computers and software. The prototype testing described in this work was performed in the Civil Engineering Structures Laboratory with substantial help from the staff.

I am thankful for the help and support offered by my advisers, Sue Mantell and Jane Davidson, as well as by the other faculty on the roof project: Taichiro Okazaki, Carol Shield, and John Carmody. Thanks go to the staff of the Civil Engineering Structures Laboratory: Paul Bergson, Jonathan Messier, and fellow graduate student BJ Siljenberg, who provided significant assistance in the design and implementation of the prototype tests. Thank you also to the other graduate students and postdocs whose collaboration has guided my way, notably Ben Schoenbauer, Dongsheng Huang, Garrett Mosiman, and Giovanni Di Muoio. Other lab mates have contributed to the quality of my education by providing good insights and good humor, including S. Mubassar Ali, William Camisa, and Gyanender Singh. That this list could go on is a testament to the quality of the education I have been so fortunate to receive.

Thank you to all of my friends and family, without whom an undertaking like this could never have succeeded. Above all, I am thankful to my wife Lindsey, who has been a constant source of support, encouragement, and joy throughout this process and with whom I will be proud to share the fruits of these efforts.

Abstract

Steel sandwich panels with integrated structural and thermal insulating performance offer several advantages over conventional construction methods for residential roofs. These advantages include improved energy efficiency, reduced construction time, architectural benefits, and amenability to other energy-saving technologies such as integrated solar photovoltaic panels. Traditional foam core panels are unsuitable for roofs, however, because they rely on the core material (which has low stiffness and is subject to creep) for long-term structural performance. One way to overcome this problem is to use a structural core with a separate thermal insulating layer, but the specific strength of such designs is limited because they do not exploit the structural properties of the core material. This work focuses on an alternative solution, web core panels, consisting of foam-filled panels with interior webs, with or without an additional insulating layer.

The structural performance of web core panels is provided by the face sheets and webs. The core is used both as an insulating material and to strengthen the thin sheet metal components against local buckling failure. The webs, in particular, must be thin and widely-spaced to minimize their impact on thermal performance. As a result, they are subject to a variety of potential failure modes, particularly shear buckling and bearing failure, that limit the range of feasible roof designs. The influence of the core material on these failure modes has not been investigated in the literature and is thus examined in this work. A model for shear buckling strength is developed by treating the webs as plates on a Pasternak elastic foundation, with expressions for the foundation constants derived using energy methods. The foundation model and its applicability to panels is validated through finite element analysis and prototype testing. A model for bearing strength is developed as an extension of mechanism solutions available in the literature. This model is validated through prototype testing. The model is used to develop a modification to existing prescriptive design code equations that accounts for the effect of the core.

The factors that limit the range of feasible web core designs are investigated. The limiting factors for design are thermal performance, panel deflection, face sheet buckling strength, and shear buckling strength of the webs. Thermal performance is particularly limiting due to the high thermal conductivity of the steel webs, and large panel depths are generally required. One way to reduce the panel depths is to use a web

material with lower thermal conductivity, such as stainless steel. Another way is to use two-layer panels, in which part of the thermal performance is provided by an external insulating layer. Design procedures are developed for panels with and without an external insulating layer and used to investigate the tradeoff between panel depth and weight. Panel designs are developed for load conditions corresponding to three United States climate zones based on minimum weight, minimum depth, and minimum material cost. In each case, web core panel designs with carbon steel webs are compared to panels with stainless steel webs and to two-layer panels. The designs with minimum weight were found to also provide minimum material cost. Depending on load and R-value requirements, reductions in depth and weight are possible with both the use of stainless steel webs and with two-layer panels.

Contents

Acknowledgments **i**

Abstract **ii**

Table of Contents **iv**

List of Tables **viii**

List of Figures **x**

Nomenclature **xvi**

Chapter 1 Introduction **1**

1.1 Steel Roof Panels 4

1.2 Roof Panel Concepts 5

1.3 Research Objectives 9

1.4 Outline of the Thesis 9

Chapter 2 Polymer Foam Considerations **11**

2.1 Physical Properties of Foams 11

2.2 Types of Foam 16

2.2.1 Polystyrenes 16

2.2.2 Polyurethanes 17

2.2.3 Sustainable Foam Technology 19
2.3 Typical Foam Properties 20
2.4 Summary 23

Chapter 3 Thermal and Structural Design Considerations 25

3.1 Panel Loads 25
3.2 Thermal Insulating Performance 28
3.3 Panel Deflection 29
3.4 Face Sheet Buckling 32
3.5 Web Shear Buckling 34
3.6 Bearing Stress Failure 36
3.7 Core Shear Stress Failure 37
3.8 Web Flexural Buckling 38
3.9 Buckling of the Face Sheet into the Webs 39
3.10 Summary 40

Chapter 4 Shear Buckling in Foam-Filled Web Core Panels 41

4.1 Introduction 42
4.2 Plate Buckling Model 45
4.3 Evaluation of Foundation Constants K_W and K_P 50
4.3.1 Foundation Stiffness Model 50
4.3.2 Model Validation 53
4.3.3 Impact of Core Properties on Shear Buckling 56
4.4 Application to Panels 57
4.5 Conclusions 61

Chapter 5 Bearing Failure of Foam-Filled Web Core Panels 64

5.1 Previous Work 65

5.2 Hinge Model 68
5.3 Modified AISI Model 71
5.4 Model Comparison 72
5.5 Summary 75

Chapter 6 Design of Web Core Roof Panels 77

6.1 Introduction 77
6.2 Foam Selection 79
6.3 Design Approach 81
6.3.1 Thermal Performance 81
6.3.2 Panel Deflection 82
6.3.3 Face Sheet Buckling 84
6.3.4 Panel Shear Strength 86
6.3.5 Panel Bearing Strength 88
6.3.6 Design Criteria 89
6.4 Design Procedure 90
6.5 Failure Mode Examination 92
6.6 Roof Panel Designs 96
6.7 Conclusions 103

Chapter 7 Prototype Testing 105

7.1 Overview of the Tests 106
7.2 Deflection and Shear Buckling Model Validation 108
7.2.1 Shear Buckling Test Model 108
7.2.2 Shear Buckling Prototype 110
7.2.3 Test Procedure 110
7.2.4 Results 112

7.2.5 Discussion 114
7.3 Bearing Strength Model Validation 115
7.3.1 Bearing Failure Test Model 115
7.3.2 Bearing Failure Prototypes 117
7.3.3 Test Procedure 118
7.3.4 Results 119
7.3.5 Discussion 124
7.4 Conclusions 125

Chapter 8 Design of Two-Layer Web Core Roof Panels 127

8.1 Introduction 128
8.2 Design of Two-Layer Panels 130
8.2.1 Effect of the Insulating Layer on Panel Performance 130
8.2.2 Validation of the Thermal Performance 132
8.2.3 Effect of the Insulating Layer on Feasible Designs 136
8.3 Minimum Weight Design 137
8.4 Roof Panel Designs 141
8.5 Material Cost 143
8.6 Comparison of Panel Concepts 144
8.7 Conclusions 148

Chapter 9 Conclusions 150

9.1 Conclusions 151
9.2 Recommendations for Future Work 153

References 155

Appendix A Loads and R-Value Requirements **165**

A.1 Roof Loads 165

A.2 Thermal Requirement 166

Appendix B Non-Limiting Failure Mode Models **168**

B.1 Flexural Buckling 168

B.2 Buckling of the Face Sheet into the Webs 173

Appendix C Modeling of Shallow Foundations **176**

Appendix D Rigid Polyurethane Foam Data Sheets **179**

List of Tables

2.1 Typical nominal properties of polymer foams commonly used for thermal insulation in buildings 21

2.2 Recommended constants for calculating the creep coefficient ϕ_t (Equation 2.3) 23

2.3 Nominal Physical Properties for *in-situ* foamed PUR at 36 kg/m^3 . . 23

3.1 Loads and R-value requirements for panels with a 6:12 roof pitch . . . 26

5.1 Steel and core material properties 72

6.1 Properties of steels used in the analysis 78

6.2 Properties of rigid polyurethane (PUR) foam used in the analysis . . 80

6.3 Safety factors used in the present analysis 90

7.1 Geometry and material properties for the shear buckling prototype . 111

7.2 Predicted behavior for the shear buckling test 111

7.3 Predicted vs. observed shear buckling test behavior 115

7.4 Geometry of the bearing failure prototypes 117

7.5 Material properties for the bearing failure prototypes 118

7.6 Strength predictions for the bearing failure tests 118

7.7 Predicted ($\overline{\mathcal{Q}}_a$) vs. observed ($\overline{\mathcal{Q}}$) bearing strength results 125

8.1 Loads and R-values used for panel design 141

8.2 Minimum weight panel designs with carbon steel webs 142

8.3 Minimum depth panel designs with carbon steel webs 143

8.4 Web core component material costs κ_i per unit weight 144

8.5 Panel designs with carbon steel webs and minimum material cost . . 145

8.6 Minimum cost designs with stainless steel webs 145

8.7 Summary of minimum cost designs for each panel type; truss core designs are included for comparison 146

A.1 Loads and R-value requirements for panels with a 6:12 roof pitch . . . 167

List of Figures

1.1 Roof structure concepts: (a) conventional (trussed) construction, and (b) panelized construction with (c) closeup of a (truss core) panel concept proposed in the literature 2

1.2 Slotted steel studs to reduce heat transfer through walls 4

1.3 All-steel residential construction in Sorochany, Russia: (a) house under construction, and (b) close-up of the attic/roof structure 5

1.4 Spectrum of panel designs based on the function of the insulating material: structural foam meets the thermal requirements incidentally (no need for specific thermal design); insulating foam does not contribute to panel structural performance 7

1.5 Web core panel concept: (a) panels with no external foam layer, and (b) two-layer panels with external foam layer 8

2.1 Simplified model for open-celled foam microstructure; cells are elongated in the rise direction 13

3.1 Climate zones used to establish panel load requirements 26

3.2 Panel coordinate system and the associated distribution of internal shearing forces and bending moments 27

3.3 Locations of the local failure modes in the face sheets and webs . . . 27

3.4 Isothermal planes (lumped thermal resistance) approximation for panels (a) without and (b) with an external foam layer 29

3.5 Load and deflection conventions for determining deflection limit . . . 30

3.6 Face sheet buckling mode: view of the buckled face sheet, assuming one intermediate web (dashed line); loading corresponds to the bending moment distribution illustrated in Figure 3.2 33

3.7 Web shear buckling mode: view of a buckled web; loading corresponds to the shear force distribution illustrated in Figure 3.2 34

3.8 Relationship between adjacent buckled webs: (a) antisymmetric buckling, and (b) symmetric buckling 35

3.9 Bearing failure mode 37

3.10 Flexural web buckling mode: view of a buckled web; loading corresponds to the bending moment distribution illustrated in Figure 3.2 . 38

3.11 Vertical buckling of the face sheet into the webs: view of the web and face sheets; loading corresponds to the bending moment distribution illustrated in Figure 3.2 39

4.1 Web core panel concept geometry and coordinate system 43

4.2 Buckling displacement models based on (a) elasticity solution, (b) linear decay, and (c) exponential decay 44

4.3 Simply supported plate and elastic foundation model 46

4.4 Buckling mode shapes with varying elastic foundation stiffness ($\beta = 1$ and $\beta = 4$) 50

4.5 Model used for the determination of foundation stiffness constants . . 51

4.6 Plate model used for FE validation of the expressions for determining foundation constants 54

4.7 Plot of the normalized deflection w/W in the foundation vs. normalized distance z/H from the plate surface; FE results are compared to the present model for $Hk = 0.85$ and 4.5 55

4.8 Plot of error in the present foundation model vs. the non-dimensional foundation depth Hk based on the foundation constants in Equation (4.23) 55

4.9 Plot of buckling coefficient χ_∞ vs. f_W for $f_W/f_P = 2$, 5, 10, and 15 . 56

4.10 Finite element model used for the analysis of panels under distributed load (core elements not displayed for clarity) 58

4.11 Buckling mode shape in the webs of a panel under distributed load ($E_c = G_c = 500$ kPa); due to symmetry, only half the panel length is shown 59

4.12 Variation in analytical and numerical buckling coefficient vs. web slenderness h_c/t for two different web spacing ratios 60

4.13 Comparison of χ_∞ and χ_{FE} vs. web aspect ratio a/h_c ($h_c/t = 400$, $p/a = 0.200$, $E_c = G_c = 500$ kPa) 62

4.14 Comparison of χ_∞ and χ_{FE} vs. non-dimensional web spacing ratio p/a ($h_c/t = 400$, $a/h_c = 10$, $E_c = G_c = 500$ kPa) 62

5.1 Early elastic buckling models for bearing failure: (a) opposing concentrated loads, (b) opposing patch loads, (c) patch load and supports . 65

5.2 End bearing failure mechanism in the webs 66

5.3 Damage zone assumption for the determination of bearing strength: (a) in the webs, and (b) in the face sheet 69

5.4 Comparison of hinge and modified AISI bearing failure models: plot of $\overline{Q}/\overline{Q}_A$ vs. web slenderness h_c/t_w 74

5.5 Contribution of core crushing to total bearing strength: plot of $\overline{Q}_c/\overline{Q}$ vs. h_c/t_w assuming carbon steel webs and 36 kg/m^3 PUR core with $t_f/t_w = \sigma_{yf}/\sigma_{yw} = 1$, $c/t_w = 150$, $p/t_w = 1200$, and $R/t_w = 0$ 74

6.1 Roof panel application and loading 79

6.2 Plot of minimum panel depth vs. length for foam core panels with 2.0 mm steel face sheets and PUR core. Designs that neglect the influence of core creep are shown with dashed lines, and designs that include the effect of creep are shown with solid lines. 80

6.3 Plate approximation for face sheet buckling analysis 85

6.4 Plate approximation for web shear buckling 87

6.5 Flowchart of the web core design procedure 91

6.6 Failure mode map for panels with carbon or stainless steel webs spaced at 1.2 m and a 36 kg/m^3 core, subjected to a transverse load of 1500 N/m^2 and an R-value requirement of 5.3 m^2-K/W ($t_f = 2.0$ mm) . . 93

6.7 Failure mode map for panels with (a) carbon or (b) stainless steel webs spaced at 1.2 m and a 36 kg/m^3 core, panel length of 7 m, subjected to a transverse load of 1500 N/m^2. R-value requirements of 3.5, 5.3, and 6.7 m^2-K/W are compared for each web material. 95

6.8 Core depth vs. panel length for foam core panels and web core panels with carbon and stainless steel webs with an R-value requirement of 5.3 m^2-K/W and an applied load of: (a) 1500 N/m^2, (b) 2000 N/m^2, and (c) 3000 N/m^2. Web spacing of 0.8 and 1.2 m are compared for the web core panels. 97

6.9 Face sheet thickness vs. panel length for panels corresponding to the designs shown in Figure 6.8 100

6.10 Web thickness vs. panel length for panels corresponding to the designs shown in Figure 6.8 101

6.11 Panel weight vs. length for panels corresponding to the designs shown in Figure 6.8, applied load of: (a) 1500 N/m^2, (b) 2000 N/m^2, and (c) 3000 N/m^2. 102

7.1 Prototype panel geometry and load configurations 107

7.2 Shear and bending moments for the shear buckling test 109

7.3 Dimensions and setup for the shear buckling test 111

7.4 Load-deflection data for the shear buckling test 113

7.5 Observed panel failure modes: (a) web shear buckling, and (b) core shear fracture. 114

7.6 Shear and bending moments for the bearing failure tests 116

7.7 Bearing failure mode: (a) end view, and (b) side view showing the location of yield lines 120

7.8 Interior bearing failure mode with yield line 121

7.9 Load vs. displacement for the tests on Panel A 122

7.10 Load vs. displacement for the tests on Panel B 123

7.11 Predicted vs. observed bearing strength; the predicted strengths indicate the relative contribution from the webs (dark shading) and the core (hatched) 126

8.1 Sandwich panel concepts for roofs: (a) web core, (b) two-layer web core, and (c) two-layer metal core 128

8.2 Two-layer web core panel geometry and coordinate system; the insulating layer is placed on the exterior or interior face of the structural layer depending on climate 129

8.3 Isothermal planes approximation for two-layer web core panels; each component has a thermal conductivity k_i corresponding to a resistance R_i in the circuit diagram 131

8.4 Finite element model and boundary conditions for the analysis of thermal performance in two-layer panels: (a) schematic illustration with metal thicknesses exaggerated for clarity, and (b) typical mesh 133

8.5 Plot of R-value ratio R/R_i vs. R_e/R_i for panels with carbon and stainless steel webs 135

8.6 Relative temperature gradient $\Delta T_i/\Delta T$ across the structural layer vs. R_i/R for panels with carbon and stainless steel webs 135

8.7 Failure mode map for web core panels with $a = 7$ m, $q = 1500$ N/m^2, and $R = 5.3$ m^2-K/W ($p = 1.2$ m, $t_f = 2.0$ mm); minimum depth designs for panels with and without an external insulating layer are indicated 136

8.8 Pareto optimal curve (weight W vs. panel depth H) for panels with $a = 7$ m, $q = 1500$ N/m^2, and $R = 5.3$ m^2-K/W ($p = 1.2$ m) 139

8.9 Flowchart of the minimum weight design procedure for two-layer web core panels 140

8.10 Material cost for each panel concept; the three columns correspond to Climates I, II, and III respectively 147

A.1 R-value requirement vs. heating degree days (HDD), as specified by building code 167

B.1 Model used for determination of the web flexural buckling load 169

B.2 Buckling mode shapes with varying elastic foundation stiffness and α ($\beta = 2$) 171

B.3 Long plate flexural buckling coefficient $\chi_{fb,\infty}$ vs. f_W for $f_W/f_P = 10$ and 15; $\alpha = 0$, 1, and 2 171

B.4 Buckling of the face sheet into the webs: (a) curvature of the web due to panel bending, and (b) distribution of compressive stress (denoted f_c in the figure) on a web element 174

C.1 Model for the determination of shallow foundation stiffness constants 176

C.2 Comparison of the shallow and deep foundation models vs. depth Hk 178

Nomenclature

a = Panel length, plate length, m
b = Panel width, plate width, m
c = Bearing width, m
c_e = Bearing width at panel supports, m
c_i = Bearing width at actuator load point, m
C = Material cost per unit area, \$/m^2
d = Distance between the face sheet centroids ($d = h_c + t_f$), m
D = Panel deflection, plate deflection, m
D_{Qx} = Panel shear stiffness, N/m
D_x = Panel bending stiffness, N-m
E = Elastic modulus, Pa
E_t = Creep-reduced core modulus, Pa
f_P = Non-dimensional (Pasternak) foundation parameter
f_W = Non-dimensional (Winkler) foundation parameter
F_C = Reduction factor for panel bearing strength
F_R = Reduction factor for web crippling strength
G = Shear modulus, Pa
h_c = Depth of the structural core layer, m
h_D = Core depth damaged by bearing failure, m
h_e = Depth of the insulating foam layer, m
H = Foundation depth, total panel depth, m
k = Foundation characteristic length parameter, m^{-1}
k_c = Core material thermal conductivity, W/m-K
k_e = Insulating layer thermal conductivity, W/m-K
k_w = Web thermal conductivity, W/m-K
K = Panel stiffness in four-point bending, N/m
K_P = Pasternak elastic foundation constant, N/m
K_W = Winkler elastic foundation constant, N/m^3
L_D = Length of panel region damaged by bearing failure, m
N_0 = Maximum in-plane bending force, N/m
p = Web spacing, m
q = Applied roof load, N/m^2
$\hat{q}$ = Elastic foundation restoring force, N/m^2
Q = Concentrated load, N
$\mathcal{Q}$ = Line load for prototype testing, N
R = R-value, m^2-K/W
t = Sheet thickness, m
ΔT = Temperature gradient across the panel, K
ΔT_i = Temperature gradient across the structural layer, K
w = Panel deflection, plate deflection, m
$\hat{w}$ = Local plate deflection, m
W = Panel weight per unit area, N/m^2

$\mathcal{W}$ = Mid-span deflection observed in prototype testing, m
α = Parameter to determine neutral bending axis location
α_f = Face sheet coefficient of thermal expansion, m^{-1}
β = Plate aspect ratio
γ = Specific weight, $\mathrm{N/m}^3$
ϵ_f = Face sheet strain due to bending
ζ_n = Fatigue reduction factor
κ = Material cost per unit weight, \$/N
λ = Distance from actuator load to supports, m
ν = Poisson's ratio
ξ = Shear lag reduction factor
ρ_c = Core density, $\mathrm{kg/m}^3$
σ = Normal stress, Pa
σ_{uc} = Core crushing strength, Pa
σ_y = Yield strength, Pa
τ = Shear stress, Pa
τ_{uc} = Core shear strength, Pa
$\tau_{u,n}$ = Fatigue-reduced core shear strength, Pa
ϕ_t = Creep reduction factor
χ = Buckling coefficient
χ_f = Face sheet buckling coefficient
χ_w = Web shear buckling coefficient
χ_{wf} = Web flexural buckling coefficient
ψ = Safety factor

Subscripts/Modifiers

w = Refers to webs
f = Refers to face sheets
c = Refers to core material
$\overline{(\cdot)}$ = Refers to limit state (load or stress at failure)
FE = Refers to values obtained by finite element analysis
$(\cdot)_{,x}$ = Refers to differentiation with respect to the subscripted variables

Chapter 1

Introduction

Energy efficiency and conservation are growing concerns globally and in the United States. One area with high potential for improvements in efficiency is residential construction. According to recent energy statistics [1], residential buildings account for 21% of US energy consumption, of which more than 39% goes into space conditioning (heating and cooling). In a typical house, thermal losses through the roof make up 14% of the building component energy load, and infiltration through the building envelope (including the roof) accounts for 28% of the heating load. Improvements to the roof system thus represent an important opportunity for decreasing residential energy consumption.

Advanced roof designs also have the potential to reduce construction waste. The construction of a typical 2000 square foot house produces some 3600 kg (8000 lb) of waste, of which 38% comes from lumber and engineered wood products, and another 25% comes from drywall [1]. Much of this waste comes from the on site production and assembly of structural features and finishing layers. The waste generation is up to four times higher if demolition of an existing structure is required. Overall, construction and demolition account for 24% of the US annual municipal solid waste stream. Alternative construction systems (e.g. factory-built wall and roof panels) that minimize waste and encourage recycling can significantly impact material use.

Conventional home construction involves the use of wall studs (typically assembled on site) and roof trusses, illustrated in Figure 1.1(a). The trusses are typically spaced at no more than 610 mm (24 in.) on center to provide adequate support for the

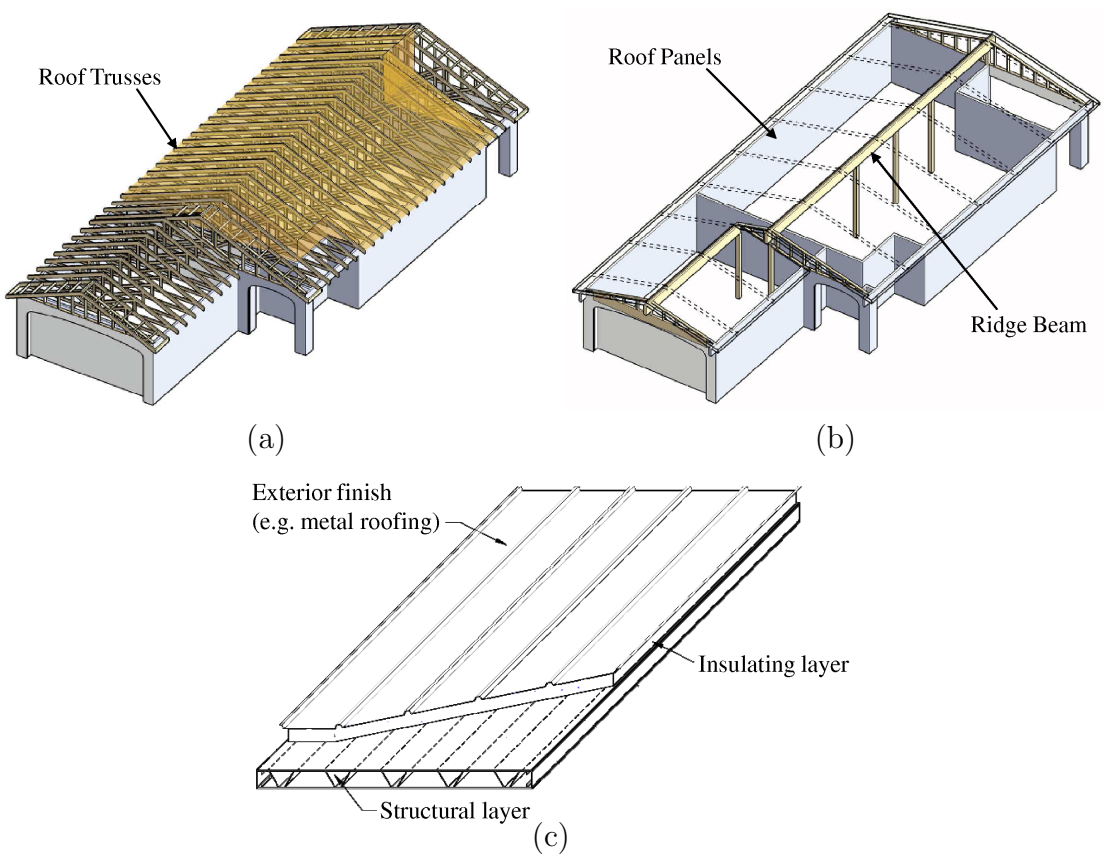

Figure 1.1. Roof structure concepts: (a) conventional (trussed) construction, and (b) panelized construction with (c) closeup of a (truss core) panel concept proposed in the literature (all figures from Reference [2]; annotations added for clarity)

roof against snow and wind loads. Roofing typically consists of plywood or oriented strandboard (OSB) sheets onto which asphalt shingles or other finishing materials are attached. The close spacing of the trusses results in an unusable attic space, which is typically vented to the outside. Insulation (usually fiberglass batts or other loose fill material) is placed in the ceiling layer. Penetrations through the ceiling layer are difficult to seal and, combined with the loose insulation material, allow substantial infiltration of unconditioned outside air into the conditioned space. The placement of HVAC systems in the unconditioned attic (common in warmer climates) and leakage from ventilation ducts in the ceiling layer contribute additional thermal losses. The system also requires significant construction time, both for the installation of the trusses and for the on-site attachment of the exterior roofing layers.

An alternative to the conventional roof structure is the panelized roof, illustrated in Figure 1.1(b). The panels are supported at the soffit and the ridge (using a ridge

beam). An example of a truss core roof panel (developed in Reference [2]; also described in Section 1.2) is illustrated in Figure 1.1(c). As illustrated, a major benefit of roof panels is the ability to integrate structural, thermal, and exterior finishing layers into a single unit, manufactured off site. As a result, roof panels offer the ability to insulate at the roof plane, creating conditioned attic space. Simulations have predicted annual energy savings of up to 40% for conditioned versus unconditioned attic space [2–5]. Additional savings of 20% or more are possible if the walls are also panelized and filled with polymer foam insulation [6–8]. The improvements are largely attributed to reduced infiltration (through the use of polymer foam instead of loose fill insulation) and the confinement of HVAC systems and duct leakage within conditioned space.

The constructibility benefits of panelized houses were studied by Mullens and Arif [9]. They supervised the side-by-side construction of two similar houses, one using structural insulated panels (SIPs) and one using conventional construction, and monitored several performance metrics. They found overall reductions for the panelized house, in terms of labor and construction time, of 65%. The labor reduction for the panelized roof was 70%. The authors also suggest that a smaller proportion of skilled labor is necessary with panelized construction, though they do not quantify the amount. Recognition of the reductions in construction time and costs is growing and is a key component of SIP marketing and, coupled with the known energy benefits, may contribute to builder acceptance in spite of the increased material cost.

An additional benefit of roof panels is the ability to create usable attic space (with steep roofs) or cathedralized ceilings (with shallower roof slopes) [2]. These benefits add architectural value to a house[1]. Open attics also allow for increased living space within a fixed footprint. As single family homes continue to grow (average square footage increased by 44% from 1980 to 2006 [1]), the use of attic space is a particularly cost-effective means to meet customer demands. Additional benefits include the ability to partially or fully attach finishing layers in the factory (reducing construction time even further) and improved quality control compared to on-site construction.

[1]From conversations with Professor John Carmody of the University of Minnesota

1.1 Steel Roof Panels

The present work focuses on improving the design of roofs using steel sandwich panels with polymer foam insulation. Steel roof panels offer the potential for increased durability and reduced life cycle costs compared to wood-based construction (discussed below). The use of steel roofing offers additional benefits over traditional roofing materials (e.g. asphalt shingles), including reduced maintenance [10] and amenability to other energy-saving technologies, such as integrated solar photovoltaic panels and cool roofs [11].

As a structural material, steel has several advantages over wood, including [13] durability, dimensional stability, consistent manufacturing quality, resistance to mold and pests, and recyclability (wood is rarely ever recycled from houses and, due to the use of chemical treatments, must be disposed of as toxic waste [13]). The life cycle cost of recycled steel is competitive with other building materials, particularly in climates where the availability of wood is limited [14]. The thermal performance of steel can be made competitive to that of wood through the use of perforations [12,15] or added insulation. The perforations, illustrated in Figure 1.2, reduce heat flow by greatly increasing the path length of heat flow through the wall. The benefits of steel construction are well known in very cold climates (e.g. Scandinavia and Russia), where steel is a building material of choice. Figure 1.3, for example, shows an all-steel residential construction in Sorochany, Russia (about 54 km north of Moscow). The slotted steel wall studs can be seen in Figure 1.3(b).

Figure 1.2. Slotted steel studs to reduce heat transfer through walls (from Reference [12])

(a) (b)

Figure 1.3. All-steel residential construction in Sorochany, Russia: (a) house under construction, and (b) close-up of the attic/roof structure (http://profilesolutions.lindab.com)

Acceptance of steel construction is occurring more slowly in the US, where wood is readily available and economically feasible. However, building envelope studies have suggested steel may become an increasingly viable building material, particularly as considerations of quality, material waste, and life cycle cost become more important [10, 11, 13]. The same considerations are expected to increase the prevalence of metal roofing in the US.

Two recent studies [16, 17] have investigated the viability of stainless steel as a construction material for buildings. Although both works focused on larger projects (e.g. commercial buildings), the main principles apply to residential construction as well. The thermal conductivity of stainless steel is about a third of that of carbon steel, while the stiffness is comparable. A drawback to stainless steel is the cost, which is about 3.5 times that of carbon steel [18]. Gedge [16] points out that much of the increased cost of stainless steel structures is due to overspecification of surface finish and can therefore be mitigated by using lower standards for non-architectural (i.e. non-visible) structural members. It is also worth pointing out that the increased strength (and reduced thermal conductivity) may lead to designs which are ultimately cost-competitive with carbon steel.

1.2 Roof Panel Concepts

Energy efficient roofs must provide adequate structural performance while simultaneously fulfilling thermal insulation requirements. A handful of roof panel concepts

that attempt to meet these goals have been examined in the literature. Note that several works already cited [6–9] have examined the non-structural impacts of panel use. The discussion in this section is limited to the work focused on the structural design of roof panels.

The early concepts [19, 20] rely on the use of wood (primarily OSB) structural materials. For example, Kucirka [19] studied the use of foam core panels for roofs. The panels consist of OSB face sheets and a core layer made of rigid polyurethane. Panel design was strongly limited by thermal and hygroscopic deflections. In addition, the panels rely fully on the core material to resist shear deformation due to the structural loads. Polymer foam core materials have low shear stiffness (compared to steel) and are subject to creep. Because roofs are subjected to long-term loading, the core layer must be deep enough to compensate for the effects of creep.

To overcome the design difficulties associated with the use of a polymer foam core, Crowley [20] proposed a panel consisting of OSB face sheets and webs. Nonstructural loose-fill insulation is located in the voids between the webs. A similar concept later proposed by Dweib, et al. [21, 22] uses face sheets and webs made from a novel bio-based composite material. Polymer foam fills the spaces between the webs, but it is not used structurally. Both designs neglect the impact of the webs on thermal performance. More critically, both designs neglect key durability considerations, including creep (of the face sheets and webs) and hygrothermal warping. These considerations are particularly important for the bio-based material, for which the creep and warping behavior is currently not understood.

A limitation of the work described in References [19, 20] is the focus on OSB as a structural material. In addition, the literature on roof panel design [6, 8, 20–22] has almost universally neglected the effect of creep, particularly in the core material. Thomas [23, 24] studied the design of foam core roof panels using a wide variety of face sheet and core materials, accounting for the effect of core creep. He found the use of non-hygroscopic (steel) face sheets results in reduced hygrothermal deflection and improved panel stiffness. Designs are still limited, however, by the reliance on the core material for stiffness under long-term loading. The effect of creep on foam core panel design, illustrated in Chapter 6 of this work, is a dramatic reduction in the maximum span length. As a result, foam core panels are ruled out as viable design options for residential roofs.

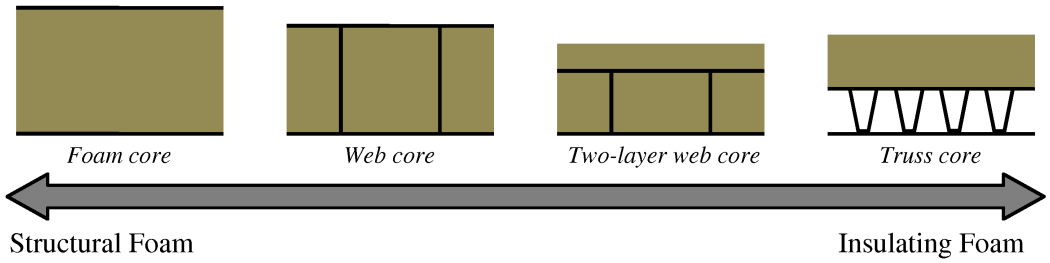

Figure 1.4. Spectrum of panel designs based on the function of the insulating material: structural foam meets the thermal requirements incidentally (no need for specific thermal design); insulating foam does not contribute to panel structural performance

As an alternative to the foam core concept, the truss core panel [25–27] was developed at the University of Minnesota. Truss core panels (see Figure 1.1(c)) consist of two layers. The structural layer is a sandwich panel with steel face sheets and cold-formed V-channel webs. The thermal layer is rigid polyurethane foam and is attached to the structural layer on either the interior or exterior surface, depending on climate (see Chapter 8). Exterior finishing consists of either metal roofing or OSB with asphalt shingles attached. Truss core panel designs have been specified for climate scenarios throughout the US and for roof spans up to 6.1 m (20 ft) [27].

Foam core and truss core panels represent limits on a spectrum of panel designs. This spectrum is illustrated in Figure 1.4. In foam core panels, the foam acts directly as a structural material: the amount of foam necessary to meet the structural requirements is more than sufficient to meet the thermal insulating requirement [23]. In truss core panels, the foam acts only as an insulating material and provides no contribution to structural performance. In addition to these concepts, hybrid designs are possible in which the thermal and structural design cannot be separated[2]. Examples of the latter category are web core and two-layer web core panels, both of which are described below.

A potential drawback to designs on either end of the spectrum in Figure 1.4 is the suboptimal use of material. Foam core panels require considerable foam and thick face sheets to achieve the required structural performance (Chapter 6). Truss core panels allow minimum foam use but require relatively thick face sheets and webs to meet the structural requirements without contribution from the foam. However, by

[2]Note "separated" in this context refers to the ability to design for thermal and structural requirements independently. All of the panels considered in this work are designed to meet both requirements in one integrated unit.

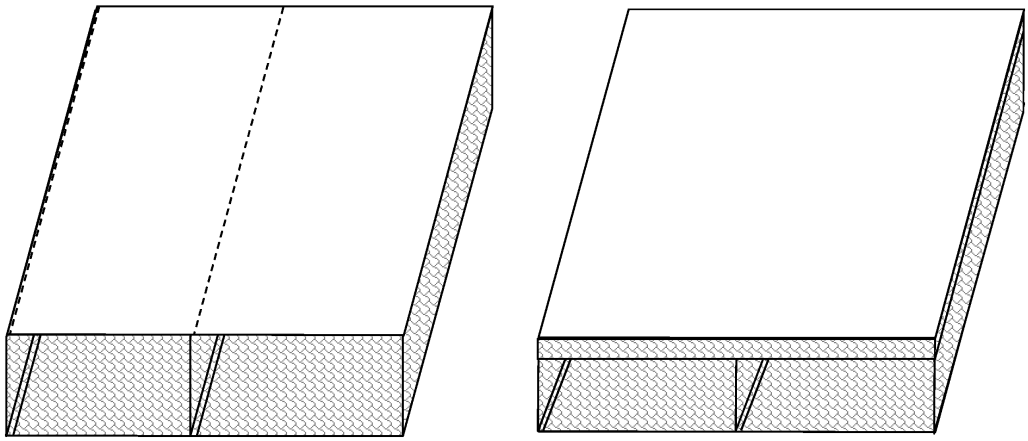

Figure 1.5. Web core panel concept: (a) panels with no external foam layer, and (b) two-layer panels with external foam layer

exploiting the structural properties of the foam, it is possible to design panels that meet the structural requirements using thinner wall sections (face sheets and webs). Web core panels, illustrated in Figure 1.5, achieve this gain by using steel webs to achieve the necessary stiffness, while the foam core strengthens the structure against local buckling. The tradeoff is a reduction in thermal insulating performance because the webs provide thermal shorts between the face sheets. Assuming the impact of the webs on thermal performance can be limited, however, the thinner wall sections enable lighter-weight design.

Two methods are available to compensate for the effect of webs on thermal performance. Web core panels with no external foam layer, Figure 1.5(a), resemble foam core panels in that the structural and thermal functions are achieved in a single panel layer—compensation for the webs is achieved by increasing the core depth. Two-layer panels, Figure 1.5(b), use an external insulating layer, analogous to truss core panels. The exterior roof finishing is achieved either by attachment to the insulating layer or through the use of lightly profiled exterior face sheets. In addition to stiffening the panel structure, the webs act as joints between adjacent panels. This function suggests an alternate interpretation of the web core panel concept: the same functions are achieved using foam core panels with webs acting as the panel-to-panel joints[3].

[3]This interpretation is strengthened by the result that panel designs typically require wide (1.2 m) web spacing, see Chapter 8.

1.3 Research Objectives

To meet the structural and thermal requirements of roofs using web core panels, it is necessary to exploit the strengthening effect of the core material on the various local structural failure modes. Although the interaction between face sheets and core material has been studied extensively (mainly in foam core panels), the interaction with the webs is not well understood. Roof panels require the use of thin webs, so an understanding of the effect of core material on web strength is essential. For that reason, a key objective of the present work is the development of models by which the core material can be incorporated into the design of panels with thin webs. Emphasis is placed on the failure modes (shear buckling and bearing failure) most likely to limit the design of roof panels, but application to the other failure modes is also presented.

Another objective of the present work is the development of an approach to the design of web core panels for residential roofs. To provide perspective, designs are developed for a representative house under different load scenarios and compared to the corresponding truss core designs reported in Reference [2]. From these results, recommendations are made regarding the design and applicability of web core panels to residential roofs.

The work described in this thesis is broadly applicable to the design of lightweight panels, with or without thermal insulating requirements. In aerospace structures, for example, specific strength requirements are becoming increasingly rigorous, and the use of composite or super alloy structural materials is increasingly expensive. This work demonstrates the significant effect that core material can have on local buckling strength. Polymer foams provide a particularly effective means of achieving minimum weight panel design. It can thus be expected that understanding the interaction between structural and core materials will become increasingly important to structural design, and the models provided here are a significant contribution toward that understanding.

1.4 Outline of the Thesis

This work details the structural and thermal design considerations for the use of web core sandwich panels in lightweight residential roofs. The choice of core material is a particularly important concern for roof panels. Therefore, an overview of poly-

mer foams is presented in Chapter 2 along with recommendations for core material selection. Chapter 3 describes the failure modes relative to web core panels under distributed load and provides an overview of the relevant literature on modeling those modes. In practice, only a few of the relevant failure modes affect panel design.

Models for the failure modes relevant to panel design are presented in Chapters 4–6. A particularly important failure mode, for which no relevant models are currently available in the literature, is shear buckling of the webs. For that reason, a model for shear buckling strength that accounts for the effect of the foam core is developed in Chapter 4. Another important failure mode for which existing models are inadequate is bearing failure at the panel supports. A different technique must be employed to model the effect of the core material. Bearing failure is modeled in Chapter 5. The other failure mode models are provided along with a procedure for minimum depth design of web core panels with no external insulating layer in Chapter 6. Chapters 4 and 6 are in press as References [28] and [29] respectively.

Validation of the structural failure mode models developed in this work was performed in part through prototype testing as described in Chapter 7. Chapter 8 presents the design considerations for two-layer web core panels. Designs for minimum weight and material cost are developed and compared to designs for panels with stainless steel webs and no external insulating layer. The designs are also compared to truss core panel designs developed in Reference [27]. Conclusions regarding the use of web core roof panels are given in Chapter 9.

Chapter 2

Polymer Foam Considerations

Polymer foams are well suited to building insulation applications. Their hygrothermal properties are superior to those of traditional insulating materials like fiberglass [30], and their mechanical properties allow them to be used where they will be subject to external loads. As with any insulating material, however, several considerations must guide foam selection. These considerations include structural and thermal requirements, building code compliance, safety, and manufacturability issues.

This chapter describes the foam considerations that are specific to web core roof panels. A brief overview of the properties and the mechanics of foam relevant to roof panel design is provided, followed by a summary of the loading and residential code requirements pertaining to the use of foams in roof panels. A summary of the foams commonly used in building applications, as well as some potentially viable emerging technologies, is also presented, along with typical properties for the commonly-used foams. Based on the roof requirements and the property data, recommendations are made regarding foam material selection for roof panels.

2.1 Physical Properties of Foams

Roof panels are designed subject to a variety of requirements, including strict deflection limits under a combination of short- and long-term loads, long service life, and large temperature variations. As a result, polymer foams used in roofs must have several characteristics, including

- High specific stiffness and strength
- Low thermal conductivity
- Stable under long-term loading
- Stable under high service temperatures
- Safe performance under fire conditions

All of these characteristics can be obtained through careful foam selection, as outlined in this work. The first three properties depend on density as well as composition of the foam and can therefore be adjusted, in general, for a particular foam. The last two properties are functions of the material and are used in Section 2.2 to narrow the set of available foams for use in roofs.

Foams are highly structured materials. At the micro scale, a foam can be approximated by a lattice of struts arranged in various space filling geometries. The simplest such model is the face centered cubic cell, illustrated in Figure 2.1. The cell walls of closed-cell foams may also contribute to structural behavior; however, for many foams (including polyurethanes) this contribution is small and can be ignored without loss of accuracy. The lattice-type microstructure of foams has important consequences on the constitutive behavior. For example, tensile, compressive, and shear stresses translate into different loads on the cell structures[1]. As a result, foams typically have different properties in tension, compression, and shear.

Many foams (like the one in the figure) have elongated cells due to pressures from the foaming process. The elongation, known as "rise," also affect foam behavior. Stresses oriented in the rise direction act mainly on the smaller struts, so foams are typically stiffer and stronger in the rise direction. The elongation occurs when foams are prevented from expanding freely in all directions. For example, in web core panels, polyurethane cores can be foamed *in-situ* (see Section 2.2.2). In that case, the foam is essentially free to expand in the direction of panel length. The face sheets and webs limit expansion perpendicular to panel length. Thus, foam rise is in the longitudinal panel direction.

The mechanics of foams have been studied extensively, and several reference books (e.g. [31–33]) are now available that summarize the results. The most important result is the observation, discussed in detail by Gibson and Ashby [33], that the properties

[1] E.g. compressive stress causes buckling of some struts; shear stress causes bending of struts that are stretched (with no bending) under tensile stress

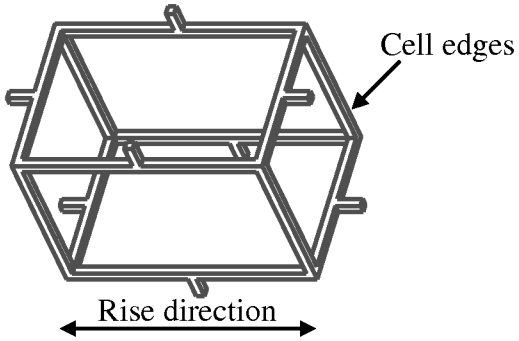

Figure 2.1. Simplified model for open-celled foam microstructure; cells are elongated in the rise direction

of a foam scale with density in a straightforward manner. Consider a foam of density ρ, for example, made out of a material with elastic modulus E_s and density ρ_s. The compressive modulus E_c of the foam follows the power law model

$$\frac{E_c}{E_s} = C\left(\frac{\rho}{\rho_s}\right)^n. \tag{2.1}$$

The other mechanical properties of foams follow the same model, though with different values for the constants C and n. In the absence of experimental data on the values of C and n, Gibson and Ashby [33] derived models for a variety of physical properties assuming the cubic cell structure illustrated in Figure 2.1. Most foams have cell geometry more complex than cubic (tetrakaidecahedral, for example) and models have been developed that account for other geometries. These models typically require experimental calibration of more than two constants, however. As a result, most design is performed using the model given in Equation (2.1), with C and n determined experimentally.

The thermal conductivity k of foams is a function of foam density and of the gas that is trapped within the cells of the foam [33]. Heat conduction through a foam occurs via three modes: conduction through the solid material, conduction through the gas, and radiation across cell voids. Due to the balance between conduction and radiation, foams have an optimum density at which the thermal conductivity is minimized. In polyurethane foams, for example, the optimum density is around 48 kg/m^3 (assuming the cells are filled with air) [33]. The thermal conductivity of most foams increases slightly as the foam ages. The aging mechanism has been reported in the literature and is summarized by Gibson [33], among others. Foams

are typically processed using blowing agents with low thermal conductivity, such as HFC's, hydrocarbons, or carbon dioxide. Over time, the blowing agents diffuse out of the foam and are replaced by air, which has a higher thermal conductivity. Under normal service conditions, the aging process takes several years, particularly if the foam is faced with an impermeable material such as steel.

An important consideration for foams used in roof panels is long-term performance. Roof panels are subjected to sustained loading, as well as to cyclic loading. Creep and fatigue are thus important aspects of foam behavior. Assuming that the applied stresses on the foam are not great enough to cause rupture, creep effectively reduces the stiffness of the material, and fatigue reduces the strength. These phenomena are particularly problematic in foam core sandwich panels, where the foam is an integral part of the panel structure. They can have an important impact on the long-term livability of the affected house and thus should not be ignored in roof panel design.

The approach to dealing with the creep of polymer foams is to reduce the stiffness according to a creep reduction factor ϕ_t. For an initially undeformed foam under constant load with initial elastic modulus E_0, the modulus E after a loading time t is given by

$$E = \frac{E_0}{1 + \phi_t}. \tag{2.2}$$

The reduced shear modulus G is found from the initial modulus G_0 in the same manner. For polymer foams, ϕ_t is best described by the power law model [34]

$$\phi_t = At^n. \tag{2.3}$$

Long-term creep testing on polystyrene [35] and other foams [36] has demonstrated that good estimates of the creep parameters can be determined through relatively short-term testing. Test data for polystyrene over a period of 1000 hours, for example, have been shown to be sufficient for the accurate prediction of creep behavior for at least 100,000 hours [35, 36].

The influence of fatigue on foam strength is accounted in this work through a fatigue reduction factor ζ_n. Fatigue results for foams are typically presented using the standard Basquin (stress-life) model for high cycle fatigue [37]. The shear strength τ_u of a foam after n loading cycles is found by reducing the monotonic shear strength τ_{u0}

according to

$$\tau_u = \zeta_n \tau_{u0}, \tag{2.4}$$

and likewise for the compressive strength. Equation (2.4) is particularly convenient for foams because ζ_n is independent of density [38]. Fatigue test results for a wide variety of foams are reported (using standard stress-life plots) by Zenkert [37].

Several failure theories have been proposed and applied to foams, as described in a review by Abrate [39]. The most generally applicable failure criteria are of the form

$$\left(\frac{\sigma}{\overline{\sigma}}\right)^n + \left(\frac{\tau}{\overline{\tau}}\right)^n \leq 1, \tag{2.5}$$

where the overlined variables refer to the maximum stress at failure. Equation (2.5) has been shown to fit well with data for PVC foams with $n = 2$ [40]. By extension, the model is often applied to other foams as well. It is worth pointing out that, in practice, the stress state in the core of sandwich panels is not mixed: as described in Chapter 6, the bending stresses in the panel are taken by the face sheets, so the core material is essentially in pure shear. As a result, Equation (2.5) simplifies to $\tau \leq \overline{\tau}$ as used in Chapter 6.

Depending on several factors—e.g. R-value, roof orientation and slope, roofing color, and the presence of solar panels—the outer surface of the roof can reach temperatures of 80°C or higher [41, 42]. These temperatures are approaching the glass transition temperature for many polymer materials and therefore can have important implications for foam material selection. The maximum service temperature is typically specified by foam manufacturers to be slightly below the glass transition temperature. In foams that are loaded while exposed to higher temperatures, substantial creep or compression setting can occur. The increased creep can cause substantial (and possibly irreversible) panel deformation. Compression setting can lead to localized densification, resulting in reduced thermal insulating performance over time. Thus, foams should not be used in applications where the maximum service temperature is routinely exceeded.

One other requirement for roof panels is the fire performance of the foam. US residential codes [43] specify that foams should be separated from the interior living space by a minimum 1/2 in. (13 mm) gypsum board. They also specify the minimum performance of the foams per ASTM E-84 [44], which deals with the amount of flame

spread and smoke generation under exposure to flames. However, a growing body of evidence (e.g. [42, 45–48]) suggests that the current standards are not adequate for evaluating the safety of the materials under realistic fire conditions. As described in Section 2.2.1, for example, fire tests have revealed very troubling performance when roof panels are used with thermoplastic core materials. Rakic [47] notes a growing trend among insurers of commercial buildings in Australia and the EU to impose requirements much stricter than the current building codes on fire performance. Thus, recommendations are made in the present work based on test results reported in the literature rather than on the current building code requirements.

2.2 Types of Foam

The most commonly used foams in building applications are polystyrenes and rigid urethanes. Polystyrene foams are thermoplastic foams available in boardstock form, though expanded polystyrene can be pre-molded into a desired shape. Urethane-based foams are thermoset foams available either in boardstock or as resins that can be mixed and foamed into the panel *in-situ*. Polystyrenes and urethanes are broadly representative of the full range of rigid polymer foams, thermoplastic and thermoset respectively. The panel design considerations regarding these foams are discussed in Sections 2.2.1 and 2.2.2 respectively. A brief review of some emerging technologies for sustainable foams is given in Section 2.2.3.

2.2.1 Polystyrenes

Polystyrene foams come in two varieties. Expanded polystyrene (EPS) is produced from solid polystyrene beads in a two-step process: first, the beads are pre-expanded through exposure to heat, then the pre-expanded beads are fused and molded into their final shape [49]. Extruded polystyrene (XPS) is formed by mixing the molten polymer with a blowing agent under high pressure and then extruding it onto a conveyor under atmospheric conditions, where it expands as a foam. Both materials are commonly used in a variety of applications, including as thermal insulation.

Polystyrenes are thermoplastic foams, so they lose their shape and melt when heated. Because thermoplastic foams tend to have lower glass transition temperatures than thermoset foams, the maximum service temperatures are relatively low as well. Polystyrene foams typically have a maximum service temperature in the range of 75–

90°C [50]. When EPS and XPS foams are used in roofs, where temperatures can readily reach the upper end of that range, substantial softening has been observed [41]. Softening leads to compaction of the foam, which in turn leads to reduced R-values and can potentially be aesthetically unpleasing. Care should be taken, therefore, not to use polystyrenes in environments where the roof temperatures exceed 70°C.

The fact that polystyrenes are thermoplastic foams has important consequences for the performance under fire conditions. Several authors (e.g. [41, 42, 45–47]) have reported on the behavior of polystyrene foam sandwich cores under medium- and large-scale fire tests. When exposed to high temperatures, the foam melts and draws away from the heated panel surface, creating voids within the panel. Substantial bowing of the affected panels is accompanied by failure of the panel-to-panel joints. The failed joints allow flaming foam droplets to flow from the panel and draw hot air into the void left by the melted foam. This hot air contributes to the rapid spread of the fire within the panel. The spread is so rapid that, even under highly-controlled test conditions, it allows the fire to burn out of control [45].

The flaming droplets and contribution to fire spread have led researchers to recommend against the use of roof panels with polystyrene cores [41, 42, 45–47]. It should be noted that the poor fire performance is not unique to polystyrene cores. The real issue, particularly with regard to fire spread, is the use of thermoplastic foams. Any other thermoplastic foam is expected to behave in the same manner (with the possible exception of the flaming droplets). It can therefore be concluded that thermoplastic foams are inappropriate for use in residential roof panels.

2.2.2 Polyurethanes

The category of rigid polyurethanes consists of two types of foam formed by the reaction of isocyanates with polyols [51]. The difference between rigid polyurethane (PUR) and polyisocyanurate (PIR) is in the ratio of isocyanate to polyol used in the formulation. PUR contains the two components in roughly equal proportion, while PIR typically contains 2–3 parts isocyanate for each part polyol [52]. The excess isocyanate reacts with itself to form trimer ring structures that are thermally stable up to high temperatures, thus affording improved thermal resistance.

Rigid urethane foams are formulated with a high degree of cross linking. As a result, PUR and PIR are both thermoset foams. This cross linking is beneficial from

the standpoint of thermal conductivity and resistance to fire and high temperatures. Excessive cross linking can make the foams friable (brittle to the touch), however, particularly for PIR foams. Friability is an undesirable characteristic because it reduces the adhesive quality of the foam [52], the fatigue strength of the foam [41], and the ability of the foam to withstand impact or localized loads.

Because of their useful structural characteristics and their ability to be readily foamed *in-situ*, urethane foams are available in a wide range of densities. PUR, for example, is readily available at densities of 400 kg/m^3 or higher [53]. While the mechanical properties improve with density, the thermal conductivity also increases [33], to the detriment of thermal performance. As a result, PUR is rarely used at densities higher than 48 kg/m^3 for building insulation applications.

The fact that rigid urethanes are thermoset foams causes them to behave under fire conditions in a manner quite different from polystyrenes and other thermoplastic foams. Urethane foams do not melt at high temperatures; instead, they form a stable char that prevents flame spread and provides a small amount of thermal protection to the surrounding foam [41, 42, 47]. Because the foam does not melt, voids are not created, and fire cannot spread within the panel. Urethane foams, and PIR in particular, also tend to have slightly higher ignition temperatures than thermoplastic foams; consequently, they have slightly longer fire resistance times. As with polystyrene foams, the behavior of PUR in fire tests is representative of thermoset foams in general.

One other thermoset, phenolic foam (PF), has been used in limited commercial insulation applications [30, 42, 50] and is therefore worth noting here. PF has insulating characteristics similar to XPS and structural characteristics slightly better than PUR [50]. Because it is very highly cross linked, it has better fire performance than PUR and PIR [41], but at the cost of particularly high friability [42]. PF has the additional drawback in that it must be absolutely protected against moisture and condensation due to the use of water soluble sulfonic acid as a foaming catalyst [54]. Water that comes in contact with the foam becomes highly acidic and poses a strong corrosion risk to the underlying panel structure. Due to the high friability and the increased corrosion risk, PF is not recommended for use in residential roofs.

2.2.3 Sustainable Foam Technology

Sustainable polymer foam technology is an area of active research. The work is primarily focused on flexible foams, which have applications (e.g. packaging and seat cushions) that demand much higher production volumes than structural foams. However, some advances in sustainable rigid foam technology are worth noting here. Sustainable rigid foam is achieved primarily through three avenues: bio-based foams, bio-based (rather than petroleum-based) constituents to traditional foams, and recyclability.

Research in bio-based structural foams is actively occurring. Wool [55], for example, reports on a thermoset foam made from acrylated epoxidized soybean oil (AESO) blown with carbon dioxide. The work on AESO foam suggests bio-based foams may be a viable option for structural core materials in the future. The results are currently too preliminary to be useful for design, however, especially with regard to durability considerations. As with any material derived from food crops, further study is also needed to determine whether soybean production would be sufficient to keep up with the demand for foam products. The work does, however, illustrate the potential for novel bio-based foam products as a potential replacement for petroleum-based foams.

Another line of research regarding bio-based foams is in sustainable sourcing of raw materials for traditional foams. The polyol component of PUR, for example, can be derived from various vegetable oils [56]. The foams can be made at lower cost and with mechanical properties comparable to petroleum-based PUR; however, the isocyanate component currently comes only from petroleum sources. Thus, coupled with the energy required to create the polyols, the bio-based foams provide limited benefit over petroleum-based foams [55]. Foams can also be made from recycled content. Azim et al. [57], for example, report the synthesis of PUR foams from recycled beverage bottles. Although this technology is in the very early stages of development, it too may be a promising avenue for sustainable foams.

A third line of research in sustainable foam technology is in the processing, particularly the development of sustainable foaming agents. Polyurethanes were traditionally blown using CFC or HCFC blowing agents [58], which have ozone depleting potential. A variety of physical blowing agents are used currently, but HFC's and C_5-hydrocarbons (e.g. pentane) are the most common, and these have global warming potential [58]. A variety of chemical blowing agents have also been developed [58–60].

Chemical blowing agents react in the mixing process, producing a gaseous byproduct (usually carbon dioxide or water vapor). A drawback to these foams is increased heat generation, which can damage the newly-formed cells [58]. A potential solution to this problem is to use froth-in-place foam [58]. Froth-in-place foams are formed by allowing the foam components to react while mixing (rather than after mixing as in foam-in-place processes). Slightly greater thermal control is possible during the mixing process (e.g. through cooling of the mixing head), so the impact of the reaction heat can be reduced. In addition, froth-in-place foams expand and gel very quickly when exposed to air, so the foam properties tend to be more uniform compared to other foaming techniques.

A major drawback to the use of sustainable foam technologies is the preliminary state of the research. Methods of mass production, particularly methods that do not require the use of fossil fuels, do not yet exist. Even when methods are developed, it will be necessary to assess the viability of the foams in terms of the impact on existing seed crop production. It will also be necessary to perform substantially more testing of the mechanical and hygrothermal properties and on how those properties change over time. Creep and fatigue testing, and testing on the resistance of the foams to chemical breakdown will be necessary, particularly for the novel foam materials, before they can be considered suitable for roof applications.

2.3 Typical Foam Properties

To provide a basis for comparison of the different foam types, some typical property values for styrene and urethane foams are provided in this section. Each of these foam types is associated with ASTM materials standards [61–63], from which the data presented in this section are drawn.

Typical values of the material properties relevant to roof design are provided in Table 2.1 for comparison. Note that, due to the unavailability of exhaustive lists of property values, the table relies on several sources. The property values that have been specified in the appropriate ASTM standards are used. The one exception is the thermal conductivity range for PUR. The ASTM standard [62] specifies a range of 0.036–0.037 W/m-K, which is substantially higher than the values reported in vendors' data sheets. The other mechanical properties not specified by ASTM standards are taken from vendors' data sheets.

Table 2.1. Typical nominal properties of polymer foams commonly used for thermal insulation in buildings

	EPS[1]	**XPS**[1]	**PUR**[2]	**PIR**[3]
Density (kg/m^3)	15–29	21–48	30–64	29–96
Compressive modulus (MPa)	1.4–3.3[5]	9.3–26[6]	2.3–5.8[7]	3.4–20[8]
Shear modulus (MPa)	2.1–4.3[5]	2.9–6.2[6]	1.0–4.5[7]	1.2–3.9[8]
Compressive strength (kPa)	69–73	104–690	145–448	137–862
Shear strength (kPa)	140–240[5]	100–280[6]	145–276	110–441[8]
Thermal conductivity (W/m-k)	0.040–0.034	0.029	0.023–0.033[7]	0.029–0.032
Max service temperature[4] (°C)	75–85	75–90	90–120	90–120

1. All values specified by ASTM C-578-08 [61] unless otherwise noted.
2. All values specified by ASTM E-1730-04 [62] unless otherwise noted.
3. All values specified by ASTM C-591-08 [63] unless otherwise noted.
4. Typical values as provided by Davies [50].
5. Typical values as provided in manufacturer's data sheets [64].
6. Typical values as provided in manufacturer's data sheets [65].
7. Typical values as provided in manufacturers' data sheets [53, 66, 67].
8. Typical values as provided in manufacturer's data sheets [68].

Table 2.1 indicates the range of densities over which the ASTM standards apply and in which the foams are typically available for use as building insulation. With the exception of maximum service temperature, the physical properties vary with foam density. Because higher density foams are more "solid" than lower density foams, most of the properties increase with density. As noted above, however, the thermal conductivity is minimized at a density that depends on the material and foaming agent. Because of the large cell sizes typically associated with polystyrene foams (the optimum density for insulation is around 50 kg/m^3 [33]), their thermal conductivity actually decreases with density over the range indicated in the table. For clarity, the property value ranges in Table 2.1 are reported as they vary with increasing density.

Note that polystyrene foams come in a lower density range than urethane foams. This difference does not significantly affect panel weight (since steel, with a density of 7870 kg/m^3, far dominates the total weight), but it may have other implications. For example, all other things being equal, the cost of a foam is proportional to its density [49, 51, 69]. Given that the foams in Table 2.1 are all currently produced in large volumes for various applications [69], a reasonable first cost comparison of the foams can be made based on density. In situations where other considerations do not rule out the use of a particular foam, it is more economical to use materials with low density.

Referring to Table 2.1, polystyrene foams tend to have higher strength and stiffness than urethane foams at a given density, but they also tend to have higher thermal conductivity. A tradeoff thus exists between structural and thermal performance. Significantly, polystyrene foams have a lower maximum service temperature than urethane foams. Thus, as noted previously, PS foams should not be used in applications where the roof temperatures are expected to exceed 70°C for appreciable lengths of time.

Note that the property data provided in Table 2.1 are nominal values. That is, long-term effects such as creep and fatigue are not included. These effects should be evaluated for specific applications through testing. For design purposes, however, some results available in the literature can be used. For example, creep data are available in the literature for polystyrenes [35] and polyurethane [34]. Fatigue data for a variety of foams are available in Reference [37]. The reduction factors used throughout this work are obtained from these references and are listed in Table 2.2. The assumed panel life is based on considerations that follow.

The creep coefficients ϕ_t are calculated based on loading times recommended by European design codes for sandwich structures [70]. The standards specify loading times for live (snow and wind) and dead (self weight) loads. The live load time is based on (unspecified) data on the maximum duration of snow loading for climates in central Europe, and the dead load time is based on typical manufacturers' warranties for building panels. The specified loading times are 100,000 hours for dead loads (ϕ_{DL}) and 2,000 hours for live loads (ϕ_{LL}). An obvious assumption in the recommendations is that the creep deformation is fully reversed during the summer months (i.e. no creep ratcheting effects). The assumption is accepted in this work, and the creep coefficients are calculated from the loading times specified in Reference [70].

The fatigue reduction factor ζ_n is calculated assuming the live load is unidirectional (i.e. varies from zero to the maximum value). The dead load is constant. Based on a dead load of 700 N/m^2 (see Appendix A), the load ratio q_{min}/q_{max} therefore varies from 0.2–0.4. Fatigue data in the literature are available for load ratios of ≈0 and 0.5 [37]. The fatigue strength decreases as the load ratio is reduced. Thus, a slightly conservative approximation of fatigue behavior is obtained by using the fatigue data corresponding to a load ratio of ≈0. Based on a life of 36,500 cycles and a load ratio ≈0, the fatigue reduction factor is $\zeta = 0.6$ for both polystyrene and urethane foams.

Table 2.2. Recommended constants for calculating the creep coefficient ϕ_t (Equation 2.3)

	A	n	ϕ_{LL}	ϕ_{DL}	ζ
EPS/XPS [35]	0.195	0.177	0.8	1.5	0.6
PUR/PIR [34]	0.260	0.177	1.0	2.0	0.6

One particular foam has been considered in the present work as a potential material for roof panel applications and has been used for design purposes. It is a PUR formulation developed by BASF that is designed to be foamed *in-situ* to a density of 36 kg/m^3 (2.25 pcf). The physical properties of the foam relevant to panel design have been evaluated, partially as a part of this project, and are provided in Table 2.3. As with Table 2.1, the effects of aging and long-term loading are not included. Because these effects have not been tested, the constants listed in Table 2.2 are used to account for creep and fatigue.

2.4 Summary

The design considerations that guide the use of polymer foam in a residential roof panel have been presented. These conditions include structural and thermal performance, including an understanding of how the foam properties are expected to change over time and how the service conditions might affect the foam. Two classes of foams are currently used in building insulation applications: polystyrenes (EPS and XPS) and urethanes (PUR and PIR). Other materials, including a variety of more environmentally sustainable foams, may become viable in the future, but the technologies are currently not mature. Comparison between polystyrenes and urethanes has been made, as well as some notes on the applicability of foams to truss core and stiffened plate panels.

Table 2.3. Nominal Physical Properties for *in-situ* foamed PUR at 36 kg/m^3 [66, 67]

Property	**Value**
Density (kg/m^3)	36
Compressive modulus (MPa)	2.99
Shear modulus (MPa)	1.29
Tensile strength (kPa)	231
Compressive strength (kPa)	138
Shear strength[1] (kPa)	>173
Thermal conductivity (W/m-K)	0.023

1. Specimen debonded from substrate at the given load prior to failure

Based on the current state of foam technology, PUR is the recommended foam for residential roof applications. PUR has several advantages over EPS and XPS:

- Thermoset foams are now known to be much safer under fire conditions than thermoplastic foams
- PUR can be used at higher temperatures than PS (the expected service temperature of 80°C is too high for many EPS or XPS formulations)
- PUR generally has lower thermal conductivity than PS
- PUR can be foamed *in-situ*, bonding to other materials without the use of additional adhesives

Based on these considerations, other thermoset foams may be viable for roofs in the future. Thermoplastic foams, including polystyrene, are not recommended.

Chapter 3

Thermal and Structural Design Considerations

Several limit states applicable to the design of web core roof panels have been identified in the present work. Specifically, these are:

- Thermal insulating performance
- Panel deflection
- Buckling of the face sheet
- Shear buckling of the webs
- Bearing stress failure at the support locations
- Shear stress failure of the core material
- Flexural buckling of the webs
- Buckling of the face sheet into the webs

A subset of these modes play a key role in the determination of feasible panel designs. Descriptions of each failure mode and the relevant modeling techniques described in the literature are presented in this chapter.

3.1 Panel Loads

The applied loading and thermal requirements for roofs in the United States are specified by building codes [43, 71]. The requirements are climate dependent. Colder climates are subject to larger loads (due to snow loading) as well as higher insulating

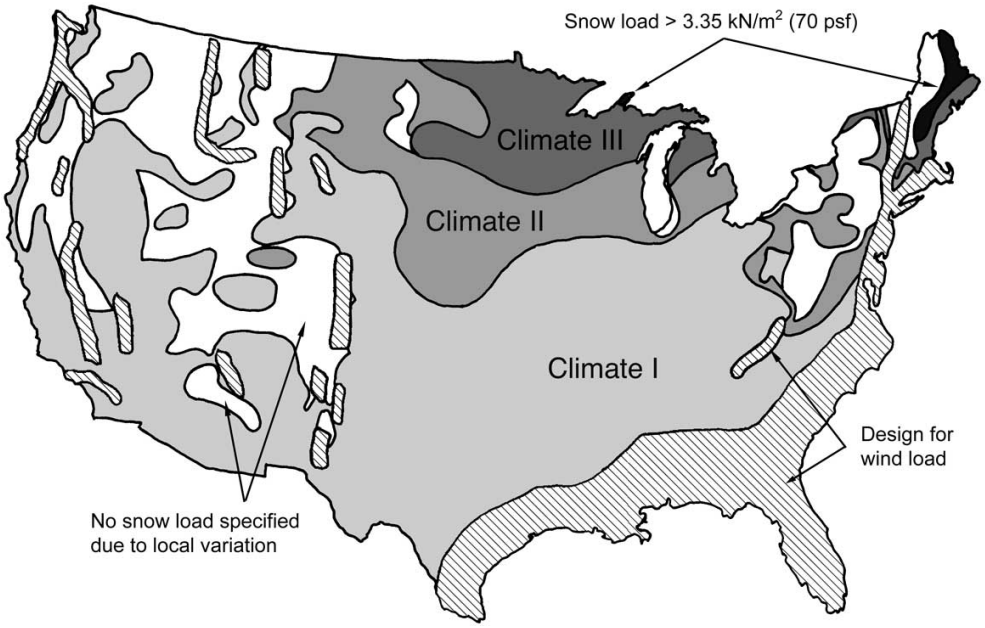

Figure 3.1. Climate zones used to establish panel load requirements (from Reference [23])

requirements. For simplicity, the continental US has been divided in the present work into three climate zones, designated Climate I, II, and III [23] in order of increasing snow load. These climate zones are illustrated in Figure 3.1 [23]. The regions not covered by these designations are subject either to high wind loads or to extreme local variations in snow loading. Panels can be designed for those regions, according to the considerations in this work, based on the appropriate local loads. The load and R-value requirements for these three regions are summarized in Table 3.1 for panels with a 6:12 roof pitch. Further details on the load requirements are given in Appendix A.

The structural failure mode models developed in the present work are derived by treating the panel assembly as a simply supported beam under uniform distributed load. The beam assumption is reasonable because the panel-to-panel joints do not resist deflection. The panels therefore behave as plates under cylindrical bending,

Table 3.1. Loads and R-value requirements for panels with a 6:12 roof pitch

	Load (N/m^2)	**R-value (m^2-K/W)**
Climate I	1576	5.3
Climate II	2173	6.8
Climate III	3322	6.8

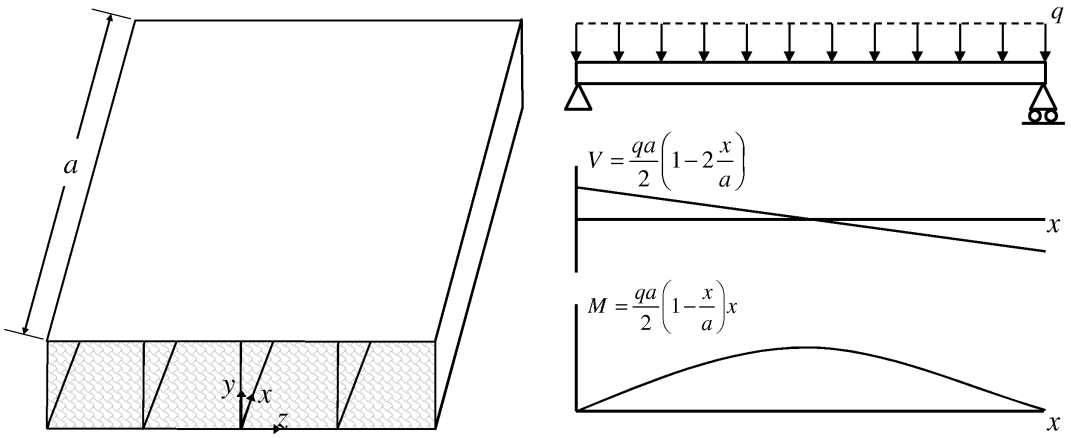

Figure 3.2. Panel coordinate system and the associated distribution of internal shearing forces and bending moments

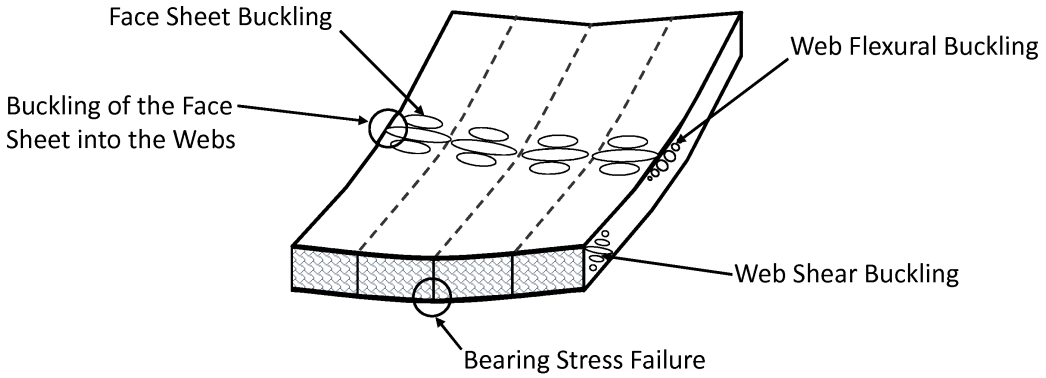

Figure 3.3. Locations of the local failure modes in the face sheets and webs

for which the behavior can be approximated using beam theory assumptions [72]. Modification to the basic theory is necessary to account for the relatively wide web spacing and is discussed in Section 3.3.

From first principles, the internal shearing forces and bending moments in a panel of length a under a distributed load q follow the distributions plotted in Figure 3.2. For reference, the coordinate system used throughout this work is included in the figure. The stresses in the face sheets and webs are not uniform along the panel length (the shearing force varies linearly, and the bending moment varies parabolically). Thus, failure modes (e.g. face sheet buckling) that are caused by bending stresses will be localized at the panel midspan, while modes (e.g. web shear buckling) caused by shear stress will occur near the supports. This localization of the failure modes is illustrated in Figure 3.3 and has a minor effect on panel strength, as described in Chapter 4.

More importantly, it means that interaction effects between failure modes will be minimized. Such interactions have therefore not been considered in the present work.

3.2 Thermal Insulating Performance

The thermal performance of roof panels is measured by the R-value of the assembly. The R-value is a measure of the resistance of the panels to conductive heat transfer. Following the concept of the "clear wall" R-value [73], the influence of the webs is taken into account, but localized details of the overall roof structure (e.g. insertions for ventilation, skylights, etc.) are ignored. Higher R-values translate to improved energy performance by reducing the energy required to maintain a set temperature in the interior space.

For the panels described in this work, the R-value is determined using the isothermal planes method [30]. In this method, illustrated in Figure 3.4, the panel assembly is broken down into a set of layers, defined by (assumed) isothermal interfaces. Following the well-known electrical circuit analogy, the thermal performance of the panel assembly is determined by treating the layers as thermal resistances in series. The structural layer of the panel is similarly broken down: assuming no lateral heat transfer between the webs and core material, these components act as parallel resistances. The R-value of the panel assembly is determined from the equivalent thermal resistance of the components.

For the web core panels illustrated in Figure 3.4(a), the isothermal planes assumption is reasonable. However, in two-layer panels, Figure 3.4(b), the interface is not isothermal in general. The webs provide a thermal short to the interior surface temperature, so the temperature T_m varies with distance from the webs. Schoenbauer [74] investigated to a limited extent the thermal performance of panels with non-isothermal interface between the layers. He found the isothermal planes approach is conservative in the sense that it underpredicts the R-value of the assembly. In the panels he investigated, the structural layer of the panel provided less than 20% of the total R-value, and the error caused by using the isothermal planes method was less than 5%. As the contribution of the structural layer to the total R-value decreases, the error decreases as well.

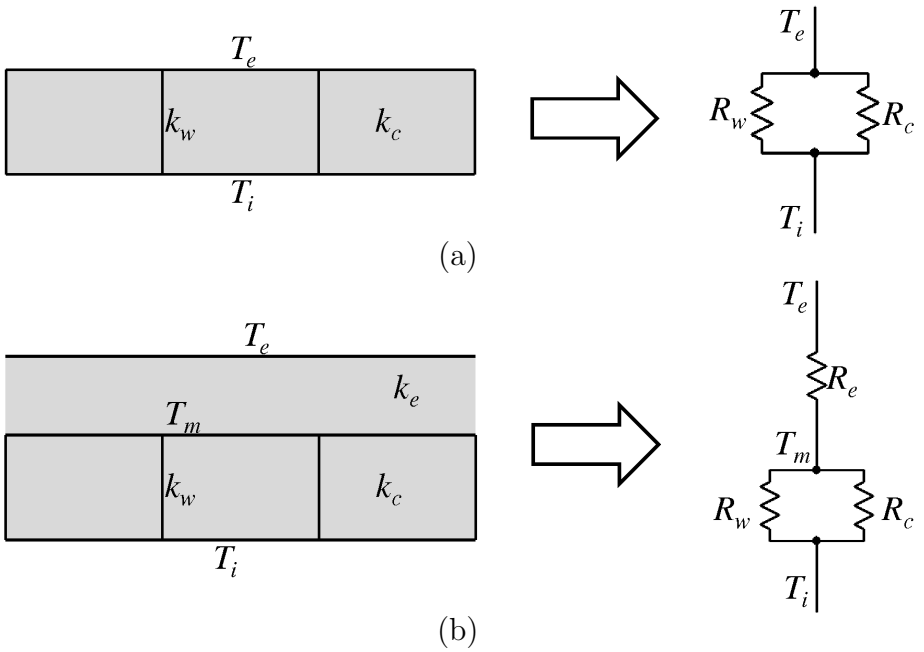

Figure 3.4. Isothermal planes (lumped thermal resistance) approximation for panels (a) without and (b) with an external foam layer

Schoenbauer's [74] results make sense because, referring to the circuit diagram in Figure 3.4(b), the temperature drop across the structural panel layer decreases along with the R-value contribution. As the temperature drop decreases, the interface between the two layers becomes more nearly isothermal. Thus, in web core panels, where much of the thermal performance comes from the exterior foam layer, the accuracy of the isothermal planes method is reasonable. Based on these results, the method is used in the present work for the thermal analysis of panels with and without an exterior foam layer.

3.3 Panel Deflection

As with the thermal insulating requirement, the limit on allowable roof deflection is specified by building codes. For example, the International Residential Code (IRC) [43] establishes a deflection limit of $span/240$, where *span* refers to the projected distance spanned by the panel. For clarity, the conventions by which load, deflection, and *span* are defined (in this work and in the residential code) are illustrated in Figure 3.5. Both the load q and the deflection w refer to the components of load and deflection acting normal to the panel surface. The specified deflection limit

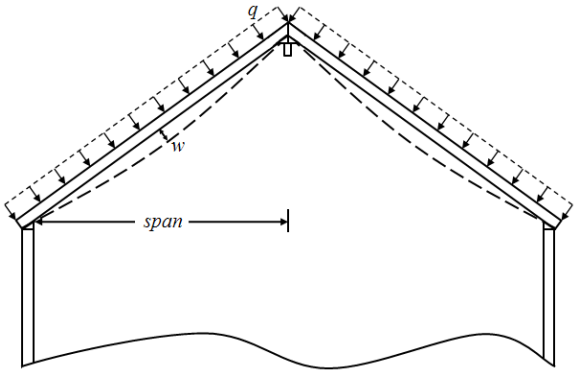

Figure 3.5. Load and deflection conventions for determining deflection limit

is set based on building experience and is meant to limit the stresses in the panel joints, prevent plastic deformations, and to maintain aesthetic appeal [42]. Because the panels are insulated, a temperature gradient occurs between the two face sheets resulting in thermal deflection. Analysis of deflection should thus account for thermal deflection as well as deflection due to the applied loads.

Durability considerations require that the deflection limit be satisfied over the full life of the roof—the effects of creep, fatigue, and other long-term phenomena should therefore be considered in determining panel deflection. Creep can have a particularly important impact on proper panel design when wood or polymer materials are used structurally. Over a period of 50 years, for example, the deflection of wood and wood-based composites can more than double as a result of creep [75,76]. In humid climates, the problem may be exacerbated by the mechano-sorptive effect (the tendency of wood to creep at highly accelerated rates when subjected to varying ambient humidity levels) [77]. These issues, which are often not adequately addressed in current building practice, are particularly problematic with the use of wood-based SIPs for roofs. The long-term warping that results from inadequate panel design has been cited by at least one major home builder[1] as an obstacle to builder acceptance of SIP roof panels (and an important opportunity for improvement).

The thermal deflection of foam core sandwich panels was studied in depth by Hartsock [78] both theoretically and experimentally. Depending on the stiffness of the core relative to the face sheets, panels deform by a combination of bending and in-plane shear. Hartsock found that panels with very weak core material deform in pure

[1]From a conversation with Larry Wrass, formerly of Pulte Homes

shear, panels with strong core material (including most polymer foams) and thin face sheets deform in bending, and panels with strong core and profiled face sheets deform by a combination of shear and bending. Shear deformation is not noticeable to the occupants of the house; excessive thermal bending, however, can increase panel deflection beyond the allowable limits. The addition of stiffeners (webs) effectively strengthens the core, so the thermal warp of web core panels is thus most effectively modeled by pure bending.

A considerable body of literature exists on the deflection models for sandwich panels with various core configurations. In general, depending on the application and boundary conditions, sandwich panels are modeled as shear-deformable beams or plates [37], with stiffness coefficients derived from the cross section geometry. Libove and Batdorf [79] developed the governing equations for shear-deformable orthotropic plates. The bending and buckling solutions were determined for foam core panels by Hoff [80] and for generic orthotropic panels by Robinson [81]. For orthotropic panels, the theory requires the determination of five stiffness coefficients: two each for bending and transverse shear deformations, and one for in-plane twisting. The panels can be modeled as beams if the length is much greater than the width and if the long edges are not supported. In that case, deflection is modeled using Timoshenko (shear-deformable) beam theory, which is characterized by two stiffness constants: one each for bending and shear deformation in the longitudinal direction.

The stiffness coefficients for a variety of panel constructions have been developed, particularly for panels with prismatic structural cores. Models have been developed for three types of web core geometry: I-cores [82–84], C- [85, 86], and Z-channels [87, 88]. The I-core consists of generally thicker straight webs that can be welded directly to the face sheets. The channel (C- and Z-) sections are used when thin webs are required; the use of channel sections provides a surface that can be used for welding or fastening to the face sheets.

Two key results arise from the prior work. First, an accurate model of panel stiffness is obtained by superimposing the independent face sheet and web stiffnesses. This result also holds for foam-filled web core panels [89], i.e. the foam acts as a third independent stiffness contribution. Second, the choice of web section is inconsequential. The only stiffness component affected by local web geometry is the shear stiffness perpendicular to the webs. In this direction, the webs interact with the face sheet, causing slightly

different stiffness for I-, C-, and Z-sections. This difference is unimportant for panel design because shear deformation perpendicular to the webs is negligible, especially in foam-filled panels. The web cross section also has negligible impact on thermal performance of thin webs [74].

Stiffness modeling of web core panels is most accurate when the web spacing is small relative to the panel width. When the spacing is relatively large, the stress distribution in the panel changes somewhat due to local deflection in regions of the face sheets far from the webs. This phenomenon, known as shear lag, results in a stress concentration in the face sheets near the webs and a decrease in panel stiffness. Winter [90] accounted for the shear lag effect by introducing an effective face sheet width, the value of which depends on factors such as cross-sectional geometry, length, and material properties. Following that approach, subsequent research has focused on the determination of effective width for specific cases.

The most comprehensive investigation of effective width for geometry relevant to web core panels was performed by Hildebrand and Reissner [91], who used energy methods to analyze the shear lag in box beams under various loading and boundary conditions. More recently, Lertsima, et al. [92] used FE analysis to investigate the effective width of box beams under uniform load. They found effective widths smaller than those predicted by Hildebrand and Reissner; however, in their analysis the load is concentrated on the webs rather than distributed over the entire face sheet. This has the effect of artificially increasing shear lag [91] and is therefore less accurate than the approach in Reference [91] for panels under uniformly distributed load. The latter case is the most realistic approximation for the loads on roof panels, so the analysis from Reference [91] is used in the present work.

3.4 Face Sheet Buckling

The possibility of face sheet buckling is an important consideration to the design of web core panels because the face sheets bear almost all of the bending stresses. The face sheet buckling mode for web core panels under distributed load is illustrated in Figure 3.6. The localization of buckling damage to a region near the midspan is a result of the quadratic bending moment distribution (see Figure 3.2). The buckling waves are largest at the midspan, where bending stresses are highest; the buckling amplitudes decay quickly with distance from the middle.

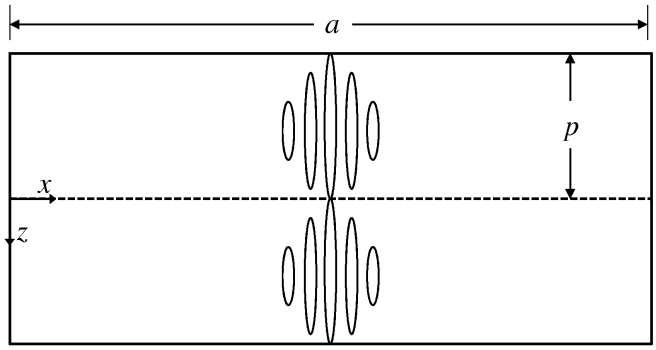

Figure 3.6. Face sheet buckling mode: view of the buckled face sheet, assuming one intermediate web (dashed line); loading corresponds to the bending moment distribution illustrated in Figure 3.2

The face sheet buckling phenomenon of sandwich structures is bounded by two cases. Face sheets supported by webs with no core material (e.g. truss core panels) experience the buckling mode typically associated with plates loaded in compression. To this case, the standard plate buckling model [93] can be applied. Face sheets supported by a solid core material with no webs (foam core panels) or webs with very low stiffness fail in a buckling mode that is characterized by very short wavelengths in the loaded direction and almost no curvature in the unloaded direction [94]. This buckling mode is generally referred to as "wrinkling" in the literature and results in ultimate panel failure with little or no postbuckling strength. In web core panels, the failure mode is a hybrid of the two cases. The face sheet, as illustrated in Figure 3.6, buckles with short wavelengths in the direction of loading (due to the influence of the foam) and at least one half-wave in the other direction (due to the webs) [89].

The face sheet wrinkling strength of foam core panels with no webs has been modeled by several authors (e.g. [95–97]), with all of the models yielding nearly the same strength predictions. The slight differences between the models result from assumptions about the buckling deformation in the core. The models have been considered from a slightly different angle in this work to develop expressions for the foundation constants used in the shear buckling model. They are therefore described in more detail in Chapter 4.

The problem of face sheet buckling in web core panels has only recently received attention in the literature. The analogous problem of the buckling of highly profiled face sheets in compression has been solved using an elastic half space model (e.g. [42]) for the core. Solution of this model results in an equation that must be solved numer-

ically and is impractical for design. Similarly, Aimmanee and Vinson [98] modeled the face sheets of web core panels as plates on a one-parameter elastic foundation, with foundation properties derived from the model by Allen [97] noted above.

Kolsters [89] showed that one-parameter foundation models are insufficient for panels containing core materials with high shear modulus. Instead, he modeled the core as a two-parameter (Pasternak) foundation. The foundation constants are derived from the core material properties based on curve fits to the results of an FE study. Those results were, in turn, validated experimentally. Using the empirically determined values for the foundation constants, Kolsters found the Pasternak foundation model to be an accurate approach to the prediction of face sheet buckling strength. The results are directly applicable to web core roof panels, so the model by Kolsters [89] is used for face sheet buckling in the present work.

3.5 Web Shear Buckling

Shear buckling of the webs is an important concern in the design of web core panels because the webs carry almost all of the internal shearing forces in the panel. In panels under distributed load, the shearing forces vary linearly along the panel length (Figure 3.2), so shear buckling occurs in a region close to the panel supports, as shown in Figure 3.7. The buckling pattern occurs at an angle of about 45° to the horizontal (the principle stress direction for a material in pure shear) because the bending stresses in the web are small due to the face sheets.

The analysis of shear buckling depends on several factors, including the non-uniform stress distribution in the webs, interaction effects with the face sheets, and the contribution of the core material. The latter effect is particularly important due to the wide web spacing. The effect of core material properties on the local buckling

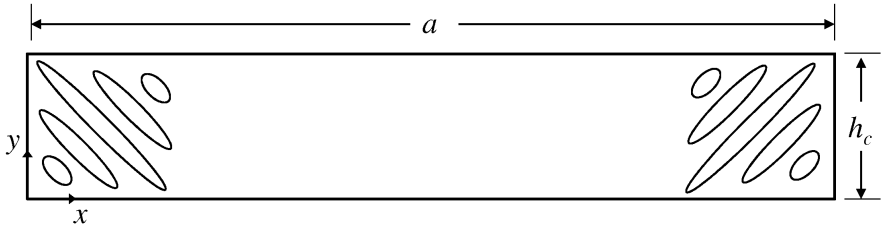

Figure 3.7. Web shear buckling mode: view of a buckled web; loading corresponds to the shear force distribution illustrated in Figure 3.2

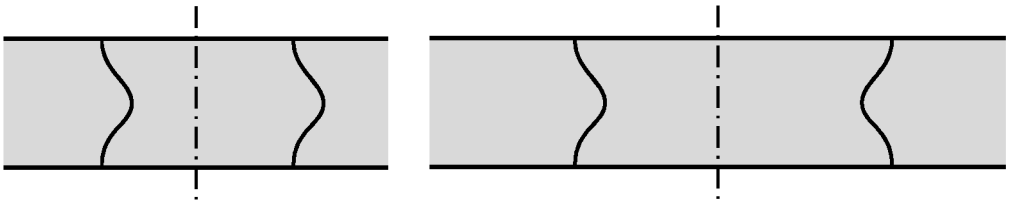

Figure 3.8. Relationship between adjacent buckled webs: (a) antisymmetric buckling, and (b) symmetric buckling

strength of sandwich panels has received little attention in the literature, especially for deep foundations (as in the case of shear buckling in widely spaced webs) with high shear stiffness. Kolsters [89] demonstrated that the shear stiffness of the core contributes substantially to *face sheet* buckling strength in such cases and provided empirical foundation constants for moderately deep foundations. He also showed that the face sheets buckle in one of two relationships to each other. These relationships are illustrated in terms of the buckling of adjacent webs in Figure 3.8. If the webs are spaced very closely ($p/t_w < 50$), the adjacent webs buckle in an antisymmetric manner, illustrated in Figure 3.8(a). Wider-spaced webs buckle in the symmetric manner illustrated in Figure 3.8(b). It will be shown that, for web core panels, $p/t_w \gg 50$, so the symmetric assumption is adopted throughout this work.

The foundation constants developed by Kolsters [89] are not applicable to the analysis of *web* buckling in panels with wide web spacing because the foundation depth is much greater than in his work. The buckling deformation field in deep foundations is fundamentally different from that of shallower foundations, as described in Chapter 4. The result is that the approach by Kolsters tends to greatly over-predict the contribution of deep foundations to buckling strength. A more accurate model for the determination of foundation constants is thus necessary for the shear buckling analysis.

For the above reasons, and because of the particular importance of shear buckling as a limiting failure mode, the development of a shear buckling model has received particular attention in the present work. Of particular importance to the model is an accurate approach to modeling the effect of the core material on buckling strength. A full discussion of shear buckling, including a review of the relevant literature on buckling and foundation modeling, is presented in Chapter 4.

3.6 Bearing Stress Failure

Local failure of the webs and core can occur at the support locations, where the panel is subjected to concentrated loads. In foam-filled panels, the failure mode consists of a combination of local foam crushing and inelastic web failure (web crippling). The web crippling mechanism, illustrated in Figure 3.9, is the formation of yield lines meeting at a plastic hinge in the face sheet at a distance from the support location. The webs lose load bearing capacity following failure.

Bearing failure can be prevented by two methods:

- Choose core material and web geometry to withstand bearing forces everywhere
- Stiffen the bearing region of the panel, e.g. through the use of wood or dense foam blocking

The second approach is useful when the thermal requirement or other considerations make it impractical to design panels with webs thick enough to resist bearing failure. An obvious drawback of that approach is the need for additional materials and manufacturing steps to attach the blocking. It may be justified, however, if the blocking is also used to meet other non-structural needs (e.g. aesthetics, moisture sealing, etc.). A model for choosing web geometry to resist bearing failure is presented in this work.

Web crippling strength depends on several factors, including sensitivity to material and load imperfections, residual stresses, support location (i.e. distance from the edge of the panel), and stress concentrations at the support [99]. A few models developed in the literature have attempted to account for these factors. The most successful, applicable to webs with no foam support, was developed by Roberts and Newark [100] based on the assumed failure mechanism illustrated in Figure 3.9. Slightly different models are used for bearings located near the end of the panel or in the interior. Romanoff [101] adapted the model in Reference [100] to predict the bearing strength of foam-filled panels loaded in the interior region by a circular indenter.

The models in References [100, 101] are adapted in the present work to predict the bearing strength of foam-filled web core panels supported at the ends by rectangular bearings. The resulting model is presented in Chapter 5. Analytical bearing strength models have some drawbacks in practice. They are based on assumed failure mechanisms and typically work for a limited range of web designs (e.g. slender webs). They also tend to overpredict bearing strength due to the influence of factors mentioned

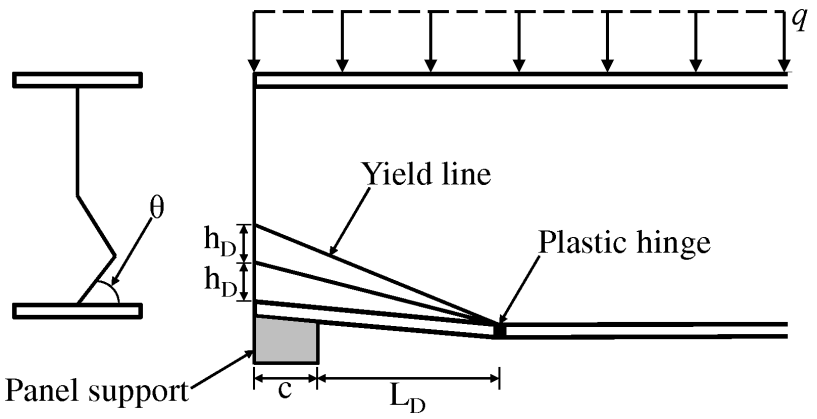

Figure 3.9. Bearing failure mode (adapted from Reference [100]): view of the failure mechanism in the web; the maximum shearing force (see Figure 3.2) is distributed over the panel support width c

above. As a result, they are not widely used in current design practice. Instead, prescriptive design codes for thin-walled structures [102] use empirical equations calibrated to match the test data for specific web geometry and loading conditions.

The empirical equations are typically calibrated over a wide range of web geometry and therefore not as limited in applicability as the mechanism solutions. Due to the prevalence of the empirical equations, new web crippling test data (e.g. [103]) are typically curve fit to the same form. Thus, in this work a semi-empirical model is also developed based in part on the prescriptive code equations. That model is presented in Chapter 5 and compared to the analytical model for panels with thin webs.

3.7 Core Shear Stress Failure

An important failure mode for foam core panels is stress failure of the core material. In web core panels, the webs take up the shear stresses, so core failure is normally not a concern. If the web fails (e.g. due to shear buckling), however, the shear stresses transfer to the core. In this case, the strength of the core material can be used to predict the existence of residual load-carrying capacity following web failure. The shear stress distribution in foam core panels with no webs is determined by first principles and is available in Reference [37], for example. In the present work, no contribution from the webs is assumed, so the analysis for foam core panels is used. Panels are designed to have adequate core shear strength independent of the webs.

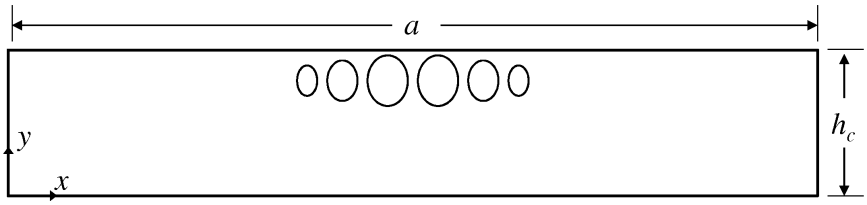

Figure 3.10. Flexural web buckling mode: view of a buckled web; loading corresponds to the bending moment distribution illustrated in Figure 3.2

3.8 Web Flexural Buckling

The in-plane bending stresses on the web can cause the buckling mode illustrated in Figure 3.10 [93]. Buckling occurs in the compressed portion of the web and, as with face sheet buckling, is localized near the midspan, where bending stresses are highest. The analysis of flexural buckling must consider the effects of the core material, non-uniform stress distribution in the longitudinal panel direction, and variable location of the neutral bending axis[2]. The webs may be widely spaced, so the elastic foundation considerations used in the shear buckling analysis are applicable to flexural buckling.

Timoshenko [93] provided a solution for the buckling strength of plates under pure in-plane bending with arbitrary neutral axis location. Curve fits to the solutions were later developed as a function of neutral axis location. These curve fits have been codified into prescriptive design codes (e.g. [102]) applicable to beams with no foam support. The curve fits are a slight simplification in that they assume the plate is infinitely long, but they do account for the neutral axis location.

In web core panels with unbuckled face sheets, the contribution of the webs to the panel bending stiffness is small (less than 10% of the total). As a result, the bending stresses on the webs are also small, and flexural buckling is unlikely to limit any web core designs. To confirm this, a flexural buckling model was developed in this work, treating the webs as plates on a Pasternak foundation. The details of the analysis are given in Appendix B. Interaction between shear and flexural buckling modes of the web has not been considered in the present work because the stresses that cause the two modes are localized to very different parts of the web.

[2]For symmetric panels with unbuckled face sheets, the neutral axis is at the midplane of the web; in general, however, the location can vary.

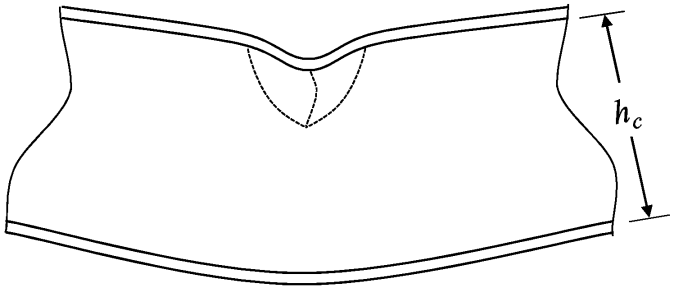

Figure 3.11. Vertical buckling of the face sheet into the webs: view of the web and face sheets (thickness exaggerated to illustrate failure); loading corresponds to the bending moment distribution illustrated in Figure 3.2

3.9 Buckling of the Face Sheet into the Webs

The face sheets provide panel stiffness by virtue of their distance from the neutral bending axis. In their own plane, however, the thin, flat sheets provide very little bending resistance. As the panel deforms under load, therefore, the webs play a key role in maintaining the distance between the face sheets and in protecting the face sheets from local failure. If the webs are too slender, they may be unable to resist the reaction forces imposed by the face sheet, resulting in the buckling failure illustrated in Figure 3.11. Adapting the terminology used in the literature, this failure mode is referred to as vertical face sheet buckling or buckling of the face sheet into the webs. It occurs when the web buckles locally beneath the face sheet, allowing unrestricted deformation of the latter and resulting in panel collapse.

The typical approach to predicting this type of failure (in plate girders and other structures with no foam support) is described by Salmon and Johnson [104]. A small element of the web is modeled by a column, with representative loads determined based on a force balance for the deformed face sheet. Using this model, it is possible to determine a web slenderness t_w/p for which buckling failure coincides with yielding of the face sheets. If the slenderness is smaller than this limit, vertical buckling of the face sheet does not occur because the panel strength is limited by face sheet yielding. In prescriptive steel design codes (e.g. [102]), the latter approach is used, and the web slenderness limit is defined as a function of face sheet yield strength.

In foam-filled web core panels, the core contributes to the strength by bearing some of the load that would otherwise occur on the webs and by strengthening the webs directly. The first contribution may be very important with the use of relatively

stiff core materials; to be conservative, however, it is neglected in the present work. The latter contribution is treated through a modification of the approach given in Reference [104]. The details of the model, including a description of how the applied forces translate into in-plane compression on the webs, are provided in Appendix B. Analogous to the approach used in prescriptive design codes, a slenderness limit applicable to foam-filled panels is developed. Using this approach, it was determined that the face sheet yielding requirement is easily satisfied for practical panel designs. Vertical buckling of the face sheets is not a limiting factor in design.

3.10 Summary

The failure modes relevant to the design of web core roof panels were reviewed in this chapter. It is worth pointing out that almost all of the structural failure modes result from the use of thin face sheets and webs. In particular, the need for thin webs to meet the thermal insulating requirement is unique to roof panels. Web core applications without thermal requirements (e.g. ship structures [89]) use thick (≈3–4 mm) webs for which local failure modes are generally not a concern. In this work it will be shown that the contribution of the foam to local buckling strength is a critical aspect of roof panel design with thin webs.

Models for thermal performance, face sheet buckling strength, and core shear strength are available in the literature and are directly applicable to web core panel design. In addition, the deflection model used in this work is developed as a combination of first principles and existing models in the literature (for thermal deflection, stiffness, and shear lag effects). Models for the other failure modes of foam-filled panels are not available in the literature and are developed in this work. From these models is is shown that two failure modes—flexural web buckling and buckling of the face sheet into the webs—do not influence the design of web core panels because other failure modes are more limiting.

Chapter 4

Shear Buckling in Foam-Filled Web Core Panels

Web core panels, foam filled sandwich panels with interior webs, are a structurally efficient option for transverse load bearing applications[1]. In web core panels, the interaction between the webs and core material can have a substantial impact on web shear buckling strength and is a key element of lightweight structural design. The present work is an investigation of web buckling behavior in web core panels under a distributed load. To solve this problem, web shear buckling was analyzed for the case of pure shear loading with foam support, and this analytic model was extended to the case of panels with a transverse distributed load. The webs are modeled as simply supported plates resting on a Pasternak elastic foundation. To that end, a buckling model for plates on a Pasternak foundation is presented, along with closed-form approximations of the solution for square and infinitely long plates. An accurate model for the foundation constants is developed using energy methods. Applicability of the plate buckling model to web core panels with transverse loads is presented via a finite element study. In panels, the slenderness and spacing of the webs have a slight effect on the boundary conditions between the webs and face sheets. The effect is relatively small, however, and the model presented in this work underpredicts buckling strength by less than 25%. The model in this work is thus a reasonable approach to the practical design of web core panels.

[1]This chapter is reprinted from Reference [28], with permission from Elsevier.

4.1 Introduction

Sandwich construction is known to be an effective approach to the design of lightweight structures. Foam core sandwich panels, comprised of two face sheets separated by a polymer foam core, are extensively used in the building industry [8, 24, 42] to satisfy both structural and insulation requirements. However, these designs are not well suited for long term transverse loads due to creep of the foam core material. Sandwich panels (such as truss core panels [26]) that include interior webs for shear support are well suited for transverse loads, but the webs create a thermal short between the face sheets. The web core panel described in the present study is a sandwich panel that combines the shear stiffness of webs with the thermal performance of polymer foam.

In this concept, the core consists of stiffening metal webs, with foam filling the gaps between them (Figure 4.1). Web core panels have been investigated for shipbuilding applications [89,98] and, more recently, for use in energy efficient residential roofs [29]. The requirements for the latter application include thermal insulating performance, which leads to the use of thin, widely-spaced webs to avoid large conductive thermal losses across the panel. The thin metal webs are susceptible to shear buckling; thus, an understanding of the effect of the core material on shear buckling strength is critical for developing designs that meet all of the requirements efficiently. In the present work, the shear buckling behavior of foam-filled web core panels is modeled by treating the webs as plates on a Pasternak elastic foundation. The relevant material properties of the core are incorporated into the foundation constants.

The shear buckling behavior of isotropic plates with no elastic foundation is well understood. Southwell and Skan [105] obtained direct solutions for the strength of infinitely long plates loaded in pure shear. Stein and Neff [106] used energy methods to develop solutions for simply supported plates of finite length. Solutions have also been developed for plates with clamped [107] or mixed [108] boundary conditions, as well as for orthotropic plates [109]. The only studies to date that have considered the effect of an elastic foundation are by Davies and Fragos [110, 111], who investigated the buckling of open C-channel sections ("cassettes") filled with foam and loaded in pure shear. They used a combination of physical testing and finite element modeling to develop an empirical design equation for clamped plate sections attached to foam. The open sections allow the foam to deflect under the action of plate buckling. In

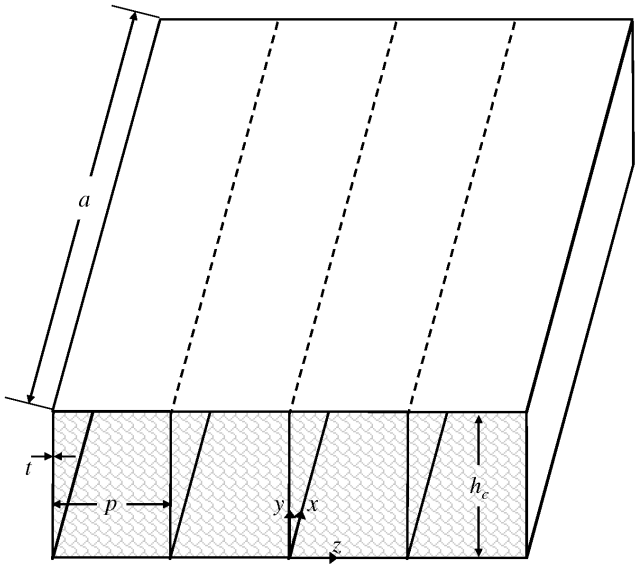

Figure 4.1. Web core panel concept geometry and coordinate system

web core panels, the foam is restricted against bending and is therefore compressed by the buckled plate. As a result, the empirical results are not generally applicable to web core design, and an analytical model that incorporates the compression effects is needed.

An important part of modeling webs as plates on an elastic foundation is the determination of foundation constants based on the physical properties of foundation materials. Some approaches to modeling the foundation behavior are suggested based on work that appears in the literature. Early models [112, 113] were obtained using the elasticity solution for a plate resting on a finite solid medium that is fixed to a rigid base. These models assume that displacement caused by the buckled plate propagates through the full depth of the medium. Foundation constants can be deduced from the results by solving for the governing equations at the plate surface. More recently, Sironic, et al. [114] used Airy's stress functions to solve for the displacement field within the foundation layer. They found that the model in References [112, 113] is inaccurate for deep foundations because the buckling displacement decays within less than the full foundation depth.

Alternative foundation models are suggested based on the work of Hoff and Mautner [95] and of Plantema [96], who assumed that the plate buckling displacement would not extend through the whole depth of the foam. Comparison between these models

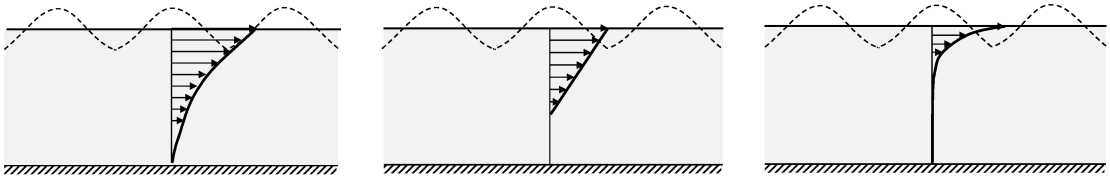

Figure 4.2. Buckling displacement models based on (a) elasticity solution (References [112, 113]), (b) linear decay (Reference [95]), and (c) exponential decay (Reference [96])

and the earlier models is illustrated in Figure 4.2. The decay of buckling displacement as predicted by the model in References [112,113] is shown in Figure 4.2(a). The decay assumed by References [95] and [96] are shown in Figures 4.2(b) and (c) respectively. Hoff and Mautner [95] assumed the displacement would decay linearly to zero at a finite depth, determined along with the critical buckling load using the principle of minimum potential energy. Plantema [96] assumed an exponential decay model. As shown in Figure 4.2(c), the characteristic length of the displacement decay is assumed to be much less than the depth of the foundation. Both of these models were used to predict the wrinkling strength of foam core sandwich panels in compression directly, i.e. without recourse to an elastic foundation model. It is demonstrated in the present work that a model similar to the one by Plantema [96] can be used to determine foundation constants for other local buckling modes by analogy to the buckling solution for beams on elastic foundation.

Application of plate buckling models to the design of web core panels requires consideration of the effects of panel geometry and load distribution on buckling strength. Geometry affects the boundary conditions on the web, particularly due to the connection with the face sheets. Wiernicki [115] investigated this effect for panels with a core consisting of corrugated light-gage metal. He found that the face sheets add rotational resistance to the webs depending on the ratio of web thickness to face sheet thickness, as well as the ratio of panel depth to web spacing. From the results of his study, it can be inferred that the boundary conditions on the web will be somewhat stronger than simply supported, but weaker than clamped.

In panels subjected to uniformly distributed loading, the in-plane shearing forces vary along the length of the panel. As a result, the stress distribution is not uniform throughout the web. Several studies [116–121] have focused on the effects of non-uniform stress distributions on plate buckling strength. Libove, et al. [116] and Zaraś,

et al. [117] used the Rayleigh-Ritz method to determine the buckling strength of a plate under uniaxial compression that varies linearly along the length. Both studies found that the variation in load causes an increase in buckling strength if calculated based on the edge loads. The increase in strength depends on aspect ratio and is greatest for square plates. The load distribution has no effect on the strength of infinitely long plates. Similar results have been found for plates under linearly varying compression balanced by body forces [118] and under parabolic variation of axial loads [119]. Two recent studies [120, 121] confirmed the phenomenon with regard to the local and distortional buckling strength of cold-formed channel sections. The studies focused on short beams, but in both cases the effect of load distribution diminished with increasing length.

The present paper investigates the shear buckling behavior of web core panels under distributed transverse loading. The analysis is performed in two parts. First, a model is developed for the buckling strength of simply supported plates on an elastic foundation, loaded in pure shear. The model includes an approach to the determination of the necessary foundation constants based on the core material properties. Second, application of the plate buckling model to the design of web core panels subjected to transverse load is presented. The impact of aspect ratio and panel geometry on the accuracy of the model is examined. The former effect is shown to be negligible, and the latter effect is quantified over a range of panel geometries.

4.2 Plate Buckling Model

Consider a thin, isotropic plate of length a and width b, as shown in Figure 4.3, and thickness t. Assume the plate has elastic modulus E and Poisson's ratio ν. The plate is simply supported on all four sides and resting on a Pasternak foundation. In the Pasternak foundation model, the restoring force $\hat{q}$ acting on the plate due to the out-of-plane deflection w is given by [122]

$$\hat{q} = K_W w - K_P \nabla^2 w, \tag{4.1}$$

where K_W and K_P are foundation stiffness constants. The first term is the resistance of the foundation material to normal deformations, and the second term is the resistance to shear deformations. If the plate is loaded by a uniform shear stress τ, then

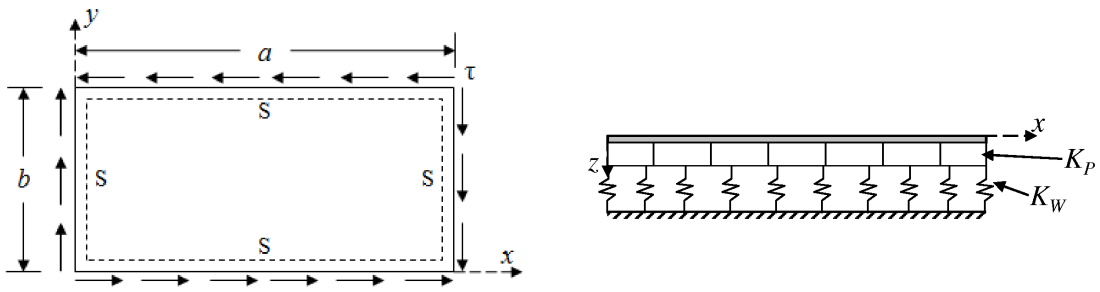

Figure 4.3. Simply supported plate and elastic foundation model

the buckling behavior is modeled using the von Kármán equation

$$D\nabla^4 w = -\left(K_W w - K_P \nabla^2 w\right) + 2\tau t w_{,xy}, \tag{4.2}$$

with the plate stiffness D given by

$$D = \frac{Et^3}{12\left(1-\nu^2\right)}. \tag{4.3}$$

The subscripted comma in Equation (4.2) represents partial differentiation with respect to the subscripted variables.

The critical buckling stress $\overline{\tau}$ for plates is given by [93]

$$\overline{\tau} = \chi \frac{\pi^2 D}{b^2 t}, \tag{4.4}$$

with buckling coefficient χ determined by the loads and boundary conditions acting on the plate. The approach used in the present work to determine χ is a Ritz solution based on the principle of minimum potential energy. According to this principle, the variation in strain energy δU of the deformed plate must be balanced by the variation in work δV caused by external loading, i.e.

$$\delta U - \delta V = 0. \tag{4.5}$$

To solve Equation (4.5), it is necessary to assume a kinematically admissible function for the displacement field w. For simply supported rectangular plates, a suitable

function is the double sine series

$$w = \sum_{m=1}^{\infty}\sum_{n=1}^{\infty} A_{mn} \sin\frac{m\pi x}{a} \sin\frac{n\pi y}{b}. \tag{4.6}$$

The strain energy U of the buckled plate is given by

$$U = \frac{1}{2}\int_0^b\int_0^a D\left\{\left(w_{,xx}+w_{,yy}\right)^2 - 2(1-\nu)\left[w_{,xx}w_{,yy} - w_{,xy}^2\right]\right\}\, dxdy. \tag{4.7}$$

The terms in square brackets cancel, leaving

$$\begin{aligned} U &= \frac{1}{2}\int_0^b\int_0^a D\left(w_{,xx}+w_{,yy}\right)^2\, dxdy \\ &= \frac{Dab\pi^4}{8}\sum_{m=1}^{\infty}\sum_{n=1}^{\infty} A_{mn}^2\left(\frac{m^2}{a^2}+\frac{n^2}{b^2}\right)^2. \end{aligned} \tag{4.8}$$

The work done on the plate is

$$V = \frac{1}{2}\int_0^b\int_0^a \left[\tau t w_{,x}w_{,y} - K_W w^2 - K_P\left(w_{,x}^2 + w_{,y}^2\right)\right]\, dxdy. \tag{4.9}$$

The three terms in the integrand of Equation (4.9) are contributions to work from the applied stress τ and the restoring forces (normal and shear) from the foundation. The work from the foundation is negative because it opposes plate deflection. Evaluation of the integral in Equation (4.9) yields

$$\begin{aligned} V = {} & 4\tau t\sum_{m}^{\infty}\sum_{n}^{\infty}\sum_{p}^{\infty}\sum_{q}^{\infty} A_{mn}A_{pq}\frac{mnpq}{\left(m^2-p^2\right)\left(n^2-q^2\right)} \\ & - K_W\frac{ab}{8}\sum_{m=1}^{\infty}\sum_{n=1}^{\infty} A_{mn}^2 \\ & - K_P\frac{\pi^2 ab}{8}\left(\sum_{m=1}^{\infty}\sum_{n=1}^{\infty}\left(\frac{m}{a}\right)^2 A_{mn}^2 + \sum_{m=1}^{\infty}\sum_{n=1}^{\infty}\left(\frac{n}{b}\right)^2 A_{mn}^2\right). \end{aligned} \tag{4.10}$$

In the first series on the right hand side of Equation (4.10), summation is taken only over those values of the subscripts such that $m \pm p$ and $n \pm q$ are both odd numbers.

The variations δU and δV are found by taking the derivative with respect to each A_{mn} coefficient. Substitution of Equations (4.4), (4.8) and (4.10) into the minimum potential energy expression (4.5) yields a set of equations (one for each A_{mn} coefficient) of the form

$$\left[\left(m^2 + n^2\beta^2\right)^2 + f_W\beta^4 + f_P\beta^2 \left(m^2 + n^2\beta^2\right) \right] A_{mn} + \frac{32\chi\beta^3}{\pi^2} \sum_{p}^{\infty} \sum_{q}^{\infty} A_{mn} A_{pq} \frac{mnpq}{\left(m^2 - p^2\right)\left(n^2 - q^2\right)} = 0, \tag{4.11}$$

where $\beta = a/b$ is the aspect ratio of the plate, and f_W and f_P are non-dimensional foundation parameters given by

$$f_W = \frac{b^4 K_W}{\pi^4 D}, \qquad f_P = \frac{b^2 K_P}{\pi^2 D}. \tag{4.12}$$

These parameters represent the ratio of the foundation stiffness (normal and shear, respectively) to the bending stiffness of the plate. The linear system of equations (4.11) is positive definite in stable equilibrium. The critical buckling load is found by solving for the minimum value of χ to make the system indefinite. The corresponding eigenvector can be substituted into Equation (4.6) to obtain the buckling mode shape.

An approximation to the buckling coefficient is made by solving a subset of the Equations (4.11) as described above. The number of terms required to achieve a given accuracy in the result depends on the values of β, f_W, and f_P. For $\beta \leq 3$ and $f_W = f_P = 0$, χ is determined to within ± 0.01 using only the terms up to $m = n = 5$ [106]; as β, f_W, or f_P increases, however, more terms are required to obtain the same level of accuracy. In the present work, buckling coefficients have been calculated (for f_W and f_P ranging from 0–300) using the terms up to $m = n = 40$.

Upper and lower bounds of the buckling coefficient were obtained by investigating two cases: $\beta = 1$ (square plates), and $\beta \geq 4$. The results have been curve fit to a function of the same form as the solution for plates in uniaxial compression [123]. For square plates ($\beta = 1$), the resulting expression is

$$\chi_1 = 2.028\sqrt{0.618 + f_W + 1.565 f_P} + f_P + 7.673. \tag{4.13}$$

For $\beta \geq 4$, the solution was evaluated over the range $4 \leq \beta \leq 10$. The buckling coefficient for $\beta \geq 4$ converges rapidly; for example, the solution for $\beta = 6$ is indistinguishable from the solution for $\beta = 10$. It can be concluded that the buckling solution for $\beta \geq 4$ is an approximation to that of infinitely long plates. An expression for the buckling coefficient of long plates ($\beta \geq 4$) was therefore developed using $\beta = 6$ and is given by

$$\chi_\infty = 2.006\sqrt{0.690 + f_W + 1.020 f_P} + f_P + 3.749. \tag{4.14}$$

The expressions fit the calculated values of χ to within ± 0.1 throughout the indicated range. Given that χ ranges from 5.48 (long plate with no foundation) to 364 (square plate with $f_W = f_P = 300$), this accuracy is acceptable for most purposes.

Comparison of Equations (4.13) and (4.14) provides insight into the influence of aspect ratio β on shear buckling strength. In relative terms, β has the largest impact on the strength of plates with no foundation, in which case square plates are 70% stronger than long plates. The difference in strength becomes much less significant as the foundation stiffness increases. For example, square plates are only about 3% stronger than long plates with $f_W = f_P = 300$. The influence of aspect ratio is thus small in plates resting on stiff foundations.

A plot of the buckling mode shape is shown in Figure 4.4 for panels with $\beta = 1$ and $\beta = 4$ and four combinations of f_W and f_P ($f_w = 0, 300$; $f_p = 0, 20$)[2]. The foundation parameters are selected to illustrate the relative importance of the normal and shear components of foundation stiffness. For the foundation parameters considered, the buckling coefficient ranges from 5.62 (no foundation, $\beta = 4$) to 64.4 ($f_w = 0, 300$; $f_p = 0, 20$; $\beta = 1$). As foundation stiffness increases, the buckling wavelength decreases because, referring to Equation (4.10), the work required to deform stiff foundations increases as the buckling wavelength a/m decreases. Comparison of the calculated buckling coefficient χ for the cases with $f_P = 0$ and $f_P = 20$ ($f_W = 300$) demonstrates the importance of the shear terms: even for $f_W/f_P = 15$, the shear stiffness of the foundation accounts for approximately 35% of the total buckling strength.

[2]As will be shown in a subsequent section, $f_W = 300$ and $f_P = 20$ are representative of slender webs on a polymer foam foundation.

f_W	f_P	$\beta = 1$		$\beta = 4$	
		χ	Mode	χ	Mode
0	**0**	9.32	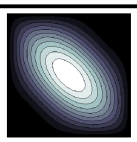	5.62	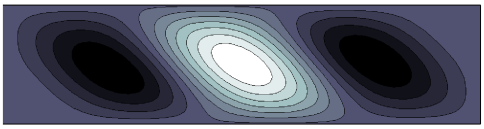
300	**0**	42.3	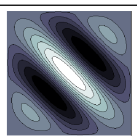	38.6	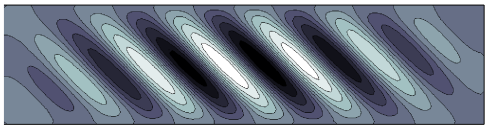
0	**20**	39.2	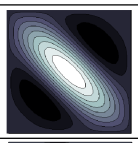	33.2	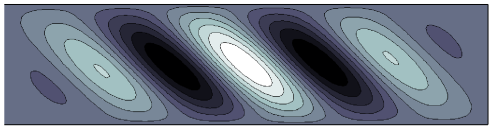
300	**20**	64.4	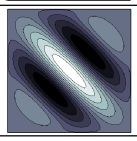	59.9	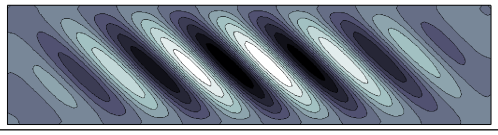

Figure 4.4. Buckling mode shapes with varying elastic foundation stiffness ($\beta = 1$ and $\beta = 4$)

4.3 Evaluation of Foundation Constants K_W and K_P

In order to apply the buckling model presented in the previous section to panel design, the foundation stiffness constants (K_W and K_P) as functions of core material properties must be determined. In this section K_W and K_P are developed for a plate resting on a solid medium following an analogy to a beam buckling model. The model is validated by a finite element study. The impact of the core properties on plate shear buckling is also demonstrated.

4.3.1 Foundation Stiffness Model

Consider a beam resting on a deep solid medium, subjected to a compressive force $\overline{Q}$ with a sinusoidal deformation pattern with amplitude α and half-wavelength L, as illustrated in Figure 4.5. This deformation pattern is transferred to the top surface of the foundation. If the bottom surface of the foundation is fixed at $z = H$, the displacement in the foundation decays with distance from the beam according to a function of the form [114]

$$w = \left[A\cosh\left(\pi z/L\right) + B\sinh\left(\pi z/L\right)\right]W, \tag{4.15}$$

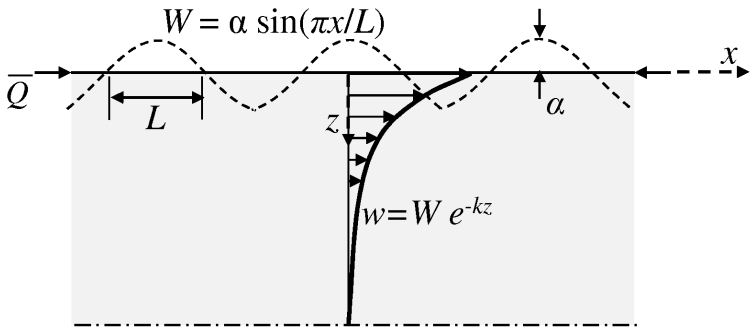

Figure 4.5. Model used for the determination of foundation stiffness constants

where $W = \sin(\pi x/L)$ is the deflection of the beam. The constants A and B are functions of the foundation depth H. If $\pi H/L$ is much less than 5, the decay is essentially linear. If $\pi H/L \geq 5$, the decay is nearly exponential, and the deformation field in the foundation can be modeled as

$$w = \alpha e^{-kz} \sin \frac{\pi x}{L}. \tag{4.16}$$

The model in this work assumes $\pi H/L \geq 5$ (equivalently $Hk \gg 1$, to assure that $w|_{z=H} \approx 0$), with the corresponding deflection field given by Equation (4.16). The range of validity for this assumption is addressed in the next section.

Following the technique of Reference [96], the foundation constants are determined by applying the principle of minimum potential energy. Assume no deformation in the plane of the beam, and consider the displacement in the region beneath a buckled half-wave. Three contributions to strain energy are present: energy U_ϵ due to normal strain in the foundation, energy U_γ due to shear strain, and energy U_f due to deformation of the beam. Assuming the foundation depth H is much greater than the characteristic length $1/k$ as noted above, the calculations are simplified without loss of accuracy by integrating to infinity in the energy expressions that follow. Noting that $\epsilon = w_{,z}$ and $\gamma = w_{,x}$, the three strain energy components are given by

$$U_\epsilon = \frac{E_c}{2} \int_0^L \int_0^\infty w_{,z}^2 \, dz dx = \frac{\alpha^2}{8} k L E_c, \tag{4.17}$$

$$U_\gamma = \frac{G_c}{2} \int_0^L \int_0^\infty w_{,x}^2 \, dz dx = \frac{\alpha^2}{8} \frac{\pi^2}{kL} G_c, \tag{4.18}$$

$$U_f = \frac{E}{2}\frac{t_w^3}{12}\int_0^L w_{,xx}^2\Big|_{z=0}\,dx = \frac{\alpha^2}{8}\frac{\pi^4}{6L^3}Et_w. \tag{4.19}$$

In the preceding equations, E_c and G_c are the elastic and shear moduli of the core material. The work W done by the applied force $\overline{Q}$ is

$$W = \frac{\overline{Q}}{2}\int_0^L w_{,x}^2\Big|_{z=0}\,dx = \frac{\alpha^2}{4}\frac{\pi^2}{L}\overline{Q}. \tag{4.20}$$

Setting $W = U_\epsilon + U_\gamma + U_f$ and solving for $\overline{Q}$ yields

$$\overline{Q} = \frac{\pi^2 E t^3}{12L^2} + E_c\frac{k}{2}\frac{L^2}{\pi^2} + \frac{G_c}{2k}. \tag{4.21}$$

The general buckling solution for a beam on a Pasternak foundation (i.e. restoring force $\hat{q} = K_W w - K_P w_{,xx}$ [122]) can be determined using minimum potential energy, analogous to the approach used in Section 4.2. If the beam buckles with one half-wavelength, the critical load $\overline{Q}$ is

$$\overline{Q} = \frac{\pi^2 E t^3}{12L^2} + K_W\frac{L^2}{\pi^2} + K_P. \tag{4.22}$$

Through comparison of Equations (4.21) and (4.22), the foundation constants are defined as

$$K_W = E_c\frac{k}{2}, \qquad K_P = \frac{G_c}{2k}. \tag{4.23}$$

The value of k is determined from the minimum potential energy solution by solving

$$\overline{Q}_{,k} = 0, \qquad \overline{Q}_{,L} = 0, \tag{4.24}$$

yielding

$$kt = \sqrt[3]{\frac{6G_c^2}{E_c E}}. \tag{4.25}$$

Equation (4.25) implies that, as the shear stiffness of the foundation increases relative to the plate stiffness, the depth affected by buckling decreases. The foundation parameters can be expressed in terms of the web and core material properties and web

slenderness ratio by substituting Equations (4.23) and (4.25) into Equation (4.12):

$$f_W = \frac{12\,(1-\nu^2)\,\sqrt[3]{6}}{2\pi^4}\left(\frac{b}{t}\right)^4 \sqrt[3]{\frac{G_c^2 E_c^2}{E^4}}, \tag{4.26}$$

$$f_P = \frac{12\,(1-\nu^2)}{2\pi^2\,\sqrt[3]{6}}\left(\frac{b}{t}\right)^2 \sqrt[3]{\frac{G_c E_c}{E^2}}. \tag{4.27}$$

These equations show that the foundation parameters increase with core modulus and web slenderness ratio, i.e. with increasing stiffness of the core relative to the plate.

4.3.2 Model Validation

To validate the foundation model described in this section, a finite element study of a plate resting on a solid foundation and loaded in pure shear is presented. The finite element model, illustrated in Figure 4.6, consists of a rectangular plate with aspect ratio β and thickness t, resting on a foundation of solid material with depth H. The plate and foundation displacement are evaluated with a commercial finite element code (ANSYS). The plate is modeled using SHELL281 elements, and the foundation is modeled using SOLID186 elements. Both element types use quadratic shape functions, which achieve better convergence than linear elements for the type of loading considered. The plate is simply supported on all four edges and loaded with a shear stress τ, distributed uniformly along the edges using SURF153 elements. The foundation is fixed at $z = H$ such that $u_x = u_y = u_z = 0$. To prevent ill conditioning of the global stiffness matrix, a very small compressive stress (of magnitude $\tau/10,000$) is applied to the edges at $x = 0$ and $x = a$. The results described in this section were obtained using $\beta = 1.5$; the results are independent of β, however, and can be generalized to other aspect ratios.

A plot of the displacement field in the foundation is shown in Figure 4.7 for two cases: $Hk = 4.5$ and $Hk = 0.85$. The normalized displacement w/W (where $W = \alpha \sin(\pi x/L)$ as shown in Figure 4.5) is plotted as a function of the normalized depth z/H. The displacements predicted by Equation (4.16) are provided for comparison. For the case where $Hk = 4.5$, the displacement matches the prediction very closely. At the fixed surface $z/H = 1.0$, for example, both the model prediction and the finite element results show that w/W decays exponentially to zero. For the case where $Hk = 0.85$, the finite element results show that w/W decays linearly to zero

at $z/H = 1.0$ while the model predict an exponential decay with $w/W = 0.42$ at $z/H = 1.0$. This result is as expected given that the model is formulated under the assumption that $Hk \gg 1$, and it leads to erroneous predictions of buckling strength as described below.

To further demonstrate the limitations of the exponential decay approximation, finite element evaluation of the buckling coefficient χ was obtained for Hk ranging from 0.5 to 8 and compared to the predicted buckling coefficient χ_β (Equations (4.11) and (4.12) for $\beta = 1.5$) using the foundation constants in Equation (4.23). Figure 4.8 shows χ/χ_β as a function of Hk. The results shown in Figure 4.8 are independent of geometry and material properties. For $0 \leq Hk \leq 2$, the exponential decay approximation for core displacement significantly overestimates the displacement in the core. Thus the model under predicts the buckling load ($\chi/\chi_\beta > 1$). For $Hk > 2$, the model slightly over predicts the buckling load ($\chi/\chi_\beta \approx 0.95$): the assumed exponential displacement is comparable to the finite element results. The difference (when $Hk > 2$) can be accommodated by including a safety factor, as is customary in buckling calculations, when evaluating χ_β.

In summary, the present shear buckling model is recommended for use in foundations for which $Hk \geq 2$. It can be noted that $Hk < 2$ corresponds to very shallow foundations for most materials. The efficient use of material in web core panels dictates web spacing much wider than that required to meet the $Hk \geq 2$ requirement, so the present model is suitable for panel design.

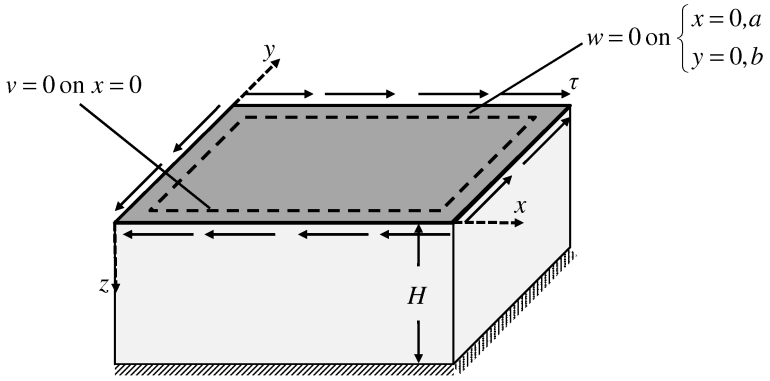

Figure 4.6. Plate model used for FE validation of the expressions for determining foundation constants

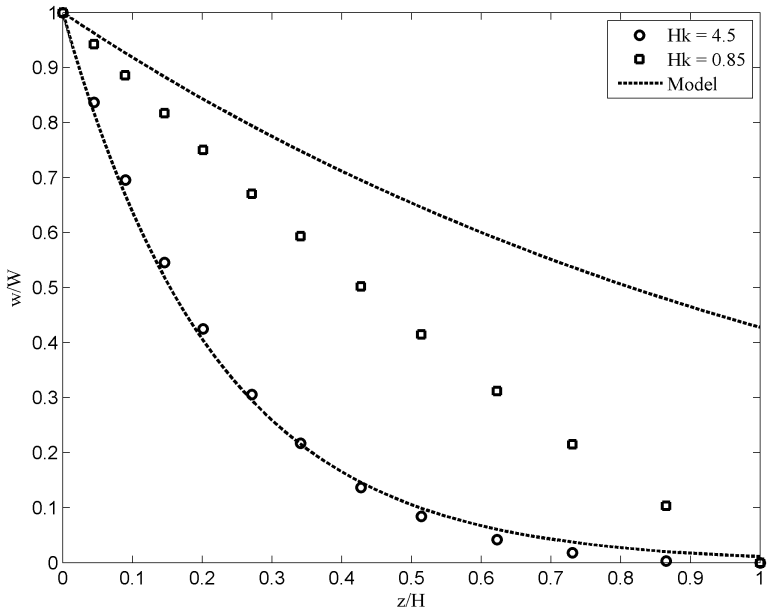

Figure 4.7. Plot of the normalized deflection w/W in the foundation vs. normalized distance z/H from the plate surface; FE results are compared to the present model for $Hk = 0.85$ and 4.5

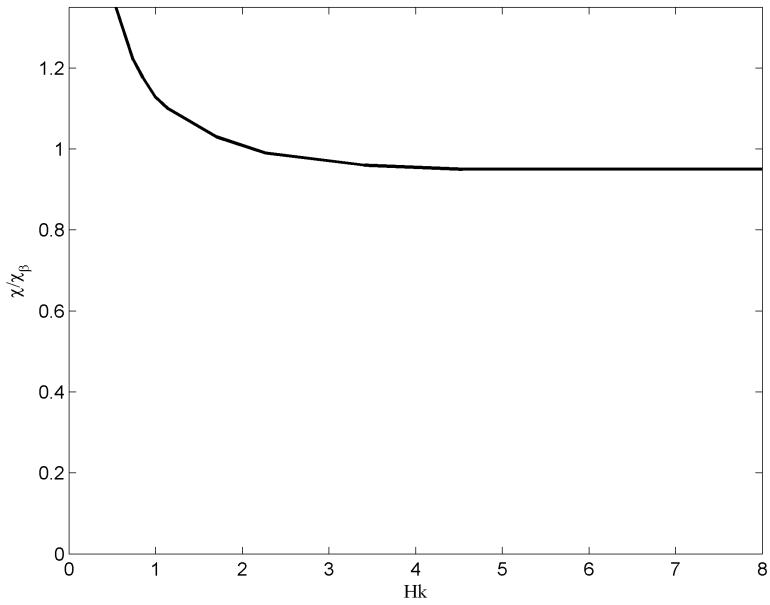

Figure 4.8. Plot of error in the present foundation model vs. the non-dimensional foundation depth Hk based on the foundation constants in Equation (4.23)

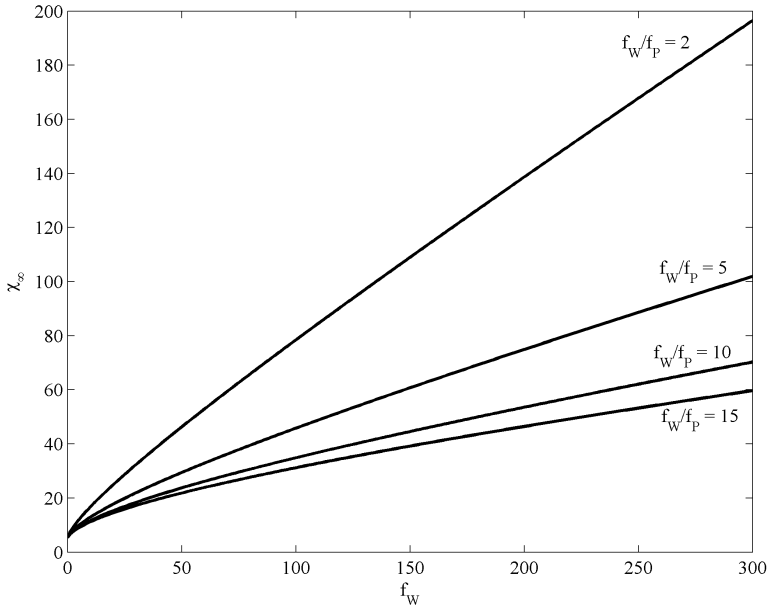

Figure 4.9. Plot of buckling coefficient χ_∞ vs. f_W for $f_W/f_P = 2$, 5, 10, and 15

4.3.3 Impact of Core Properties on Shear Buckling

Equations (4.26) and (4.27) illustrate the effect of core properties on the foundation parameters. As the foundation parameters increase, the shear buckling load increases. In this section, shear buckling load as a function of the foundation parameters for typical materials and web geometries is discussed. The buckling coefficient χ_∞ for long plates is plotted in Figure 4.9 for f_W ranging from 0 to 300, assuming various fixed values of the ratio f_W/f_P. The range of 2–15 for f_W/f_P shown in the figure represents the range likely to be found in practice: for moderately thick plates (e.g. $b/t \approx 200$) on an isotropic foundation $f_W/f_P \approx 2$; for very slender plates (e.g. $b/t \approx 500$) on a foundation with high shear stiffness $f_W/f_P \approx 15$. For a constant f_W/f_P and $f_W > 30$, χ_∞ increases linearly with f_W. Over the range of f_W/f_P considered, the buckling coefficient is inversely proportional to f_W/f_P: at $f_W = 300$, χ_∞ ranges from 196 at $f_W/f_P = 2$ to 59.7 at $f_W/f_P = 15$. This behavior can be attributed to the effect of foundation shear stiffness. Referring to Equations (4.13) and (4.14), it can be seen that the f_P term begins to dominate the expressions for χ as foam shear stiffness increases. As a result, the shear contribution is important, even in moderately stiff foundations.

4.4 Application to Panels

Application of the plate buckling model developed in this work to the analysis of web core sandwich panels is now presented. The panel geometry and coordinate system are illustrated in Figure 4.1. Note that, in this case, the aspect ratio of the web is $\beta = a/h_c$, the slenderness ratio is $b/t = h_c/t$ and the foundation depth is $H = p/2$. The panel is simply supported and subjected to a uniform distributed load q. As noted in the introduction, the buckling problem for panels must consider the non-uniform stress distribution in the webs and the interaction with the face sheets. In particular, the face sheets provide rotational resistance to the webs that depends on material properties, web spacing and geometry, and face sheet thickness [115]. Assuming the face sheet thickness is of the same order as the web thickness, the support condition will be close to simply supported. The latter assumption is reasonable for all-steel panels, and in the present work the face sheets and webs have the same thickness t.

In panels with relatively weak core material ($E_c \ll E$), the bending stresses are borne primarily by the face sheets, and the shear stresses are borne by the webs. As a result, for a panel under distributed load q, the shear stress in the webs is nearly constant through the depth of the panel. The shear stress at the support locations is

$$\tau = \frac{qpa}{2th_c}. \tag{4.28}$$

As a conservative approximation, assume the stress τ in Equation (4.28) acts uniformly over the length of the web. Then the transverse load $\overline{q}$ to cause shear buckling is found from Equations (4.4) and (4.28) to be

$$\overline{q} = \chi_\infty \frac{2\pi^2 D}{pah_c}, \tag{4.29}$$

with χ_∞ determined using Equation (4.14). Because both faces of the webs are bonded to foam, the foundation stiffness is twice as great as in the preceding examples, i.e. K_W and K_P in Equation (4.23) are both multiplied by 2.

The buckling strength predicted by Equation (4.29) is based on the maximum shear stress in the web (i.e. at the supports). The adequacy of this approach can be predicted by analogy to the solution given in Reference [116] for plates under linearly varying compressive loads. In very short panels ($a/h_c < 4$), the approach will

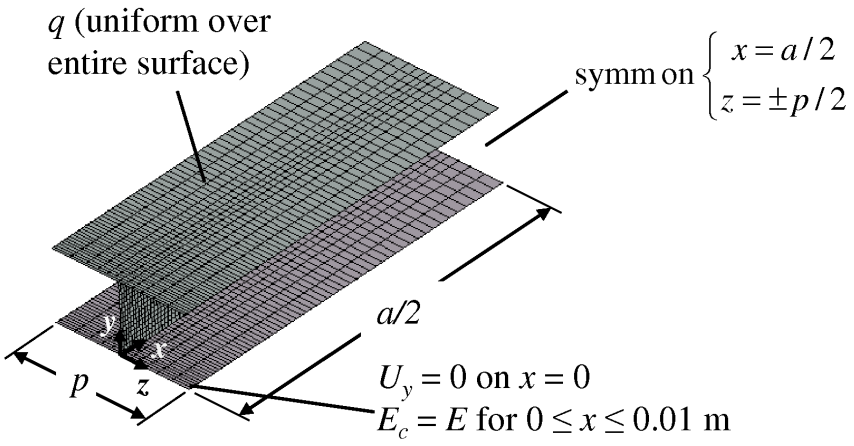

Figure 4.10. Finite element model used for the analysis of panels under distributed load (core elements not displayed for clarity)

slightly underestimate buckling strength. Most structural panels will be relatively long ($a/h_c \geq 4$), in which case the web behaves essentially as an infinitely long plate. Thus, it will be shown that the load distribution has negligible effect on the buckling strength in practice.

To evaluate the adequacy of Equation (4.29) for panel design, a finite element investigation of local web buckling behavior was performed. The face sheets and webs were modeled using SHELL281 elements, and the core material was modeled using SOLID186 elements. Perfect bonding was assumed between the shell elements and the core. The bond between the face sheets and webs was modeled by imposing equal displacements on the face sheet and web at the interface between them. The model is shown in Figure 4.10 (for clarity, only the plate elements are displayed in the figure). It consists of a panel section of width p, centered around a web. Due to symmetry, only half the panel length is modeled; symmetric boundary conditions are applied at the surfaces corresponding to $x = a/2$ and $z = \pm p/2$. The panel is loaded with a uniform pressure q on the top surface.

To prevent spurious crippling modes that arise due to the load concentration at the supports, the panel is supported on a rigid bearing of width 10 mm. The bearing region is kept small to ensure the complete transfer of shear stresses to the rest of the panel, thus minimizing any impact on panel strength. It is not considered part of the panel length. Very stiff ($E_c = E$) core material is used in the bearing region. As a result, the support condition along the short edges of the web ($x = 0$) is much

h_c/t, a/h_c	f_W, f_P	Mode
200, 20	10.7, 4.41	
400, 10	171, 17.7	

Figure 4.11. Buckling mode shape in the webs of a panel under distributed load ($E_c = G_c = 500$ kPa); due to symmetry, only half the panel length is shown

closer to clamped than to simply supported. This condition is not problematic for the present study because, for long panels, the boundary conditions on the short edges do not affect shear buckling strength [108].

The critical buckling load $\overline{q}_{FE}$ and mode shape were determined using an eigenvalue buckling analysis. The buckling mechanism for webs under the action of distributed loads is illustrated for two sample cases in Figure 4.11. The two cases correspond to webs of relatively low and high slenderness ($h_c/t = 200$ and 400, respectively). The buckling wavelengths are similar to those for panels under uniform load, though the amplitudes of the buckles diminish with distance from the support. As a result, the displacement in the core due to buckling is limited to a region of the webs near the panel supports, where the shear stresses are greatest.

To provide a basis of comparison between FE results and the present model, consider an effective buckling coefficient χ_{FE} given by

$$\chi_{FE} = \frac{pah_c}{2\pi^2 D}\overline{q}_{FE}. \tag{4.30}$$

The suitability of Equation (4.29) to model the strength of panels under distributed load is assessed through comparison of χ_∞ and χ_{FE}. In panels with $a/h_c \geq 4$, χ_∞ depends only on material properties and on the web slenderness ratio h_c/t, both of which determine the influence of the core material (see Equation 4.27). However, χ_{FE} also depends on the web spacing ratio p/a.

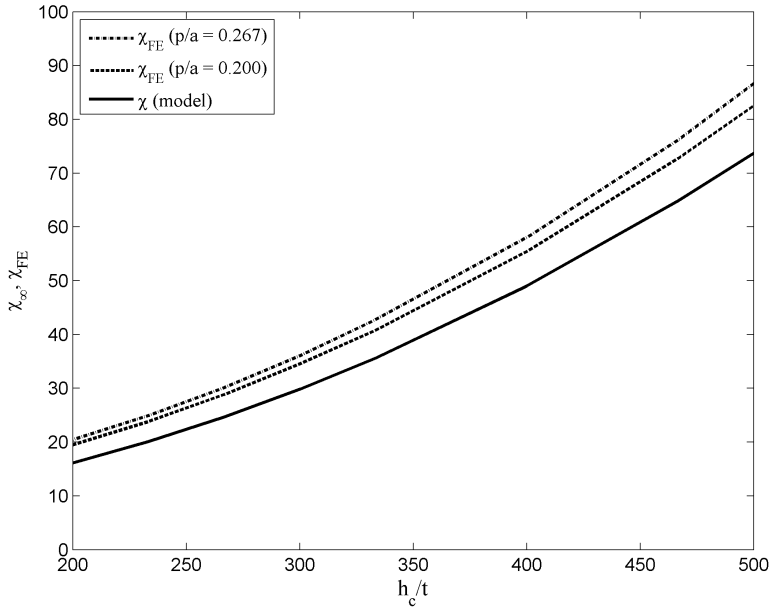

Figure 4.12. Variation in analytical and numerical buckling coefficient vs. web slenderness h_c/t for two different web spacing ratios ($E_c = G_c = 500$ kPa)

The relationship between buckling coefficient and web slenderness h_c/t is plotted in Figure 4.12 for panels with $E_c = G_c = 500$ kPa and two values of p/a (0.267 and 0.200). In all cases the dimensions were chosen so that $a/h_c \geq 8$. The foundation constants f_W and f_P range from 10.7–418 and 4.41–27.6 respectively. Over this range of h_c/t, Equation (4.29) underestimates the buckling coefficient χ_{FE} by 11–21%. The relative error is greater for small h_c/t values by virtue of the smaller value for χ_{FE}. The error increases slightly with an increase in p/a. This behavior can be understood by considering the boundary conditions on the long edges of the web. By analogy to the analysis in Reference [115], the rotational resistance from the face sheets depends on their stiffness relative to that of the webs. In foam-filled panels, the relative stiffness of the face sheets increases with p/a. Although this added resistance is small, it results in webs with slightly higher buckling strength than predicted by Equation (4.29).

Figures 4.13 and 4.14 illustrate the effects of aspect ratio and web spacing on shear buckling strength. Figure 4.13 shows the variation in χ_{FE} with aspect ratio a/h_c of the web. The data correspond to $h_c/t = 400$ and $p/a = 0.200$. The variation in χ_{FE} is about 5% and occurs almost entirely in the range $a/h_c < 7$. This difference is small enough to confirm the validity of the assumption of infinite length for panels

with $a/h_c \geq 4$. Figure 4.14 shows the variation in χ_{FE} with the web spacing ratio p/a ($h_c/t = 400$, $a/h_c = 10$). As noted above, the rotational restraint on the webs increases with p/a, resulting in an increase in χ_{FE}. The variation in χ_{FE} is about 10% and is approximately linear.

The results shown in Figures 4.12–4.14 demonstrate that panel geometry has a slight effect on the boundary conditions of the web. The insensitivity of buckling strength to aspect ratio a/h_c suggests that the load distribution in the web has little impact on buckling behavior in panel designs. The effect of the web spacing ratio p/a is greater, particularly if p/a and h_c/t are both large. Even so, however, Equation (4.29) underpredicts the buckling strength by less than 25%, particularly with slender webs at relatively close spacing. This result suggests that the use of Equation (4.29) is a reasonable and conservative approach to the analysis of shear buckling in web core panels under distributed load.

4.5 Conclusions

Web core panels have potential for use in a variety of applications, including in the building construction industry, where thin webs are necessary for thermal insulating performance [29]. The design of such panels to withstand transverse loads without shear buckling of the webs requires an understanding of the impact of the core material on buckling strength, as well as how to apply that strength in the presence of the non-uniform stresses that result from distributed panel loads.

The present work has examined the shear buckling behavior of web core panels under a distributed load. A new model has been presented for the buckling of plates on a Pasternak foundation under uniform in-plane shear. The buckling coefficients for square and long plates have been calculated and fit to analytical expressions, given by Equations (4.13) and (4.14) respectively. The solutions for square and long plates provide upper and lower bounds to the value of the buckling coefficient. Equation (4.14) is particularly useful for web core designs because the desired span is typically large enough to allow treatment of the web as infinitely long.

A key element of the plate buckling model in this work is the determination of suitable foundation constants. A foundation model was developed using the principle of minimum potential energy, based on the assumption that the displacement in the core

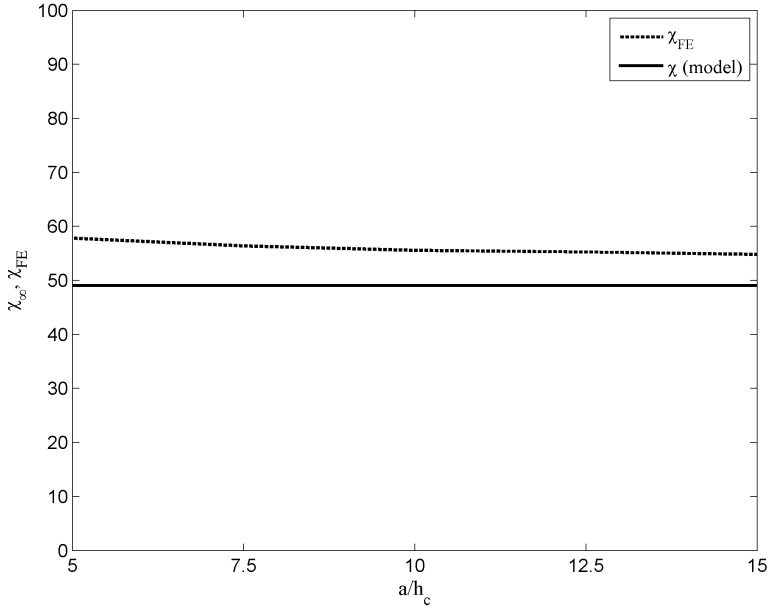

Figure 4.13. Comparison of χ_∞ and χ_{FE} vs. web aspect ratio a/h_c ($h_c/t = 400$, $p/a = 0.200$, $E_c = G_c = 500$ kPa)

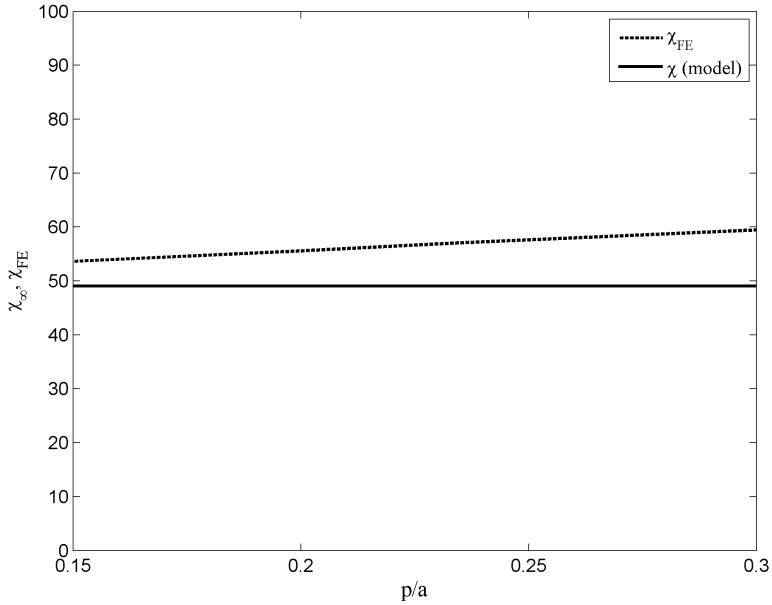

Figure 4.14. Comparison of χ_∞ and χ_{FE} vs. non-dimensional web spacing p/a ($h_c/t = 400$, $a/h_c = 10$, $E_c = G_c = 500$ kPa)

due to buckling decays exponentially with distance from the plate. The foundation constants are expressed by combining Equations (4.23) and (4.25) and are applicable for deep cores or cores with relatively large shear stiffness (i.e. $Hk \geq 2$).

Applicability of the plate buckling model to web core panels under distributed load has been demonstrated. Assuming the panel is long enough to be modeled using the basic assumptions of beam theory ($a/h_c \geq 4$), the buckling strength is determined on the basis of the maximum shearing forces in the panel (i.e. the effect of the load distribution is negligible). The accuracy of the model is affected somewhat by panel geometry. As the web spacing p/a or web slenderness h_c/t is increased, the face sheets provide increased rotational restraint. As a result, the webs are slightly stronger than predicted by the present theory. The difference in strength is small, however, (less than 25%), so for panel design purposes, it is reasonable and conservative to neglect it.

Chapter 5

Bearing Failure of Foam-Filled Web Core Panels

An important limitation to the design of panels with thin webs is the susceptibility to failure at locations of concentrated load. In roof panels, load concentrations occur at the supports. The mechanism of bearing failure in the webs is a localized buckling that develops into a set of yield lines which converge at a plastic hinge in the face sheet. This failure mode is referred to in the literature as web crippling. The associated deformations are large enough to cause crushing of the core material at the load locations. Thus, bearing failure in foam-filled panels is initiated by the combination of web crippling and core crushing.

Two approaches to predicting the bearing strength of foam-filled panels are presented in this chapter. A mechanism solution is developed using an existing plastic hinge model for web crippling [100]. This model accounts for the influence of the core material using energy methods and is applicable to panels supported along the edges by rectangular bearings. Because empirical models are more commonly used for web crippling in practice, a simplified model for the core material is also presented. This model is proposed as a modification to current AISI design codes [102] for thin steel design.

Note that, throughout this work, the term "strength" in connection with bearing failure refers to the ultimate load or resultant force at the bearings to cause failure. This usage is consistent with other work in the literature (e.g. [100, 124])

5.1 Previous Work

The bearing strength $\overline{Q}$ of foam filled panels is expressed as

$$\overline{Q} = \overline{Q}_w + \overline{Q}_{core}, \tag{5.1}$$

where $\overline{Q}_w$ is the web crippling strength and $\overline{Q}_{core}$ is the contribution of the core material. Both contributions can be modeled using energy methods corresponding to the observed failure mechanism. In practice, $\overline{Q}_w$ is generally modeled by an empirical approach as well. Both approaches are described in this work.

A handful of researchers have modeled web crippling in plates or webs with no foam support. The early work focused on the elastic stability of plates under concentrated or patch loads. Timoshenko [93], for example, found the elastic buckling coefficient for simply supported plates under opposing concentrated loads (Figure 5.1a), and Khan and Walker [125] replaced the concentrated loads with patch loads (Figure 5.1b). Rockey and Bagchi [126] used finite element analysis to find the buckling coefficient for plates with a patch load on one edge and patch supports on the opposite edge (Figure 5.1c). All of these models fail to accurately predict web crippling strength (especially with slender webs) because the plates have significant postbuckling capacity.

These models fail to account for possible end effects. The failure mechanism is different for loads applied near the ends (e.g. due to panel supports) compared to loads in the interior. Bearing failure under end loading involves the development of fewer plastic hinges and a smaller region of damage in the web compared to interior loading. A few researchers have modeled crippling behavior by mimicking the (plastic hinge) failure mechanism observed in testing. A review of this work was made by

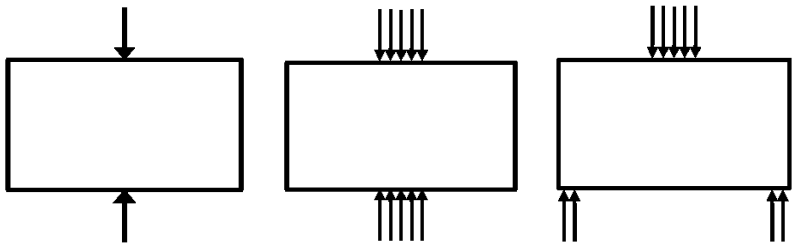

Figure 5.1. Early elastic buckling models for bearing failure: (a) opposing concentrated loads [93], (b) opposing patch loads [125], and (c) patch load and supports [126]

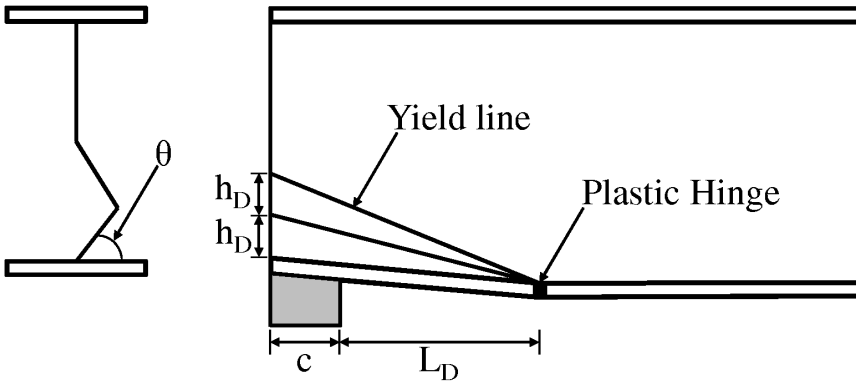

Figure 5.2. End bearing failure mechanism in the webs (adapted from Reference [100])

Elgaaly [127]. The mechanism model for which web crippling strength has been most successfully predicted is by Roberts and coworkers. The most recent version of that model, by Roberts and Newark [100], is described here.

The model by Roberts and Newark [100] is based on the assumed failure mechanism illustrated in Figure 5.2, as reported in the literature for numerous tests on slender plate girders. The web folds along yield lines that meet at a plastic hinge at the face sheet interface. The plastic hinge is located at a distance L_D from the support. The damaged region has a depth $2h_D$ at the edge of the panel. The width of the support is c. Roberts and Newark assume the load spreads through the face sheet at a 45° angle, so the support width is effectively $c + t_f$, and the total length of the damaged region is $L_D + c + t_f$. The web crippling strength with no foam support is predicted by equating the work done by the applied load to the energy dissipated in the formation of plastic hinges.

For loads applied near the panel ends, the web crippling strength $\overline{Q}_w$ predicted by the model in Reference [100] is

$$\overline{Q}_w = F_R \left[\frac{3.3}{8} t_w^2 \sqrt{E_w \sigma_{yw}} \left(\frac{t_f}{t_w} \right)^{1/4} \left(1 + \frac{8(c + t_f) t_w}{3 h_c t_f} \right) \right]. \tag{5.2}$$

The constant F_R is a calibrating coefficient used to account for the observed variability in test data. The variability is due to factors such as load and geometric imperfections, material variations, and residual stresses [99]. Based on the results of 237 web crippling tests, Equation (5.2) overestimates web strength by about 25% on average. The data had a spread of about ±45%. From these two observations, Roberts and

Newark recommended the use of $F_R = (1.25 \cdot 1.45)^{-1} = 0.55$ for predicting end failure. They do not provide limits of applicability for Equation (5.2); however, based on the test data on which their value for F_R is based, the following limits can be suggested:

$$100 \leq h_c/t_w \leq 500, \qquad c/t_w \leq 100, \qquad p/t_f \leq 50, \qquad 1 \leq t_f/t_w \leq 12. \tag{5.3}$$

Based on the same test data, the accuracy of Equation (5.2) does not appear to be systematically related to any geometric parameter. The model is applicable to relatively slender ($h_c/t_w \geq 100$) webs in which failure initiates as an elastic buckling mode. The strength of stocky webs is overestimated because failure initiates by yielding of the web in compression.

An important drawback to physical bearing strength models is the lack of acceptance in practice. Prescriptive design codes tend to rely exclusively on nonphysical empirical models for web crippling strength. The empirical models are based on a variety of tests reported in the literature and implicitly account for various effects that are neglected in the mechanism models. These include material and geometric imperfections, residual stresses, and manufacturing parameters (e.g. bending radii of cold-formed sections). The empirical models are calibrated to fit for a range of web geometry, including stocky webs (e.g. $h_c/t_w \leq 100$), for which the failure mechanism is yielding.

Prescriptive design codes (e.g. [102]) provide a unified model for web crippling strength,

$$\overline{Q}_{Aw} = C t_w^2 \sigma_{yw} \left(1 - C_R \sqrt{\frac{R}{t_w}}\right) \left(1 + C_c \sqrt{\frac{c}{t_w}}\right) \left(1 - C_h \sqrt{\frac{h_c}{t_w}}\right), \tag{5.4}$$

with C coefficients that depend on web geometry, loading, and support conditions. For example, web core roof panels will likely use C-channel webs to provide a surface for welding to the face sheets. The parameter R is the bending radius between the web and flanges of the section. Under the load conditions expected for roofs (end one-flange loading with stiffened flanges), the coefficients are [102]

$$C = 4, \qquad C_R = 0.14, \qquad C_c = 0.35, \qquad C_h = 0.02. \tag{5.5}$$

Equation (5.4) is specified subject to several geometric limits:

$$R/t_w \leq 5, \qquad h_c/t_w \leq 200, \qquad c/t_w \leq 210, \qquad c/h_c \leq 2.0. \tag{5.6}$$

These limits are based on the geometry of the beams used to obtain the test data on which the equation is based [128]. As with the data referenced by Roberts and Newark [100], no systematic trends in the accuracy of the equation due to geometry have been reported.

Due to the unique loading in web core roof panels (i.e. foam-filled panels with thin webs under transverse loading), the contribution $\overline{Q}_{core}$ of the core material to bearing strength has been investigated only once in the prior literature. Starting with the model by Roberts and Newark, Romanoff [101,124] developed a model for the bearing strength of foam-filled web core panels loaded far from the panel edges by a circular indenter. He assumed the failure mechanism and strength of the webs were identical to those in Reference [100], i.e. the damage parameters h_D and L_D are unaffected by the core material. Romanoff provides limited prototype test results suggesting his model overpredicts interior bearing strength by about 10%. This accuracy is comparable to that of the model in Reference [100] for webs with no foam.

Two important modifications to Romanoff's model are required for web core roof panels. First, as the existing model applies only to interior bearing failure, it must be redeveloped to account for the strength under end loading. The strength and failure mechanisms under end loading differ from those under interior loading because loads applied at the ends of the panel produce fewer plastic hinges and a smaller damage area. As a result, the strength is lower under end loads. The second modification to Romanoff's model is due to the geometry of the support conditions: roof panels are supported by rectangular bearings that span the full panel width.

5.2 Hinge Model

Romanoff [101] found that the core has two effects on panel strength: it acts indirectly as an elastic foundation to resist the crippling failure of the webs, and it directly increases the panel strength via its crushing capacity. The two contributions act

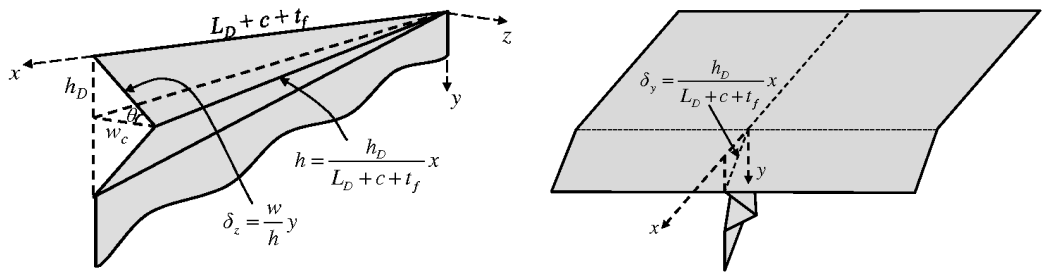

(a) (b)

Figure 5.3. Damage zone assumption for the determination of bearing strength: (a) in the webs, and (b) in the face sheet

independently, so Equation (5.1) is expressed by

$$\overline{Q} = \overline{Q}_w + \overline{Q}_f + \overline{Q}_c, \tag{5.7}$$

where $\overline{Q}_f$ is the effect of the foam as an elastic foundation, and $\overline{Q}_c$ is the contribution of core crushing strength. Both contributions are modeled in this section using energy methods.

The geometry of the bearing failure damage in the web is illustrated in Figure 5.3(a). The volume enclosed by the deformed shape and the initial shape represents core material displaced by the cripple. At any position x, the vertical (y-direction) displacement δ_y of the middle yield line is given by

$$\delta_y = \frac{h_D}{L_D + c + t_f} x. \tag{5.8}$$

Because the damage is symmetric about $y = h$, only the upper part of the crippled web (i.e. $0 \leq y \leq h$) is analyzed. The displacement δ_z of the web in the z-direction is

$$\delta_z = \frac{w}{h} y = \frac{y}{\tan\theta}, \tag{5.9}$$

Treating the foam as an elastic foundation with modulus K_{wc}, the displacement causes a restoring pressure of $K_{wc}\delta_z$. The resultant force acts in the z-direction and is equal to the applied force $\overline{Q}_z$ required to achieve the displacement. That force is given by

$$\overline{Q}_z = K_{wc} \iint \delta_z(x, y)\, dA. \tag{5.10}$$

The elastic foundation contribution $\overline{Q}_f$ acts in the y-direction and is resolved as $\overline{Q}_f = \overline{Q}_z \tan\theta$. Combining Equations (5.9) and (5.10) with this substitution and multiplying by 2 to account for the symmetry condition yield the result

$$\overline{Q}_f = 2K_{wc} \int_0^{L_D+c+t_f} \int_0^{\frac{h_D}{L_D+c+t_f}x} y \, dy \, dx = \frac{K_{wc} h_D^2}{3} \left(L_D + c + t_f\right). \tag{5.11}$$

Romanoff [101] used finite element analysis to estimate the foundation modulus K_{wc},

$$K_{wc} = \max \left\{ 0.28 E_c \sqrt[3]{\frac{12 E_c (1-\nu_w^2)}{E_w t_w^3}}, \frac{E_c}{p} \right\}. \tag{5.12}$$

The contribution $\overline{Q}_c$ of foam crushing is determined from the face sheet deformation illustrated in Figure 5.3(b). Assuming the underlying foam is crushed, the energy U required to cause the end displacement δ_y is

$$\begin{aligned} U &= \iint \sigma_{uc} \delta_y \, dA = \sigma_{uc} \int_0^{L_D+c+t_f} \int_{-p/2}^{p/2} \frac{h_D}{L_D+c+t_f} x \, dy \, dx \\ &= \sigma_{uc} \frac{h_D p}{2} \left(L_D + c + t_f\right). \end{aligned} \tag{5.13}$$

The work W done by the applied force $\overline{Q}_c$ is

$$W = \overline{Q}_c h_D. \tag{5.14}$$

Setting $U = W$ gives the result

$$\overline{Q}_c = \sigma_{uc} \frac{p}{2} \left(c + t_f + L_D\right). \tag{5.15}$$

The panel bearing strength is found by substituting Equations (5.2), (5.11), and (5.15) into Equation (5.7). The result is

$$\begin{aligned} \overline{Q} \;\; = \;\; & F_R \left[\frac{3.3}{8} t_w^2 \sqrt{E_w \sigma_{yw}} \left(\frac{t_f}{t_w}\right)^{1/4} \left(1 + \frac{8(c+t_f)t_w}{3 h_c t_f}\right) \right] \\ & + \frac{h_D^2 K_{wc}}{3} \left(c + t_f + L_D\right) + \sigma_{uc} \frac{p}{2} \left(c + t_f + L_D\right). \end{aligned} \tag{5.16}$$

The parameters L_D and h_D that define damage geometry were determined in Reference [100]. Based on empirical observations, the depth h_D is

$$h_D = \min\left\{20t_w, \frac{h_c}{2}\right\}. \tag{5.17}$$

Minimizing the crippling load $\overline{Q}_w$ with respect to L_D yields the result [100]

$$L_D = \sqrt{\frac{\sigma_{yf}^3 p^2 t_f^3 h_D}{2E_w \sigma_{yw}^2 t_w^4}}. \tag{5.18}$$

As a practical note, the relative contributions of the three terms in Equation (5.7) to total bearing strength are demonstrated in Section 5.4. It will be shown that the core crushing contribution $\overline{Q}_c$ accounts for more than 80% of the total strength in panels with thin webs. The elastic foundation contribution $\overline{Q}_f$ is negligible in practice. These results form the basis of the modfied AISI model developed in the next section, which assumes the core contribution results only from the crushing strength.

5.3 Modified AISI Model

The proposed modification to the AISI design equation is developed by assuming the core material contributes only via its crushing strength. The bearing strength $\overline{Q}_A$ predicted by the modified AISI method is thus

$$\overline{Q}_A = \overline{Q}_{Aw} + \overline{Q}_{Ac}, \tag{5.19}$$

with web crippling strength $\overline{Q}_{Aw}$ determined by Equation (5.4), and core crushing strength $\overline{Q}_{Ac}$ determined by by a simplified analytical model.

The empirical web crippling strength $\overline{Q}_{Aw}$ is used for design without *a priori* knowledge of the failure mechanism. General mechanism-based expressions for $\overline{Q}_{Ac}$ thus cannot be developed, and the modified AISI model is derived independent of the webs. The approach in this work is developed based on the core crushing strength in panels with no webs. Davies [42] lists several models for the crushing strength of foam core panels under bearing load. The differences among the models reflect differences in the assumptions about how stresses transfer from the bearing surface into the foam. The models provide similar strength predictions. A reasonable approach is to assume

Table 5.1. Steel and core material properties

E_w	205 GPa
σ_{yw}	225 MPa
σ_{yf}	225 MPa
E_c	2985 kPa
σ_{uc}	138 kPa

the bearing stress distributes evenly throughout the bearing region, i.e.

$$\overline{Q}_{Ac} = cp\sigma_{uc}. \tag{5.20}$$

This term will be equal to the core crushing contribution predicted by Equation (5.15) if $L_D \approx c$. In practice, L_D is on the same order of magnitude as c (predicted by Equation (5.18) as well as by the models in Reference [42]), so the difference between the two approximations is small.

5.4 Model Comparison

In this section, comparison of the two bearing failure models is presented based on the use of steel webs and a 36 kg/m^3 PUR core. The relevant material properties (all obtained through testing described in Chapter 7) are listed in Table 5.1. To simplify the comparison, note that Equations (5.16) and (5.19) can be non-dimensionalized into equations of the form

$$\frac{\overline{Q}}{\sigma_{yw}t_w^2} = f_1\left(\frac{h_c}{t_w}, \frac{c}{t_w}, \frac{p}{t_w}, \frac{\sigma_{uc}}{\sigma_{yw}}, \frac{\sigma_{yf}}{\sigma_{yw}}, \frac{E_w}{\sigma_{yw}}, \frac{E_c}{\sigma_{yw}}, \frac{t_f}{t_w}\right), \tag{5.21}$$

$$\frac{\overline{Q}_A}{\sigma_{yw}t_w^2} = f_2\left(\frac{h_c}{t_w}, \frac{c}{t_w}, \frac{p}{t_w}, \frac{\sigma_{uc}}{\sigma_{yw}}, \frac{R}{t_w}\right). \tag{5.22}$$

The two models have identical similarity variables with respect to the web and bearing geometry. The hinge model includes additional variables that account for the influence of the face sheets, and the modified AISI equation accounts for the bending radius of the web. To preserve similarity, the results in this section are given in terms of $\overline{Q}/\overline{Q}_A$.

Direct comparison of the models is possible by assuming the face sheet is the same material as the web (i.e. $t_f/t_w = 1$, $\sigma_{yf}/\sigma_{yw} = 1$) and by setting $R/t_w = 0$. Based on

typical web core designs (Chapter 6), a web spacing ratio of $p/t_w = 1200$ is used. The bearing strength predictions for the hinge and modified AISI models are compared in Figure 5.4 for web slenderness h_c/t_w ranging from 150–500. The ratio $\overline{Q}/\overline{Q}_A$ is plotted for c/t_w ranging from 100–200. The hinge model predicts bearing strength within about 15% of the modified AISI model. The main source of this difference is the core crushing contribution predicted by each model. The calculated damage length L_D varies from the bearing length c by about ±30% over the range of c/t_w considered. Thus, while the hinge model predicts a larger web crippling contribution (by about 5–20%) than the modified AISI model, it may predict a smaller total strength with wide bearings.

The importance of the core crushing contribution to the overall bearing strength is illustrated in Figure 5.5. Using the same materials and geometry from the previous figure, with $c/t_w = 150$, the core crushing contribution $\overline{Q}_c/\overline{Q}$ (and $\overline{Q}_{Ac}/\overline{Q}_A$) is plotted as a function of web slenderness. According to the hinge model, the core crushing term $\overline{Q}_c$ contributes 78–86% of the bearing strength. In contrast, the elastic foundation effect $\overline{Q}_f$ (not shown) supplies only about 5% of the total strength. The ratio $\overline{Q}_c/\overline{Q}$ increases with h_c/t_w because slender webs have low crippling strength. Similarly, according to the modified AISI equation, $\overline{Q}_{Ac}$ contributes 88–90% of the bearing strength in panels with slender webs. For both models, the results plotted in Figure 5.5 are insensitive to c/t_w.

The large contribution of the core material relative to the webs has implications for roof panel design. For example, the variability in bearing strength is significantly less for foam-filled versus empty panels. Neglecting the variability in foam crushing strength, a variation of ±50% in $\overline{Q}_w$ affects $\overline{Q}$ by less than ± 10%. In other words, the uncertainty in bearing strength is shifted from the webs to the core material. The core crushing strength is not affected by factors such as initial imperfections and bending radii, so the variability in the strength of foam-filled panels is lower than that of the webs alone.

The large contribution of core crushing to the bearing strength of foam-filled panels suggests a reasonable prediction of bearing strength is made by neglecting the web contribution altogether, i.e.

$$\overline{Q} \approx cp\sigma_{uc}. \tag{5.23}$$

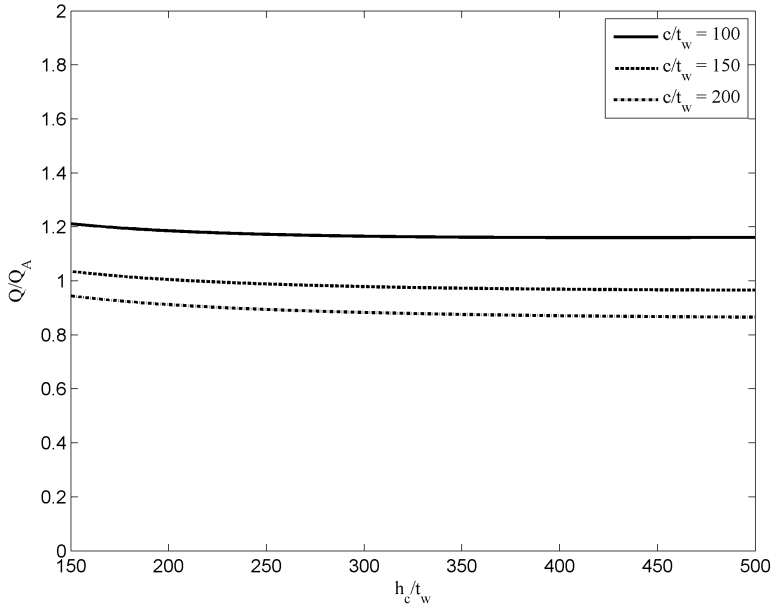

Figure 5.4. Comparison of hinge and modified AISI bearing failure models: plot of $\overline{Q}/\overline{Q}_A$ vs. web slenderness h_c/t_w assuming carbon steel webs and 36 kg/m^3 PUR core with $t_f/t_w = \sigma_{yf}/\sigma_{yw} = 1$, $p/t_w = 1200$, and $R/t_w = 0$

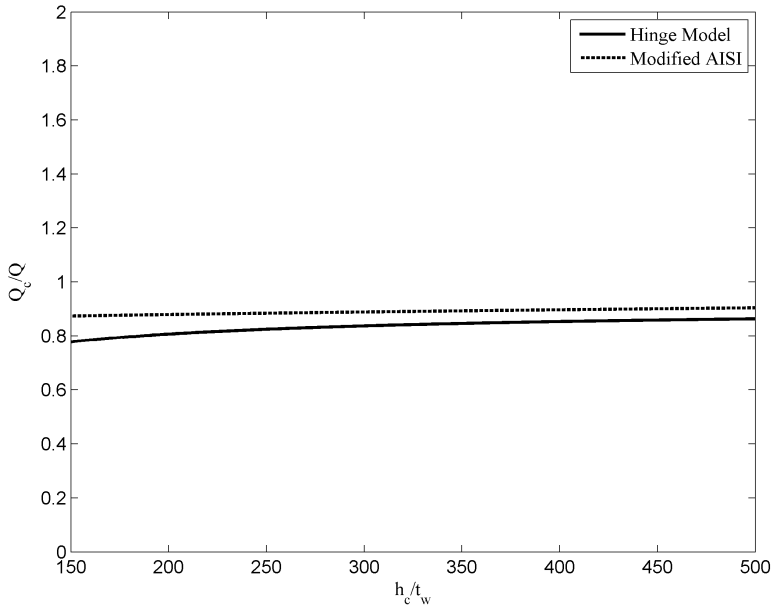

Figure 5.5. Contribution of core crushing to total bearing strength: plot of $\overline{Q}_c/\overline{Q}$ vs. h_c/t_w assuming carbon steel webs and 36 kg/m^3 PUR core with $t_f/t_w = \sigma_{yf}/\sigma_{yw} = 1$, $c/t_w = 150$, $p/t_w = 1200$, and $R/t_w = 0$

In the present example, the error from using Equation (5.23) is around 20%. This difference is reasonable for most designs. In panels with slender webs ($h_c/t_w \geq 200$), the results in Figure 5.5 suggest bearing strength is fairly insensitive to web slenderness. The important geometric parameter for bearing strength is thus the support width c. Consideration of the web crippling contribution becomes important when the strength predicted by Equation (5.23) is slightly less than needed (e.g. when relatively weak core material is used).

Bearing failure is not a concern for typical roof panel designs. For example, consider the design of a roof panel using the foam properties in Table 5.1. Based on Equation (5.23), the maximum distributed load $\overline{q}$ the panel can support without bearing failure is approximately

$$\overline{q} \approx \frac{2c\sigma_{uc}}{a}. \tag{5.24}$$

Typical residential wall panels have a depth of 165 mm (6.5 in.)[1]. The bearing width with a 6:12 roof pitch is thus 184 mm (7.25 in.). Assuming a fatigue reduction factor $\zeta_n = 0.6$ (Chapter 2), and a panel length of 6.8 m, $\overline{q}$ is 4481 N/m^2. Applying a safety factor of 2 (see Chapter 6), this strength is sufficient for roofs in most of the US (specifically, Climates I and II, see Table A.1). Other provisions must be made in northern climates (i.e. Climate III). For example, the wall panel depth can be increased to about 200 mm. The increase in wall thickness has the added benefit of increased R-value, which is typically recommended for colder climates [71].

5.5 Summary

A hinge model for the bearing strength of foam-filled web core panels was presented. The model is based on a mechanism solution that was developed and validated in the literature for web crippling strength in cold-formed steel beams. It accounts for the interactions between the face sheets, webs, and core material and can be used to gain insight into the role of each material in the prevention of bearing failure. Of particular importance is the determination that the core crushing strength contributes approximately 80–90% of the total bearing capacity in typical roof panels. The elastic foundation effect of the core is effectively negligible because the core material does not prevent plastic hinge formation. The hinge model was compared to a proposed

[1]Based on standard SIP wall panel designs obtained from the Structural Insulated Panel Association website (http://www.sips.org)

modification to the current AISI prescriptive design code for thin steel beams. Bearing strength predictions by the two approaches agree to within about 35% for typical roof panels with slender, widely-spaced webs.

The dominance of the foam crushing contribution to bearing strength suggests a reasonable first approximation can be made by neglecting the webs altogether. The resulting design equation (5.23) makes it possible to prevent bearing failure *a priori* by specifying the bearing width c. For roof panels with 36 kg/m^3 PUR core material, typical wall assemblies provide enough support width to prevent failure in US Climate zones I and II. Slightly wider bearings ($\approx$200 mm) are required for Climate III.

Chapter 6

Design of Web Core Roof Panels

Panelized construction of residential buildings is gaining popularity due to the architectural and energy efficiency benefits that can be achieved[1]. An important challenge to the design of panel structures for buildings is the balance between long-term structural performance and the thermal insulating requirement. This chapter focuses on the design considerations for web core panels for residential roofs. A design procedure is developed that considers R-value, panel deflection, core shear failure, and buckling of the face sheets and webs. The buckling models include the effect of the core material as discussed in Chapter 4. Panel designs are presented that provide an R-value of 5.3 m^2-K/W for roof loads of 1500, 2000 and 3000 N/m^2. It is demonstrated that the web core panel can be designed for these structural and thermal requirements with unsupported span lengths as long as 7 m, while span lengths for foam core panels are limited to 4 m. Web shear buckling and R-value are the two performance criteria that limit panel span length and depth.

6.1 Introduction

Panelized construction has found use in a variety of structural applications where weight and constructibility are constraints. In the building construction industry, wall and roof panels have the additional benefit of energy savings through improved thermal insulation and reduced air infiltration, particularly when polymer foam cores are used. Roof panels have the potential for even greater benefit but pose unique

[1]Portions of this chapter are reprinted from Reference [29], with permission from the publisher.

Table 6.1. Properties of steels used in the analysis

Property	**Carbon Steel [129]**	**Stainless Steel [130]**
Density (kg/m^3)	7870	7870
Elastic modulus (GPa)	205	195
Poisson's ratio	0.3	0.3
Thermal Conductivity (W/m-K)	51.9	16.1

technical challenges due to the need to provide thermal insulating performance while spanning long lengths from soffit to ridge without the use of an underlying support structure. Web core panels constructed from light gauge sheet metal have the potential to meet the requirements of roof panels. The metal webs provide substantial stiffness to meet the structural requirements, though the panel must be designed to overcome the effect of the webs on insulating performance.

In this chapter, a design methodology for web core panels with metal face sheets and thin metal webs is developed for roof applications. Light gage sheet metals, such as carbon or stainless steel, are ideal face sheet and web materials. In addition to excellent structural properties (Table 6.1), these materials can be rolled into a variety of structural shapes and can be assembled efficiently through laser welding. Metal face sheets offer strength and stiffness without absorbing moisture. The webs provide shear stiffness and are critical to increasing the unsupported span length. Because the structural foam provides an elastic support for the webs, thin webs can be utilized to minimize the conductive path (between the face sheets) introduced by the web. The thermal performance is improved even further by selecting web materials such as stainless steel, for which the thermal conductivity is 30% of carbon steel (see Table 6.1). As a consequence, for R-values typically required in homes, panels with stainless steel webs can be designed to span longer lengths than panels with carbon steel webs.

The geometry of the web core panel is illustrated in Figure 4.1. The face sheet and web thicknesses are assumed different in this chapter and are denoted t_f and t_w. The roof application is shown in Figure 6.1. The roof is constructed of multiple panels that span from ridge to soffit. The length and width of each panel are a and b respectively. Each panel is supported at the soffit by the underlying walls and at the ridge by a ridge beam; the supports have bearing width c. A ridge beam or other equivalent support is suggested to avoid overly complex connections at the soffit. Relatively little rotational restraint is expected from the ridge and soffit supports; therefore, the

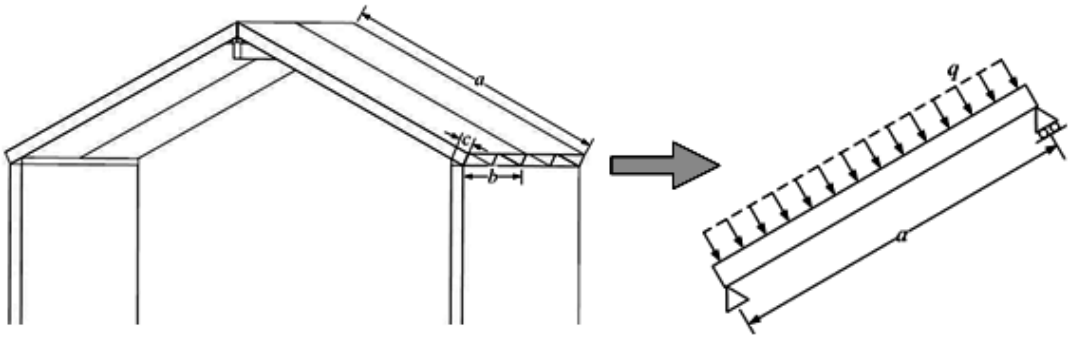

Figure 6.1. Roof panel application and loading

end conditions at the soffit and ridge are treated as simple supports. No underlying support is assumed along the longitudinal edges of the panels.

In the sections that follow, relevant panel performance measures are developed, specifically for panel deflection, core shear failure, bearing failure, buckling of the face sheets and webs, and R-value. The structural implications of using thin webs are developed and presented—particularly the influence of the foam on web buckling strength and bearing failure at the panel end supports. The chapter concludes with a case study, in which designs for foam core and web core panels are presented based on typical roof loads of 1500, 2000 and 3000 N/m^2 and an R-value of 5.3 m^2-K/W.

6.2 Foam Selection

The structural insulating core material choice is an important consideration for the design of roof panels. Polymer foams are well suited to the application because of their high stiffness-to-weight ratio and low thermal conductivity. Based on the considerations in Chapter 2, a commercially available low-density PUR that can be foamed *in-situ* [66] is selected for the present study. The properties are reduced as described in Chapter 2 to account for creep and fatigue. The thermal and mechanical properties of this foam (both nominal and reduced values) are listed in Table 6.2.

Figure 6.2 illustrates the effect of foam structural properties on foam core panel design. Panel depth as a function of span length is shown for representative residential roof loads of 1500, 2000 and 3000 N/m^2 and a temperature gradient of 55°C. All panels provide an insulation level greater than R-5.3 m^2-K/W. The panel face sheets are 2 mm thick carbon steel and the core is PUR. The dashed lines correspond to

Table 6.2. Properties of rigid polyurethane (PUR) foam used in the analysis [66]

Property	**Nominal Value**	**Live Load**	**Dead Load**
Density (kg/m^3)	36	36	36
Compressive modulus (MPa)	2.99	1.50	1.00
Shear modulus (MPa)	1.29	0.65	0.43
Compressive strength (kPa)	138	83	83
Shear strength (kPa)	173	104	104
Thermal conductivity (W/m-K)	0.023	0.023	0.023
Max service temp (°C) [50]	90–120	90–120	90–120

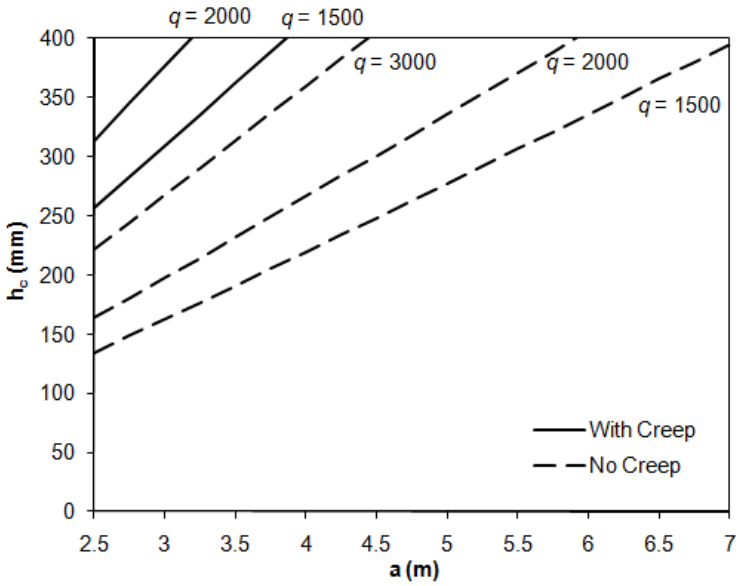

Figure 6.2. Plot of minimum panel depth vs. length for foam core panels with 2.0 mm steel face sheets and PUR core. Designs that neglect the influence of core creep are shown with dashed lines, and designs that include the effect of creep are shown with solid lines.

designs based on the nominal foam properties and the solid lines correspond to designs based on the properties adjusted for dead loads. The maximum span lengths without considering creep are 7, 5.9 and 4.4 m corresponding to increasing loads of 1500, 2000 and 3000 N/m^2. When creep of the foam is considered, the maximum span lengths are 3.8 and 3.2 m corresponding to loads of 1500 and 2000 N/m^2. The length is less than 2.5 m for a 3000 N/m^2 load. Because of the dependence on the foam for shear stiffness, foam core panel lengths are reduced significantly when creep effects are included. This example illustrates the potential impact of increasing the shear stiffness of the panel by adding webs.

6.3 Design Approach

The analysis and design of a web core roof panel requires the simultaneous consideration of thermal and structural performance. In this section, expressions describing the performance as a function of the panel geometry and loads are developed and discussed. Several limit states must be considered for the web core panel. These include the overall measures of panel performance—thermal performance and deflection—as well as local buckling and stress failure modes. Local buckling is possible for both the face sheet and the webs. The core can fail due to shear stress failure or due to crushing at the panel supports.

Models for the limit states follow. Each of the models is based on the use of thin face sheets and webs (i.e. $h_c/t_f \geq 50$ and $p/t_w \geq 50$) and a relatively flexible core ($E_c \ll E_f$). Full adhesion of the foam and the structural materials is assumed. Resulting from the use of thin webs, the strength of the core is high relative to the buckling strength of the unsupported webs.

The foam is treated as isotropic, using the compressive or shear properties measured perpendicular to the rise direction. This simplification is representative of the load conditions on the foam in the models described below. Because foams tend to be stronger in tension (and in the direction of rise), the approach is also slightly conservative.

6.3.1 Thermal Performance

The thermal performance of the web core panel is determined using the isothermal planes method [30] for one-dimensional heat conduction. Lateral heat flow between the webs and the insulation is negligible, so the panel is modeled as a network of thermal path resistances in series and parallel. The R-value of the overall assembly is found from the equivalent resistance of the network. The contribution of the thin metal face sheets to the R-value of the panel assembly is negligible. The R-value is thus given by

$$R = \frac{h_c}{k_w \frac{t_w}{p} + k_c \left(1 - \frac{t_w}{p}\right)}, \tag{6.1}$$

where k_w and k_c are the thermal conductivity of the web and insulating materials, respectively. Equation (6.1) can be rearranged to find the core depth required for a

desired R-value, i.e.

$$h_c = R\left[k_c + (k_w - k_c)\,\frac{t_w}{p}\right], \tag{6.2}$$

from which it can be seen that the depth to achieve the target R-value without webs is Rk_c. The second term on the right hand side of Equation (6.2) is the penalty, in terms of increased core depth, that results from the use of stiffening webs. For metal webs, $k_w \gg k_c$ (see Tables 6.1 and 6.2), so the webs have a strong impact on the thermal performance of the panel. To minimize the detrimental effects of conducting materials like steel, it is necessary to use thin, widely-spaced webs.

United States building codes [71] prescribe an R-value requirement for roofs that is heavily dependent on the number of heating degree days (HDD) at the building location. The heating degree days vary substantially throughout the country (from near zero to ≈10,500), so it is convenient for the present discussion to define thermal climate zones. Locations within the southern half of the continental US (excluding the Rocky Mountain range) have less than 4500 HDD. The R-value requirement for 4500 HDD is 5.3 m^2-K/W [71]. In the mountains and in the northern half of the US, the R-value requirement ranges up to a maximum of 6.8 m^2-K/W [71].

6.3.2 Panel Deflection

The temperature gradient and the roof loading cause the panel to deflect. The temperature gradient across the panel thickness causes differential thermal expansion of the face sheets, leading to a thermal deflection component w_{th}, and the applied load on the roof causes a mechanical component w_{load}. The two components are independent, so the total panel deflection w is found by superposition:

$$w = w_{th} + w_{load}. \tag{6.3}$$

The webs add significant shear stiffness to the panel. As a result, the differential expansion of the face sheets results solely in panel bending [78], and the thermal component of deflection (evaluated at the panel mid-span, $x = a/2$) is

$$w_{th} = \frac{a^2 \alpha_f \Delta T}{8d}, \tag{6.4}$$

where α_f is the coefficient of thermal expansion of the face sheets, ΔT is the temperature gradient across the panel, and $d = h_c + t_f$ is the distance between the centroids of the face sheets.

The flexural stiffness of the panel is comprised of two components: the bending stiffness D_x and the shear stiffness D_{Qx}. The stiffness coefficients are found by adding the stiffness of the webs to the stiffness expression for foam core panels [89], i.e.

$$D_x = \frac{E_f d^2 t_f}{2} + \frac{E_w h_c^3}{12}\left(\frac{t_w}{p}\right) + \frac{E_c h_c^3}{12}\left(1 - \frac{t_w}{p}\right), \tag{6.5}$$

$$D_{Qx} = 2G_w t_w \left[\frac{d^2 t_f}{p h_c t_w} + \frac{1}{6}\left(\frac{h_c}{p}\right)^2\right]\left[\frac{tf}{t_w} + \frac{h_c^2}{3pd}\right]^{-1} + G_c \frac{d^2}{h_c}\left(1 - \frac{t_w}{p}\right). \tag{6.6}$$

The last term in each of Equations (6.5) and (6.6) represents the effect of the core material on panel stiffness. In steel panel designs, $E_f \gg E_c$ and $E_w \gg E_c$; therefore, the effect of the foam on the stiffness coefficients and panel deflection is negligible. Comparison of the first two terms of D_x shows the influence of the webs on bending stiffness is also small. Thus, the bending stiffness of the panel is provided by the face sheets, while the shear stiffness is provided by the webs.

For a simply supported panel under a uniformly distributed load q, the maximum deflection occurs at the panel mid-span ($x = a/2$) and is given by

$$w_{load} = \frac{5qa^4}{384\xi D_x} + \frac{qa^2}{8D_{Qx}}. \tag{6.7}$$

The first term in the right hand side of Equation (6.7) is the deflection due to bending, and the second term is the shear deflection. The parameter ξ is a reduction factor to account for the effects of shear lag, as described below. The maximum allowable panel deflection $\overline{w}$ is specified for residential roofs as $\overline{w} = a/240$ [43]. The global deflection constraint can thus be expressed as

$$w_{th} + w_{load} \leq \bar{w}. \tag{6.8}$$

The thermal component of panel deflection can be substantial in the presence of large temperature gradients. With steel face sheets and $\Delta T = 55°\text{C}$, for example, the thermal deflection is comparable or larger in magnitude than the deflection due to

the load for many roof applications. Over the full range of panel lengths and loads considered in this study, the thermal component of deflection consistently accounts for more than 50% of the total deflection.

For designs that use thin, widely-spaced webs, the panel bending stiffness is effectively reduced due to shear lag effects. These effects are accounted for in the present analysis by reducing the bending stiffness D_x by a shear lag factor ξ as shown in Equation (6.7). Neglecting the influence of the foam and assuming that the face sheets do not buckle as a result of panel bending (see the next section), the analysis of Hildebrand and Reissner [91] can be used to determine ξ. For a simply supported beam under uniformly distributed transverse load, ξ is given by

$$\xi = \frac{1 - \frac{m-1}{3} f}{1 + \left(1 - \frac{m}{3}\right) f}, \tag{6.9}$$

where f is a shear lag function that depends on loading and boundary conditions, and is defined in [91]. For web core panels with thin face sheets (i.e. $h_c/t_f \geq 50$), the non-dimensional stiffness parameter m is approximated by

$$m \approx \frac{2}{1 + 6\frac{t_f}{t_w}\frac{p}{h_c}} + 1. \tag{6.10}$$

For short panels, the reduction factor ξ is as low as 0.7 (indicating a 30% reduction in bending stiffness). However, the bending component of deflection is small for short panels, so the effect of shear lag is negligible. For longer panels, where the bending component is a larger percentage of the total deflection, $\xi > 0.95$. To meet the deflection requirement for these designs, the core depth must be increased by less than 0.5% compared to the value obtained when shear lag is neglected.

6.3.3 Face Sheet Buckling

Because the bending stiffness of the panel is provided almost entirely by the face sheets, the face sheets bear the bending stress of the panel. The top face sheet is in compression and therefore subject to buckling. The top face sheet is modeled as a set of plates, each of width p and length a, simply supported along the webs and transverse edges. The model for the individual plates is illustrated in Figure 6.3. Each plate is loaded in uniform, uniaxial compression along the edges at $x = 0$ and

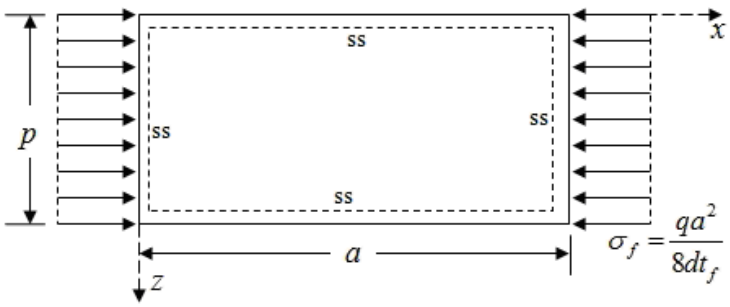

Figure 6.3. Plate approximation for face sheet buckling analysis

$x = a$ by a stress σ_f equal to the maximum bending stress imposed by the panel loading.

As the buckled face sheet deforms, it forces a corresponding deformation in the core. Relatively stiff core materials resist this deformation both in compression and in shear, thus increasing the buckling strength. Kolsters [89] studied this effect in web core panels loaded in pure compression and in bending. He found that the core material can be modeled as a Pasternak foundation, for which the restoring pressure $\hat{q}$ due to a local deflection $\hat{w}$ is given by [122]

$$\hat{q} = K_{Wf}\hat{w} - K_{Pf}\nabla^2\hat{w}. \tag{6.11}$$

The Winkler and Pasternak foundation constants K_{Wf} and K_{Pf} represent the resistance of the foundation to compression and shear deformation. The foundation constants for a panel loaded in bending were determined in Reference [89] using finite element analysis and found to be

$$K_{Wf} = \frac{E_c}{6h_c}, \qquad K_{Pf} = \frac{1}{6}G_c h_c. \tag{6.12}$$

A parabolic moment distribution exists under distributed loads with maximum moment $qa^2/8$ occurring at the panel mid-span ($x = a/2$). The resulting stress σ_f is

$$\sigma_f = \frac{qa^2}{8dt_f}. \tag{6.13}$$

The critical buckling stress $\overline{\sigma}_f$ follows the standard form for plate buckling [93],

$$\overline{\sigma}_f = \chi_f \frac{\pi^2 D_f}{p^2 t_f}, \tag{6.14}$$

where χ_f is a factor that accounts for the loads and boundary conditions imposed on the plate, and D_f is the plate stiffness of the face sheet,

$$D_f = \frac{E_f t_f^3}{12\left(1-\nu_f^2\right)}. \tag{6.15}$$

For a simply supported plate on a Pasternak foundation, χ_f is given by [123]

$$\chi_f = 2\sqrt{1 + f_{Wf} + f_{Pf}} + f_{Pf} + 2, \tag{6.16}$$

where the non-dimensional Winkler and Pasternak foundation parameters f_{Wf} and f_{Pf} are

$$f_{Wf} = \frac{p^4 K_{Wf}}{\pi^4 D_f}, \qquad f_{Pf} = \frac{p^2 K_{Pf}}{\pi^2 D_f} \tag{6.17}$$

These parameters represent the ratio of the normal and shear stiffnesses of the foundation to the bending stiffness of the plate. High values for the parameters signify a core material that strongly resists local deformation of the face sheet.

From the preceding analysis, face sheet buckling is avoided when $\sigma_f < \overline{\sigma}_f$. In determining the values of the foundation constants, the foam stiffness is reduced per Equation (2.2) to account for the effects of live load creep. Building design codes [102] allow designs within the postbuckling range. These guidelines for postbuckling behavior can be applied to the face sheets of web core panels. It will be shown, however, that face sheet buckling is not a limiting failure mode for practical panel designs due to the large core depths and thin webs required to meet the thermal requirement. Therefore, postbuckling capacity is not considered in the present study.

6.3.4 Panel Shear Strength

Shear failure of the panel is possible at the panel supports ($x = 0$ and $x = a$), where the transverse shearing forces are greatest. The shear strength of the panel has contributions from both the webs and the foam. Based on the stiffness model presented earlier, the shearing forces are supported almost entirely by the webs. The

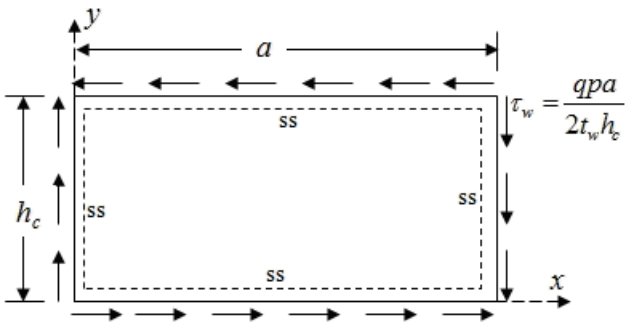

Figure 6.4. Plate approximation for web shear buckling

resulting stresses can therefore lead to shear buckling of the webs. Following the onset of shear buckling, the forces are transferred to the core material. Web core panels therefore contain some shear postbuckling strength as long as the core strength is greater than the web buckling strength. Although shear buckling of deeper panels will not lead to collapse, the loss of web stiffness will lead to a reduction in panel stiffness. In the present study, both aspects of shear strength are treated separately.

The web shear buckling analysis is performed by treating the webs as plates on an elastic foundation. Each web is modeled as a simply-supported plate of length a and width h_c, subjected to the uniform shear stress τ_w on all four edges (Figure 6.4). The maximum shearing force $qpa/2$ occurs at the panel supports ($x = 0$ and $x = a$). The shear buckling strength of the webs is approximated using the resulting average shear stress, which is given by

$$\tau_w = \frac{qpa}{2t_w h_c}. \tag{6.18}$$

The model follows standard practice for steel design [131, 132] and is slightly conservative because it neglects the interactions between face sheets and webs, as well as variations in shear loading along the length of the panel. The critical buckling stress $\overline{\tau}_w$ is [93]

$$\overline{\tau}_w = \chi_w \frac{\pi^2 D_w}{h_c^2 t_w}, \tag{6.19}$$

where D_w is the plate stiffness of the web,

$$D_w = \frac{E_w t_w^3}{12\left(1-\nu_w^2\right)}. \tag{6.20}$$

From the results given in Reference [28], the buckling coefficient χ_w is approximated by

$$\chi_w = 2.006\sqrt{0.690 + f_{Ww} + 1.020 f_{Pw}} + f_{Pw} + 3.749, \tag{6.21}$$

and the non-dimensional foundation parameters f_{Ww} and f_{Pw} are

$$f_{Ww} = \frac{12\left(1-\nu_w^2\right)\sqrt[3]{6}}{2\pi^4}\left(\frac{h_c}{t_w}\right)^4 \sqrt[3]{\frac{G_c^2 E_c^2}{E_w^4}}, \tag{6.22}$$

$$f_{Pw} = \frac{12\left(1-\nu_w^2\right)}{2\pi^2\sqrt[3]{6}}\left(\frac{h_c}{t_w}\right)^2 \sqrt[3]{\frac{G_c E_c}{E_w^2}}. \tag{6.23}$$

These parameters are developed for relatively deep foundations and are thus applicable for wide web spacing. Combining Equation (4.25) with the requirement that $Hk \geq 2$ (Chapter 4) yields the condition

$$\frac{t_w}{p} \leq 0.454\sqrt[3]{\frac{G_c^2}{E_c E_w}}. \tag{6.24}$$

This requirement is easily satisfied for roof panel designs. For example, with a PUR core and webs approximately 1 mm thick, the minimum web spacing is 250 mm[2].

As noted previously, the panel will have some shear postbuckling strength as long as the shear stresses can be transferred to the core material without causing core failure. Therefore, shear failure of the core is modeled by assuming the webs do not contribute to the shear strength of the core. The applied core shear stress τ_c is approximated from sandwich panel theory as [37]

$$\tau_c = \frac{qa}{2h_c}. \tag{6.25}$$

The limiting stress on the foam core is the shear strength τ_{uc}, where τ_{uc} is reduced per Equation (2.4) to account for fatigue.

6.3.5 Panel Bearing Strength

At the support locations the panel is subjected to concentrated loads, which can cause compressive bearing failure of the panel. This failure occurs through a combination

[2]An alternative form of the foundation constants applicable for closely-spaced webs is given in Appendix C

of local foam crushing and web crippling. Romanoff [124] identified three factors that contribute to the bearing strength of web core panels: the crippling strength of the webs, the interaction between the webs and foam as they cripple, and the crushing strength of the foam. The first contribution has been modeled by Roberts and Newark [100]. The other contributions are determined based on the assumed failure mechanism of the webs using energy methods.

Romanoff [124] found the bearing strength of panels loaded far from the edges; his method has been extended in the present study for panels supported over a rectangular area on the panel edges ($x = 0$ and $x = a$). Assuming slender webs are used ($h_c \geq 40t_w$), the concentrated load on a web $\overline{Q}$ at which bearing failure occurs is

$$\begin{aligned} \overline{Q} &= F_R \left[\frac{3.3}{8} t_w^2 \sqrt{E_w \sigma_{yw}} \left(\frac{t_f}{t_w} \right)^{1/4} \left(1 + \frac{8(c + t_f)t_w}{3h_c t_f} \right) \right] \\ &\quad + \frac{h_D^2 K_{wc}}{3} (c + t_f + L_D) + \sigma_{uc} \frac{p}{2} (c + t_f + L_D) . \end{aligned} \tag{6.26}$$

The three terms on the right hand side are the contributions from the crippling strength of the webs, the interaction between the crippled webs and the foam, and the crushing strength of the foam. The parameters K_{wc} and L_D are an elastic foundation modulus and the length of the damaged region of the web [124].

The thermal requirement necessitates the use of very slender (large h_c/t_w ratios), widely-spaced webs. For such designs, the foam crushing term typically contributes 80% or more of the total bearing strength, with most of the remaining strength coming from the web crippling term. Thus, for panels with slender widely spaced webs, it is reasonable to neglect the contribution of the webs in calculating the bearing strength. The foam must support a load $qpa/2$ along each bearing edge and the foam load capacity is $\sigma_{uc}pc$. Thus, the load $\overline{q}$ that the panel can sustain without bearing failure is approximated by

$$\overline{q} = \frac{2c}{a} \sigma_{uc}. \tag{6.27}$$

6.3.6 Design Criteria

The failure modes for web core panels can be classified either as ultimate or serviceability limit states. The serviceability limit states—deflection, thermal performance, and initial face sheet buckling—do not cause structural failure of the panel if limits are

Table 6.3. Safety factors used in the present analysis [34, 35, 102]

Failure Mode	ψ_i
Thermal	1.0
Deflection	1.0
Face sheet buckling	1.0
Web shear buckling	1.6
Core shear failure	2.0
Core bearing failure	2.0

exceeded. For deflection and thermal performance, the limits are set by prescriptive codes. For initial face sheet buckling, the panel has residual postbuckling capacity that allows loading beyond the buckling load. All other failure modes (web buckling, core shear failure and core crushing) are treated as ultimate limit states, that is, panel failure is expected if any of the states are violated.

The analysis and designs that follow are developed based on the Allowable Strength Design (ASD) criterion [102]. Following the ASD criteria, each limit state is expressed generically in terms of an applied load F_i (such as deflection or applied normal stress) and a nominal limit load $\overline{F}_i$. The following condition must be met for each limit state:

$$F_i \leq \psi_i \overline{F}_i, \tag{6.28}$$

where ψ_i is a safety factor for the limit state. The safety factors are specified based on the severity of the limit states. For the serviceability limit states (thermal, deflection, and initial face buckling), the safety factors are set to 1.0. The safety factor for web shear buckling is set to 1.6 per US building codes [102]. Prescriptive codes do not address stress failure of the core; the safety factors for core failure are set to 2.0 in order to minimize the effects on core creep rates [34, 35]. The safety factors and equations corresponding to the limit states are listed in Table 6.3.

6.4 Design Procedure

The design of roof panels is driven by the interaction between structural and thermal requirements. From a structural standpoint, thicker webs (high t_w/p ratios) are desirable, but from a thermal standpoint, thinner webs are required. A design procedure has been developed that balances the two requirements to minimize the core depth h_c. This objective was chosen based on the relatively high cost of the foam compared

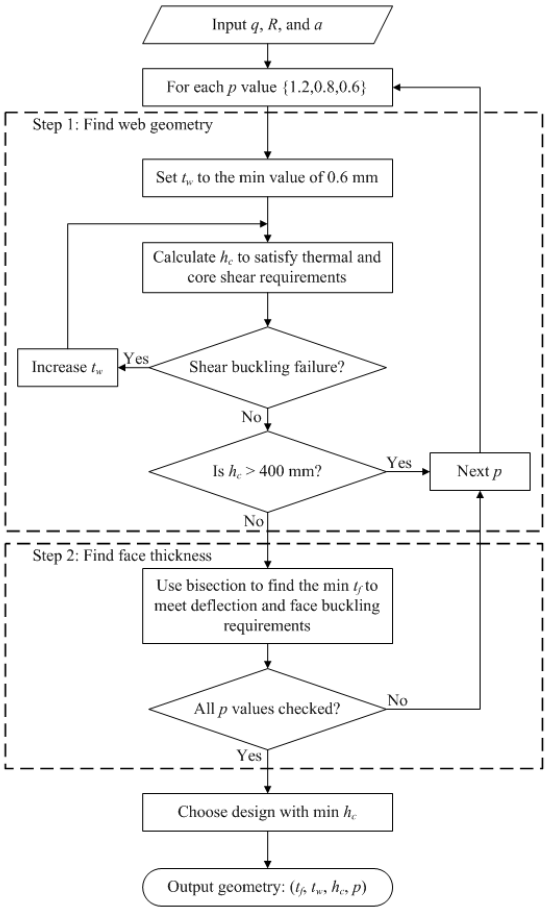

Figure 6.5. Flowchart of the web core design procedure

to the structural material, as well as the difficulty of integrating deep panels into roof architecture.

The proposed design procedure follows the flowchart illustrated in Figure 6.5. The panel length, loading, and R-value are defined by roof geometry and geographic location and are inputs to the procedure. The outputs of the procedure are t_f, t_w, h_c, and p for the design that minimizes the core depth h_c. Constraints are imposed on panel geometry to improve manufacturability. To ensure that cold-rolled steel can be used, the face sheet and web thicknesses are limited to the range of 0.6–2.0 mm. For the purposes of handling and architectural requirements, the maximum panel width and thickness are set at 2.4 m and 400 mm respectively. Web spacing is limited to integer increments of the total width (i.e. 1.2 m, 0.8 m, 0.6 m, etc. for a panel width of 2.4 m).

For the requirements of most residential roofs and the materials considered in this study, it will be demonstrated that the thermal and shear buckling requirements impose the primary restrictions on the design space for the web geometry t_w and h_c. The proposed design procedure is therefore performed in two steps. First, the web thickness and height, t_w and h_c, are determined for the maximum p based on the thermal, shear buckling, and core shear failure requirements. The web thickness is incremented in steps of 0.01 mm, starting from the minimum allowable value (0.6 mm). For each value of t_w, the h_c to satisfy the thermal and core shear failure requirements is found from Equations (6.2) and (6.25); the resulting t_w and h_c are then checked for shear buckling. If shear buckling is predicted, t_w is increased until shear buckling is avoided. If the shear buckling requirement cannot be met without violating the geometric constraints described above, then no feasible designs exist for the current web spacing and the search is repeated with a smaller value for p.

Once t_w and h_c are determined in step 1, t_f is found in step 2 based on the deflection and face sheet buckling requirements. The minimum value to satisfy both requirements is found using bisection, i.e. iterate, reducing the search space for t_f (starting with the original range 0.6–2.0 mm). The entire process is repeated for each value of p until the minimum core depth is found. In practice, the problem is convex in p; therefore, not all possible values need to be checked. It is possible to start with the largest allowable value of p, then reduce p until further reductions fail to result in smaller core depths.

6.5 Failure Mode Examination

To gain insight into the design considerations for web core panels, it is useful to examine the influence of the failure modes on panel design. This influence can be investigated by mapping the effect of each failure mode on the feasible (t_w, h_c) design space. Examples of failure mode maps are shown in Figures 6.6(a) and (b) for panel lengths of 5 and 7 m. The applied load in both cases is 1500 N/m^2, and the minimum R-value is 5.3 m^2-K/W. These requirements are representative of houses in the southern half of the United States. The curves corresponding to minimum t_w required to avoid shear buckling and minimum h_c to avoid the other failure modes are plotted for panels with carbon steel and stainless steel webs with a 1.2 m web spacing. To demonstrate the minimum allowable core depth for failure modes that depend on t_f,

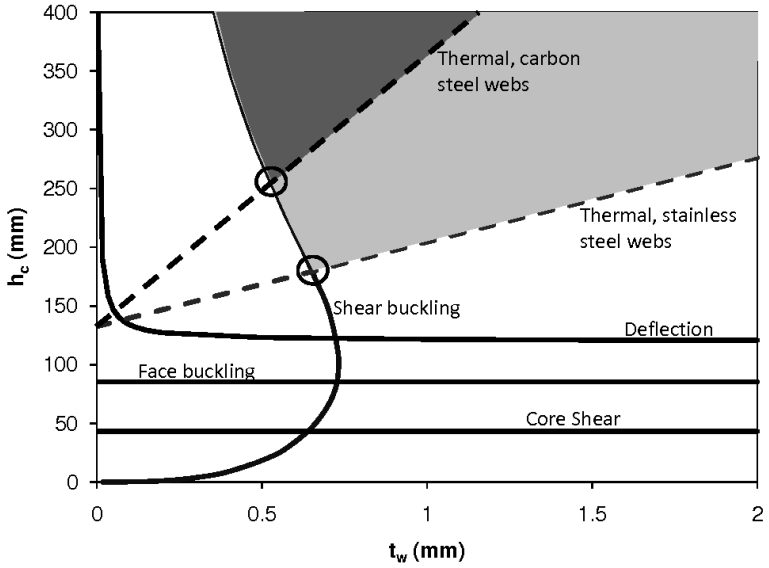

(a)

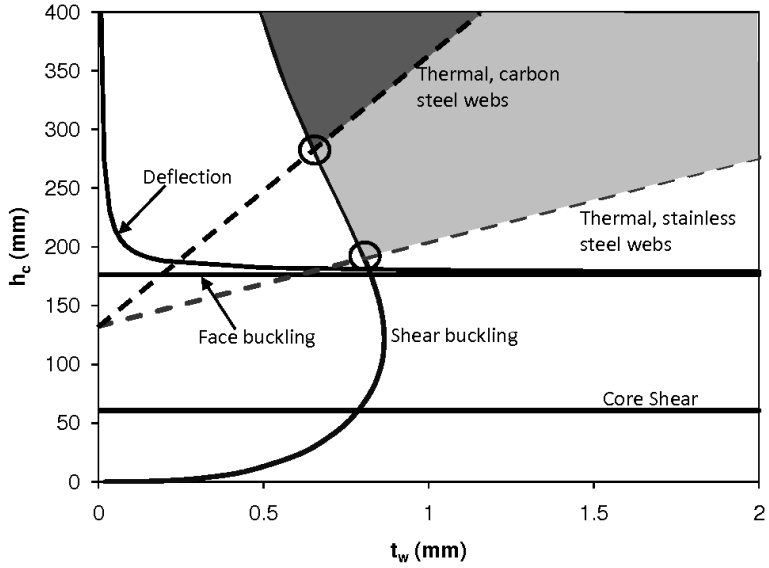

(b)

Figure 6.6. Failure mode map for panels with carbon or stainless steel webs spaced at 1.2 m and a 36 kg/m^3 core, subjected to a transverse load of 1500 N/m^2 and an R-value requirement of 5.3 m^2-K/W ($t_f = 2.0$ mm): (a) panel length of 5 m, and (b) panel length of 7 m. The regions of (t_w, h_c) combinations for which no failure modes occur for the two web materials are shaded, and the minimum depth designs are circled.

the maximum value of 2.0 mm is used. The space of permissible designs is shaded (dark shading for designs with carbon steel webs and light shading for stainless steel webs), and the design point that minimizes h_c for each material is circled. In each case, the permissible (t_w, h_c) space is determined by the thermal and shear buckling failure modes.

Core shear failure and face sheet buckling are independent of t_w. The curve for core shear failure is generated by solving Equation (6.25) for h_c. The curve for face sheet buckling is generated by setting $\sigma_f = \overline{\sigma}_f$ and $t_f = 2.0$ mm. The deflection curve does not change with t_w for t_w greater than about 0.3 mm. This independence occurs because the webs effectively eliminate the shear component of panel deflection. Very thin webs contribute less to the panel shear stiffness, so greater core depth is necessary to meet the deflection requirement. In the limit as t_w approaches zero (i.e. no webs), the core depth increases sharply to the value for foam core panels with no webs (505 and 600 mm for panel lengths of 5 and 7 m respectively).

The curve corresponding to shear buckling is the locus of points where $\tau_w = \overline{\tau}_w$, as given by Equations (6.18) and (6.19). The intersection of the shear buckling curve with the core shear curve is the minimum core depth for which the panel is expected to have postbuckling strength in shear. If sufficiently thick webs are used, then the shear buckling constraint will be satisfied regardless of core depth. In Figure 6.6(a), for example, shear buckling is avoided for all h_c when $t_w \geq 0.73$ mm, and in Figure 6.6(b) it is avoided when $t_w \geq 0.87$ mm. This comparison also indicates that the required web thickness increases with increasing panel length.

The thermal requirement is indicated by a line with a slope $R(k_w - k_c)/p$ (see Equation (6.2)). Because $k_w \gg k_c$, the slope is proportional to the thermal conductivity of the web material. Figures 6.6(a) and (b) include dashed lines representing the thermal requirements for carbon steel and stainless steel webs. Because the thermal conductivity of stainless steel is approximately one third that of carbon steel, panels with stainless steel webs are less deep than panels with carbon steel webs. For example, for a 5 m long span, a 254 mm deep panel with carbon steel webs satisfies all requirements compared to a 179 mm deep panel with stainless steel webs. For a 7 m span, panel depths are 282 mm and 190 mm for carbon and stainless steel webs, respectively. For the same R-value and web material, panel depth increases with increasing panel length.

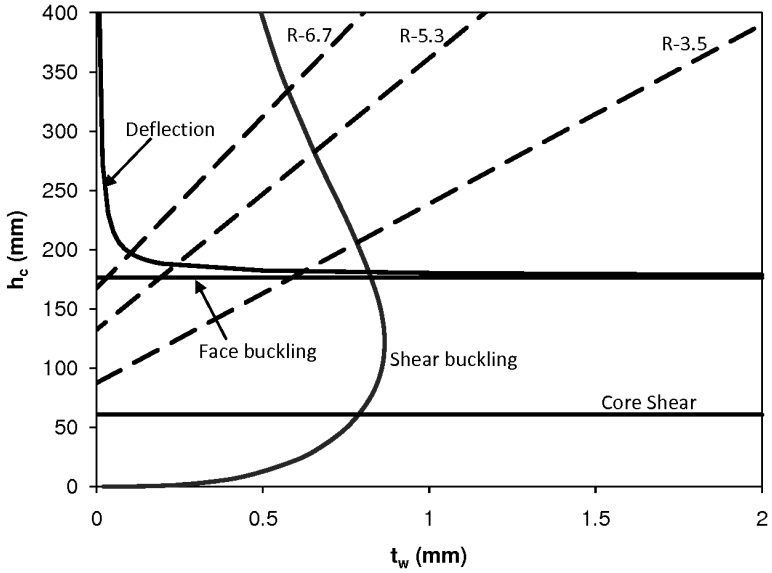

(a)

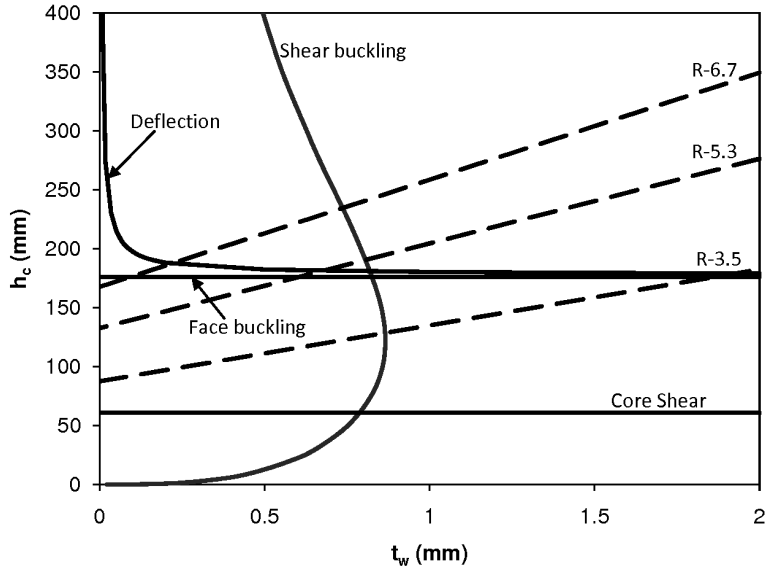

(b)

Figure 6.7. Failure mode map for panels with (a) carbon or (b) stainless steel webs spaced at 1.2 m and a 36 kg/m^3 core, panel length of 7 m, subjected to a transverse load of 1500 N/m^2. R-value requirements of 3.5, 5.3, and 6.7 m^2-K/W are compared for each web material.

To illustrate the effect of the thermal requirement on the design space, the failure mode map of Figure 6.6(b) is repeated with several different R-value requirements in Figure 6.7. Lines corresponding to R-value requirements of 3.5, 5.3, and 6.7 m^2-K/W, are shown for carbon steel webs in Figure 6.7(a) and for stainless steel webs in Figure 6.7(b). The curves from Figure 6.6(b) corresponding to structural limit states are included for reference. Designs are generally limited by the interaction between thermal performance and the shear buckling requirement. If the thermal requirement is sufficiently reduced, then other failure modes can influence the design. In Figure 6.7(b), for example, stainless steel web designs with an R-value requirement of 3.5 m^2-K/W or less are not limited by thermal performance. In this case, the deflection and face sheet buckling requirements are more restrictive than the thermal requirement. For example, with stainless steel webs 0.82 mm thick, the panel that satisfies all limit states is 181 mm deep. The corresponding R-value is 5.0 m^2-K/W.

The latter situation, in which the design is not limited by thermal performance, occurs for designs with low R-value requirements and high transverse loads. It also occurs only with the use of stainless steel (or other low thermal conductivity material) webs. The situation is unlikely in practice because high loading occurs primarily in colder climates, where the R-value requirement is higher (6.8 m^2-K/W). If the situation does occur, it is necessary to increase the depth h_c to meet the deflection and face sheet buckling requirements. In that case, step 1 of the design process (see Figure 6.5) should be repeated to ensure that shear buckling is still prevented.

6.6 Roof Panel Designs

The procedure has been applied to the design of panels for lengths from 2.5 to 7 m and the loads expected in residential applications: 1500, 2000, and 3000 N/m^2. Each of these loads includes an assumed dead load of 700 N/m^2: 500 N/m^2 for panel weight and 200 N/m^2 for additional roofing layers. An R-value of 5.3 m^2-K/W is specified. Designs are presented for web spacing of 1.2 and 0.8 m.

The minimum panel depth is plotted as a function of panel length in Figures 6.8(a)–(c) for 1500, 2000 and 3000 N/m^2. Foam core panels are compared with web core panels with carbon and stainless steel webs. In foam core panels, the foam provides minimal shear stiffness: the panel depth increases significantly with length and load to satisfy the deflection requirement. The webs provide shear stiffness, enabling web

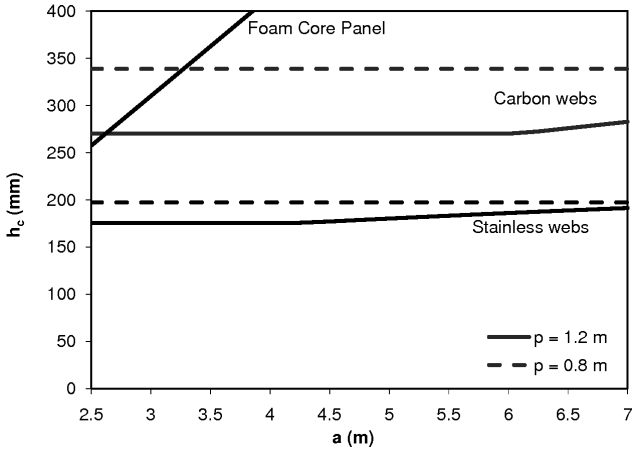

(a)

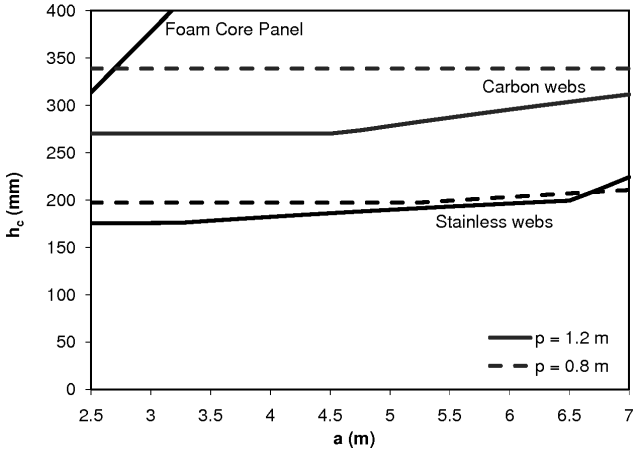

(b)

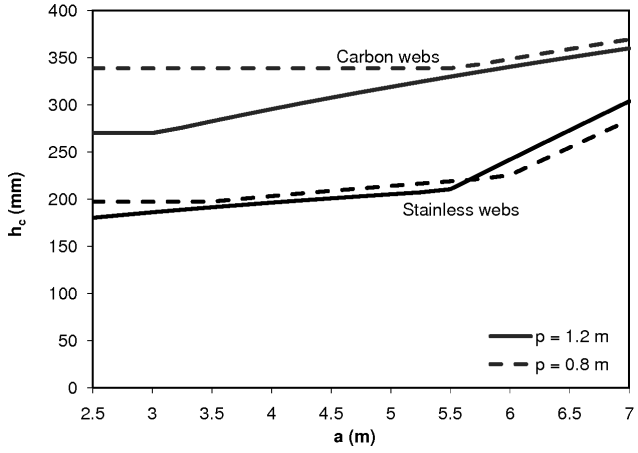

(c)

Figure 6.8. Core depth vs. panel length for foam core panels and web core panels with carbon and stainless steel webs with an R-value requirement of 5.3 m^2-K/W and an applied load of: (a) 1500 N/m^2, (b) 2000 N/m^2, and (c) 3000 N/m^2. Web spacing of 0.8 and 1.2 m are compared for the web core panels.

core designs for much longer spans. The required core depth increases with length in all cases, but the use of webs reduces the depth by as much as 57%. For example, for a load of 1500 N/m^2, webs are required for panels longer than 3.9 m, and the use of webs reduces panel depth for lengths greater than 2.6 m. The increase in allowable panel length and the reduction in panel depth attributed to the use of webs become more dramatic as the load is increased. For a load of 3000 N/m^2, webs are required for any length.

Two factors cause the increase in panel depth with span length. For longer span lengths under 1500 and 2000 N/m^2 loads, the increase in depth reflects an increase in the required web thickness to prevent shear buckling. Panel depth is correspondingly increased to meet the thermal requirement. (Some segments of the curves in Figure 6.8 are flat; these represent designs where the required web thickness is less than the minimum of 0.6 mm, hence no need to increase t_w.) If stainless steel webs are used under high loads (3000 N/m^2) with longer spans, the depth increases more rapidly with span length. It will be demonstrated that these cases are designs for which the maximum face sheet thickness (2.0 mm) must be used. It becomes necessary to increase the depth to meet the structural requirements.

Two factors cause the increase in panel depth with span length. In most cases, the depth reflects an increase in the required web thickness to prevent shear buckling. Panel depth is correspondingly increased to meet the thermal requirement. If stainless steel webs are used at higher loads (2000 and 3000 N/m^2) and longer spans, the depth increases more rapidly. In this case, the maximum face sheet thickness (2.0 mm) is required to meet the structural requirements, and it is necessary to further increase the depth to meet the structural requirements. These are the designs, described in the previous section, that are not limited by thermal performance. These trends, in terms of face sheet and web thickness, are illustrated in the figures that follow.

Figure 6.8 also shows the effect of web spacing. Closer web spacing is generally beneficial from a structural standpoint: it results in stiffer panels with less stress on the webs. On the other hand, closer webs are detrimental to the thermal performance, and, as noted above, thermal requirements control most of the designs. Thus, designs with $p = 0.8$ m require deeper cores than the designs with $p = 1.2$ m. For those designs that are limited by structural requirements, reductions of up to 20 mm (7%) in depth are possible with reduced web spacing.

The face sheet and web thicknesses corresponding to the designs in Figure 6.8 are plotted as a function of panel length in Figures 6.9 and 6.10 respectively. All foam core panel designs require the maximum face sheet thickness of 2 mm in order to minimize depth. The limit on span length for foam core panels is set by the depth limit of 400 mm. For web core designs, face sheet thickness influences both the panel deflection and face sheet buckling strength. For short to moderate span lengths (e.g. ≈4.5 m with stainless steel webs), only the minimum face sheet thickness, 0.6 mm, is required. The required face sheet thickness is smaller for panels with carbon steel webs because the depth is greater. For longer panels (with either web material), the deflection and face sheet buckling criteria require an increase in face sheet thickness. The increase is linear because the representative load varies linearly with length (see Equations (6.7) and (6.13)).

Figures 6.8 and 6.10 reflect the directly proportional relationship between web thickness and core depth. For example, for panels with carbon steel webs spaced at 0.8 m and loaded at 1500 N/m^2, the required web thickness is 0.6 mm for $a < 6.3$ m. Panel depth is 283 mm. For $a > 6.3$ m, the web thickness and panel depth increase linearly. Web spacing and material influence the web thickness. Panels with $p = 1.2$ m require webs up to about 40% thicker than those with $p = 0.8$ m. Similarly, carbon steel webs must be up to 25% thinner than stainless steel webs. These relationships between web geometry and material are consistent with the thermal requirement. As the web spacing decreases, thinner webs are required to satisfy the thermal requirement. Webs constructed from materials with higher thermal conductivity must also be thinner.

The panel weights associated with each of the designs in Figure 6.8 are plotted in Figure 6.11. All of the designs weigh less than the assumed design weight of 500 N/m^2. For 1500 N/m^2, foam core panel weight increases from 183 to 239 N/m^2 as the span length increases from 2.5 to 4 m. For 2000 N/m^2, panel weight increases from 203 to 237 N/m^2 as the span length increases from 2.5 to 3.3 m. The increase in panel weight is associated entirely with an increase in foam depth. Foam core panels weigh less than web core panels with closely-spaced carbon steel webs, but more than all other web core designs.

For web core panels, increases in face sheet thickness and foam depth affect the weight, while increases in web thickness have a minimal effect. The increase in weight (with

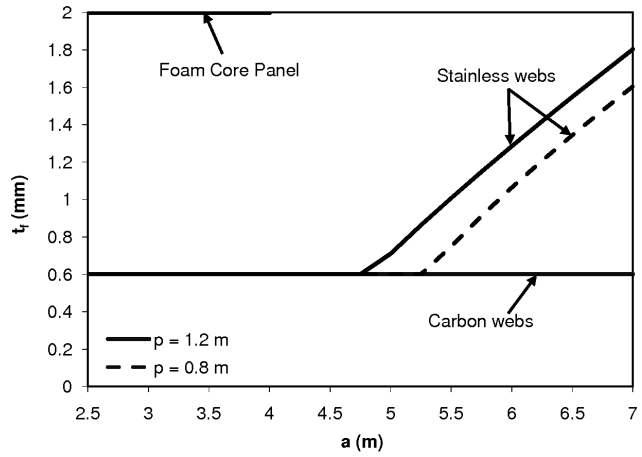

(a)

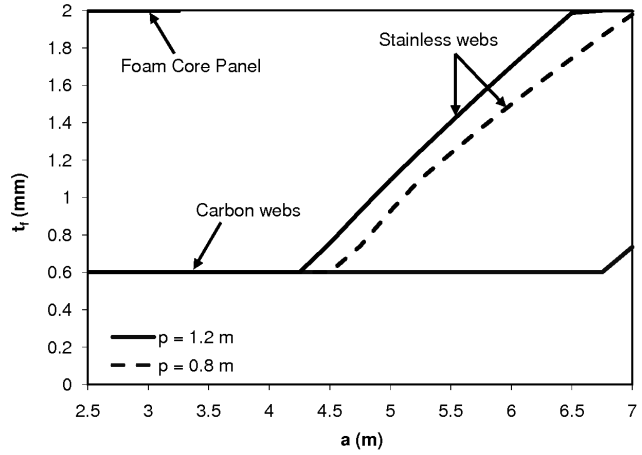

(b)

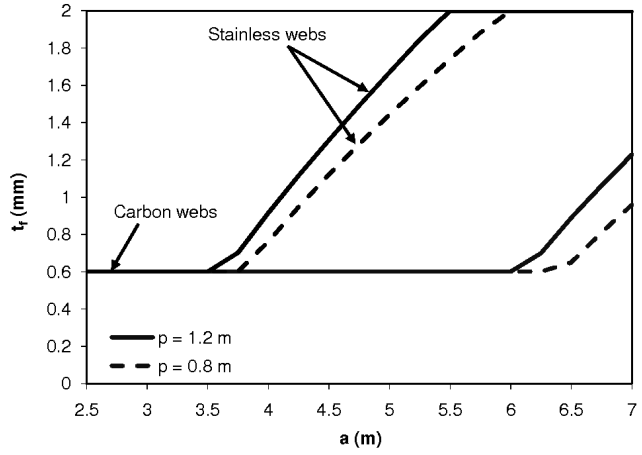

(c)

Figure 6.9. Face sheet thickness vs. panel length for panels corresponding to the designs shown in Figure 6.8, applied load of: (a) 1500 N/m^2, (b) 2000 N/m^2, and (c) 3000 N/m^2. Web spacing of 0.8 and 1.2 m are compared.

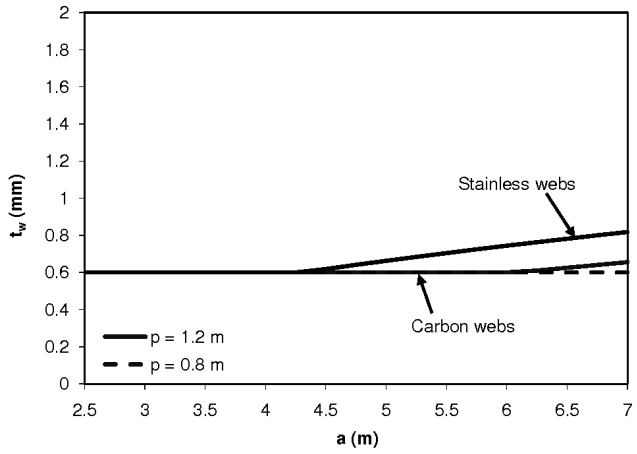

(a)

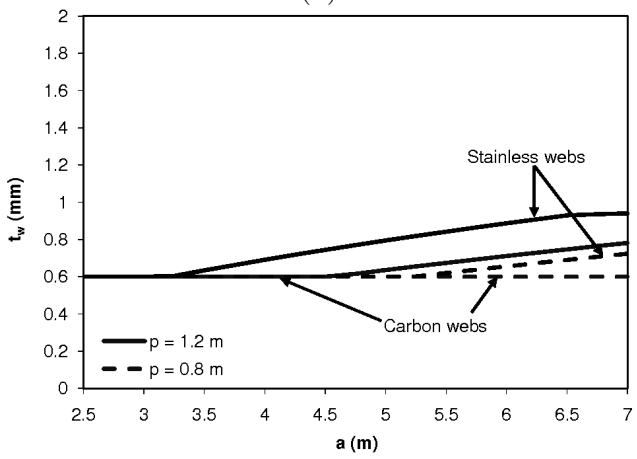

(b)

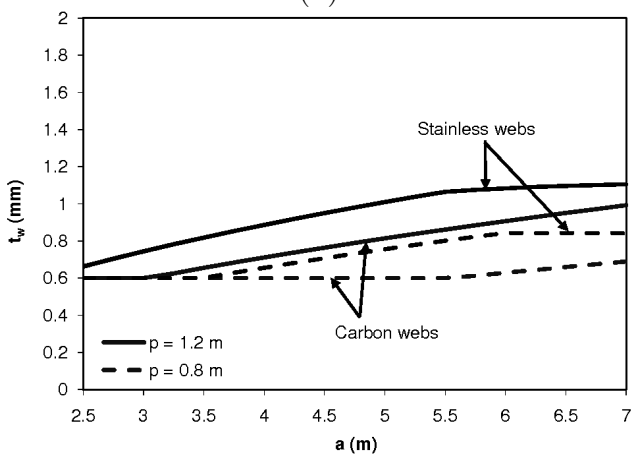

(c)

Figure 6.10. Web thickness vs. panel length for panels corresponding to the designs shown in Figure 6.8, applied load of: (a) 1500 N/m^2, (b) 2000 N/m^2, and (c) 3000 N/m^2. Web spacing of 0.8 and 1.2 m are compared.

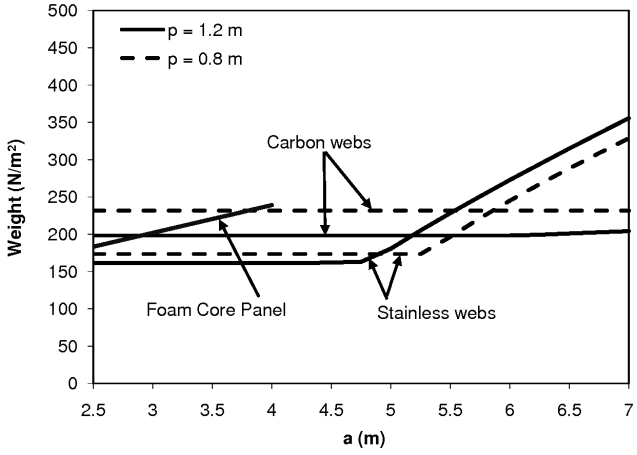

(a)

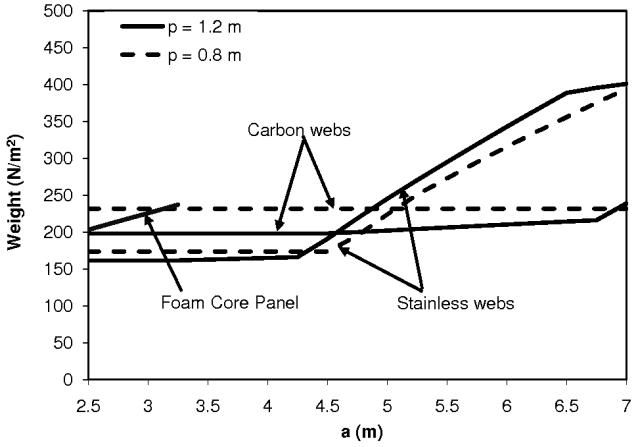

(b)

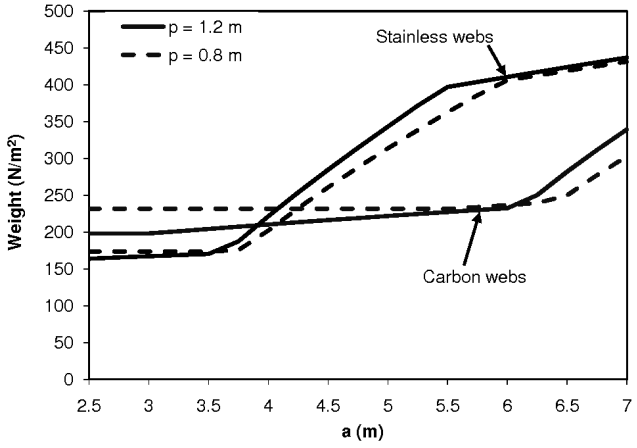

(c)

Figure 6.11. Panel weight vs. length for panels corresponding to the designs shown in Figure 6.8, applied load of: (a) 1500 N/m^2, (b) 2000 N/m^2, and (c) 3000 N/m^2.

increasing span) for web core panels with carbon steel webs follows the same trend as the increase in panel depth. This result is as expected because the face sheet thickness is 0.6 mm for all web core panels with carbon steel webs. In the range where h_c increases with constant t_f (e.g. carbon steel webs at 3000 N/m^2, $3 \leq a \leq 6$ m), the weight increases relatively slowly with length. In the range where t_f also increases (e.g. same case with $a > 6$ m), the increase is more dramatic. Because most of the panel weight comes from the face sheets, the weight is very sensitive to changes in face sheet thickness.

The effect of web spacing on panel weight is reasonably small. With carbon steel webs under moderate loading and length, panels with $p = 1.2$ m weigh about 17% less than panels with 0.8 m; longer panels under high load weigh up to 10% more with the wider web spacing. With stainless steel webs, the trends are similar but less dramatic: panels with wider web spacing weigh 7% less for moderate span and load, and up to 10% more for greater span and load. In both cases, the increased weight under greater span and load is the result of increased face sheet thickness. Panels with slightly closer web spacing can use thinner face sheets and, under the conditions described here, the reduction in face sheet thickness has more effect than the increase in depth.

6.7 Conclusions

Panelized residential roofs have several potential benefits over conventional construction techniques, including reduced construction times, improved energy efficiency, and architectural benefits. Design considerations governing the use of metal web core panels for residential roofs have been presented. The specific performance considerations relevant for roof applications are: R-value, panel deflection, core shear failure, bearing failure, and local buckling of the face sheets and webs. The webs contribute substantial shear stiffness and eliminate the effect of foam creep on panel deflection, but they also provide a thermal conduction path through the foam that reduces the insulating value of the panel. As a consequence, for most applications, more foam is required to meet the target insulating value than would be needed if no webs were present. For the metal webs considered in the present study, the depth is a strong function of the thermal conductivity of the web material. Thus stainless steel webs are preferred to carbon steel webs from a performance standpoint. A design procedure

has been developed by which the competing structural and thermal requirements are balanced to create web core designs that minimize the core depth h_c.

Web core and foam core panel designs are presented for residential roof applications with loads ranging from 1500 to 3000 N/m^2 and span lengths ranging from 2.5 m to 7 m. In all cases, the panels provide an insulating value of R-5.3 m^2-K/W. For these representative roof applications, panel designs are largely determined by the required R-value and the shear buckling strength. If panel depth is restricted to 400 mm, foam core span length is limited to 3.8 m for a 1500 N/m^2 load and 3.2 m for a 2000 N/m^2 load. There are no foam core designs that can sustain a 3000 N/m^2 load over the spans considered without increasing the depth greater than 400 mm. In contrast, web core panels with carbon or stainless steel webs can be designed to span lengths up to 7 m while supporting loads up to 3000 N/m^2. Webs fabricated from materials with low thermal conductivity but high strength and stiffness can lead to longer panel lengths. For example, panels with stainless steel webs provide an average reduction of 150 mm in core depth compared to panels with carbon steel webs. This difference may be important in cases where minimizing foam use is critical or in cases where higher R-value requirements are imposed.

In all but the most extreme cases (i.e. panels longer than 6 m under 3000 N/m^2 loading), it has been shown that the webs should be spaced widely (1.2 m) to minimize the core depth. This result suggests that an efficient manufacturing process may involve the production of panels 1.2 m wide with webs serving as the joints between adjacent panels. In other words, web core panels can be thought of as modification of foam core panels in which the webs act as longitudinal spline joints. Regardless of how the webs are treated, the present analysis has demonstrated that stiffening members spanning the depth of the core can have a significant impact on both the structural and thermal performance of panels.

Chapter 7

Prototype Testing

Four limiting structural failure modes have been identified for web core panels: deflection, face sheet buckling, web shear buckling, and bearing failure at the supports. The deflection model is derived from basic engineering principles, and Kolsters [89] validated the model for face sheet buckling through finite element analysis and testing. The effect of the core material on web strength, however, has not been investigated prior to this work. The models in Chapters 4 and 5 have shown that the core contribution is significant, and an accurate understanding of that contribution is necessary to develop feasible roof panel designs. The tests reported in this chapter were therefore performed to investigate the effect of the core on shear buckling strength (including postbuckling deflection behavior) and bearing strength.

The web shear buckling model was investigated extensively in Chapter 4 via finite element analysis. It was shown that the Pasternak foundation model can be effectively applied to the prediction of the initial shear buckling strength of foam-filled panels. It was also demonstrated that the core material can increase the shear buckling strength by an order or magnitude (see Section 4.3.3). In the present chapter, the shear buckling behavior is further validated through prototype testing to provide increased confidence in those results and to investigate the panel postbuckling behavior (stiffness and strength). Validation of the deflection model, pre- and postbuckling, was obtained in the same test. The bearing strength model, Equation (5.16), is unique to the present work and cannot be directly validated by any work appearing in the literature. Tests to validate the end bearing failure model were therefore performed. The bearing

tests had two objectives: validation of the bearing strength model, and determination of a suitable reduction factor F_C.

Tests were performed at the Civil Engineering Structures Laboratory at the University of Minnesota. An overview of the tests is provided in Section 7.1. The deflection and shear buckling models were validated using a four-point bending test, and the bearing strength model was validated using three-point bending tests. The details of the four-point bending test, including prototype design, test procedure, and results, are provided in Section 7.2. The details of the three-point bending test are provided in Section 7.3.

7.1 Overview of the Tests

The theory developed in this work focuses on the design of panels that are subjected to a uniformly distributed load. However, the facilities to test panels under distributed load were not available, so testing was performed using line loads. This substitution is acceptable because the theory developed in this work is independent of the loading. Deflection is characterized by the stiffnesses D_x and D_{Qx}, shear buckling is characterized by the coefficient χ_β, and bearing failure is characterized by the bearing strength $\overline{Q}$. These quantities are functions of cross-sectional geometry and material properties only (see Equations (6.5), (6.6), (6.21), and (6.26) respectively). Thus, only the applied stresses are affected by the type of loading, and these effects are understood through first principles.

For several practical reasons, the prototypes were filled box beam panels (i.e. web core panels with no internal webs), illustrated in Figure 7.1. The cross sectional geometry is defined by the same nomenclature used throughout this work. The panels span a distance a, with load actuators located at a distance λ from the supports. The box section allowed easy access to the webs for instrumentation and qualitative investigation of failure modes. It also allowed the web spacing to be maximized given the limits on panel width.

The panels were built up using flat face sheets and cold-formed C-channel webs. The webs were spot welded to the face sheets at a spacing of approximately 75 mm along the web flanges. The panels were filled *in-situ* with PUR by the foam vendor, BASF. They were blocked off at each end (yz-face) using 38 mm thick lumber during this

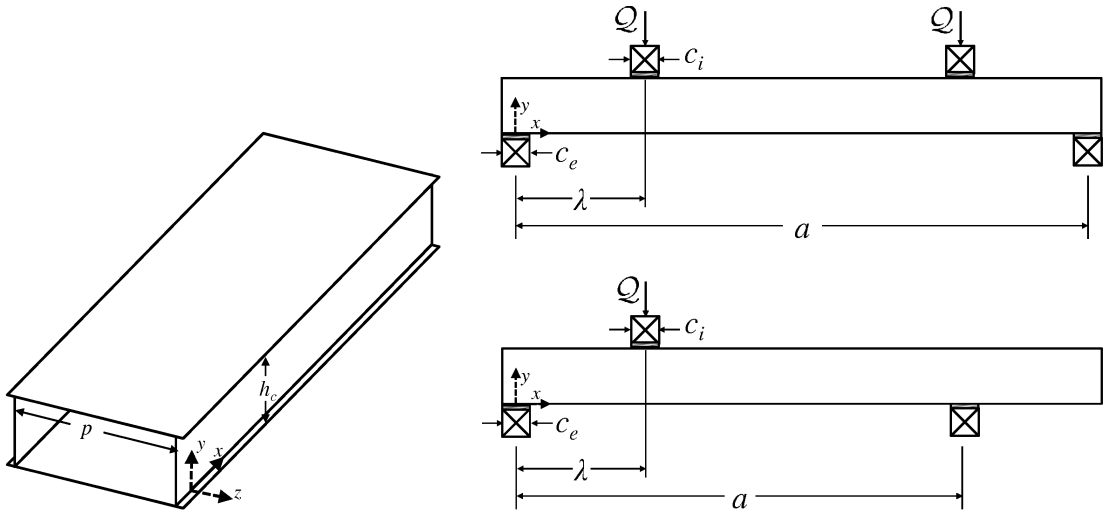

Figure 7.1. Prototype panel geometry and load configurations

process for containment of the liquid foam. In addition, the webs were reinforced by dimensional lumber to prevent excessive deformation resulting from the internal foaming pressures. Despite the stiffening, initial bowing in the webs on the order of about 6 mm was observed in all three panels. The imperfections were largest near the midspan of the panel, and smaller near the supports.

The panel length and width were constrained by limitations of the test setup and the prototype production process. The support structure for the actuators was fixed in place and allowed a maximum panel width of about 750 mm. To allow access to the webs as noted above, a width of 610 mm (24 in.) was specified for all of the prototypes. The length was constrained by the foaming process. The prototype foaming facility was tooled for a maximum length of 2.4 m (96 in.), so all of the prototypes were foamed to that length. The depths were chosen to be roughly representative of expected web core panel designs while maintaining a width ratio $p/h_c > 2$ as required for beam bending tests (see Reference [133], for example).

After completion of the tests described in this chapter, samples of foam from each panel were returned to the foam vendor for material property testing. Data sheets containing the full set of results for each foam are given in Appendix D. The properties relevant to the work described in this chapter are provided in Tables 7.1 and 7.5. As discussed in Chapter 2, foam rise in the bulk of the foam is oriented in the (longitudinal) x-direction. As a result, the loads on the foam due to local web defor-

mation occur perpendicular to the foam rise, and the properties used in this chapter are obtained perpendicular to the rise direction.

7.2 Deflection and Shear Buckling Model Validation

Validation of the deflection and shear buckling models was obtained through a four-point bending test, referred to here as the shear buckling test for simplicity. Of interest for the deflection model is the panel stiffness before and after the onset of shear buckling. The test results demonstrate that the postbuckling deflection behavior can be predicted by assuming the buckled webs are fully ineffective.

The instrumentation used in the shear buckling test allowed measurement of the applied load $\mathcal{Q}$ and the midspan displacement $\mathcal{W}$. The script $\mathcal{Q}$ and $\mathcal{W}$ are used throughout this chapter to distinguish experimentally measured values from theoretical loads and displacements (Q and w, respectively). The subsections that follow detail the modeling, prototype design, procedure, and results of the shear buckling test. The modeling section provides both the governing equations used for prototype design and the procedure by which validation of the deflection and shear buckling models is obtained from the measurements of $\mathcal{Q}$ and $\mathcal{W}$.

7.2.1 Shear Buckling Test Model

The model for the shear buckling test is shown in Figure 7.2 along with diagrams of the internal shear and bending moment distribution. The maximum shearing force occurs in the regions between each load point and support ($0 \leq x \leq \lambda$ and $a \geq x \geq a - \lambda$) and is equal in magnitude to $\mathcal{Q}$. The maximum bending moment occurs in the region between the load points ($\lambda \leq x \leq a - \lambda$) where shearing forces are absent, so the region of possible face sheet buckling is separated from the region of web failure.

To obtain the theoretical deflection behavior, consider a beam loaded in symmetric four-point bending, with load Q at each point. The deflection w at the midspan is

$$w = Q\left[\frac{\lambda}{24D_x}\left(3a^2 - 4\lambda^2\right) + \frac{\lambda}{D_{Qx}}\right], \tag{7.1}$$

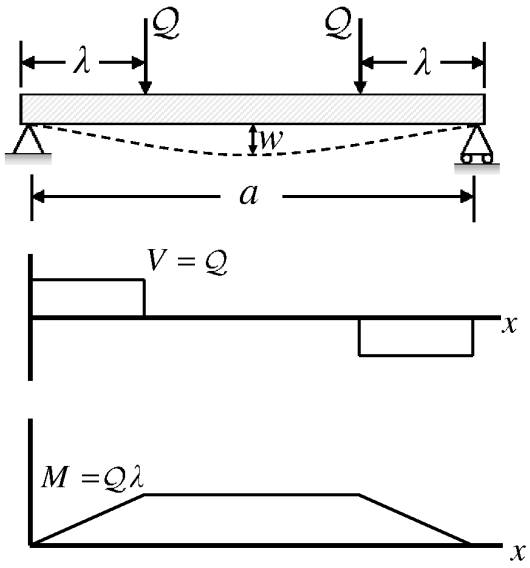

Figure 7.2. Shear and bending moments for the shear buckling test

with D_x and D_{Qx} given by Equations (6.5) and (6.6). From Equation (7.1), the predicted panel stiffness K is

$$K = \frac{Q}{w} = \left[\frac{\lambda}{24 D_x} \left(3a^2 - 4\lambda^2 \right) + \frac{\lambda}{D_{Qx}} \right]^{-1}. \tag{7.2}$$

The panel deflection model is validated by comparing the observed stiffness $\mathcal{Q}/\mathcal{W}$ to the stiffness predicted by Equation (7.2). If the observed and calculated stiffnesses match, it can be inferred that D_x and D_{Qx} are modeled correctly.

Equation (7.2) is valid assuming no buckling of the face sheet or webs. The onset of web buckling is accompanied by a dramatic loss of web stiffness [134]. The webs develop postbuckling capacity via the tension field effect [132], but only after unacceptably large panel deflections. Therefore, the initial postbuckling behavior in shear can be predicted by assuming the buckled webs are fully ineffective. In that case, the postbuckling stiffness of the panel is predicted, using Equation (7.2), by setting $E_w = 0$ in the calculation of D_x and D_{Qx}.

Equating the stress $\tau = \mathcal{Q}/2t_w h_c$ to the shear buckling strength given by Equation (4.4) yields the predicted load $\overline{Q}$ at failure

$$\overline{Q} = 2\chi_\beta \frac{\pi^2 D_w}{h_c}, \tag{7.3}$$

with χ_β determined by solving the system of equations (4.11). The aspect ratio β in this case is determined from the dimensions of the clear span of the web ($\lambda - c$). The onset of shear buckling is difficult to determine qualitatively; as noted above, however, it is accompanied by a reduction in panel stiffness. Therefore, $\overline{\mathcal{Q}}$ is determined from the load at which this reduction in stiffness is observed.

The stress on the face sheets is largest in the constant moment region ($\lambda \leq x \leq a - \lambda$). Equating the applied stress $\sigma = \mathcal{Q}\lambda d/2I_f$ to the buckling strength (Equation 6.14) yields the predicted critical load

$$\overline{Q}_f = \chi_f \frac{\pi^2 d D_f}{p\lambda}. \tag{7.4}$$

7.2.2 Shear Buckling Prototype

The shear buckling prototype was designed subject to the overall geometric constraints described in Section 7.1. The face sheet and web thicknesses were chosen to ensure shear buckling as the limiting failure mode (i.e. $\overline{Q}_f > \overline{Q}$). The search space was limited to standard US steel gauge thicknesses in the range of 0.61 mm (24 ga) to 1.90 mm (14 ga).

The geometry and material properties for the shear buckling prototype are given in Table 7.1. The sheet metal properties are assumed based on typical values for mild steel [129]. The predicted behavior of the panel under four-point bending is listed in Table 7.2. The panel is expected to have a stiffness of 7.57 MN/m up to a load of 13.2 kN, at which point shear buckling is predicted. The core shear failure is about double the shear buckling load (26.7 kN), so the panel is expected to have postbuckling strength in shear. A 64% reduction in stiffness is predicted following shear buckling. The predicted face sheet buckling load is 16.8 kN, high enough to ensure shear buckling is the critical failure mode.

7.2.3 Test Procedure

The test was performed in the Civil Engineering Structures Lab. The load was applied using hydraulic actuators with displacement control. Wood (dimensional lumber 38 mm thick) spreader blocks spanning the full panel width were used at both the load points and the support points to distribute the loads over a finite bearing length

Table 7.1. Geometry and material properties for the shear buckling prototype

t_f	0.92 mm
t_w	0.61 mm
h_c	254 mm
p	610 mm
a	2324 mm
λ	654 mm
c	114 mm
ρ_c	35.7 kg/m^3
E_c	2985 kPa
G_c	1293 kPa
E_f*	205 GPa
E_w*	205 GPa

* Assumed (typical for steel [129])

Table 7.2. Predicted behavior for the shear buckling test

Failure mode	**Load**
Shear buckling	13.2 kN
Stiffness (no buckling)	7.57 MN/m
Postbuckling Stiffness	2.74 MN/m
Face sheet buckling	16.8 kN
Core shear failure	26.7 kN

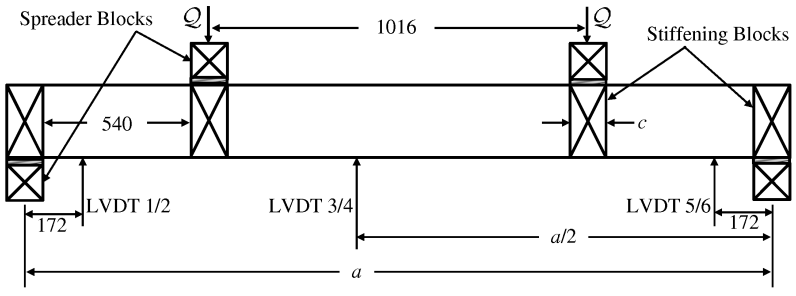

Figure 7.3. Dimensions and setup for the shear buckling test (all dimensions in mm)

of $c = 114$ mm. To ensure even load distribution and allow panel rotation at the supports, neoprene pads were placed between the spreader blocks and the panel. The load was applied by increasing the actuator displacement monotonically at a rate of 0.75 mm/min (0.03 in./min) until a drop in load was observed. Loading was applied symmetric about the panel midspan, with a separation of 1016 mm (40 in.) on-center between the load points.

To avoid the possibility of bearing failure for the shear buckling test, the webs were reinforced with 38 mm thick wood blocks at the support and load locations. These blocks had a width c and were placed to coincide with the locations of the spreader blocks at the load and support locations. The setup is illustrated schematically in Figure 7.3. The blocks were glued to the web and fastened to the flanges using screws, thus creating a load path through the wood and preventing bearing failure. The wood blocks used by the foam vendor to plug the panel for foaming were left in the panel for this test. The blocks were located in the bearing region and had no effect on deflection or shear buckling strength.

The actuators were equipped with load cells and displacement sensors. Because of the nonlinear compressive properties of the neoprene pads, the actuator displacement is not an accurate measure of panel displacement. Linear variable displacement transducers (LVDT's) were therefore used to obtain accurate measurements of panel displacement. Measurements of all sensor data were recorded at a frequency of 1 Hz. The dimensions and locations of the load points and LVDT's are illustrated in Figure 7.3. The LVDT's were located in six positions: one below each web, at the midspan and 172 mm from each support. This arrangement allowed accurate measurement of panel deflection by canceling out the rigid body motion due to compression of the neoprene pads. The midspan deflection $\mathcal{W}$ of the panel is determined by

$$\mathcal{W} = \mathcal{W}_{34} - \frac{\mathcal{W}_{12} + \mathcal{W}_{56}}{2}, \tag{7.5}$$

where $\mathcal{W}_{ij}$ is the average of the displacement readings from sensors i and j.

7.2.4 Results

The load-deflection data from the shear buckling test are plotted in Figure 7.4. Line fits to the pre- and postbuckling behavior are included. The observed stiff-

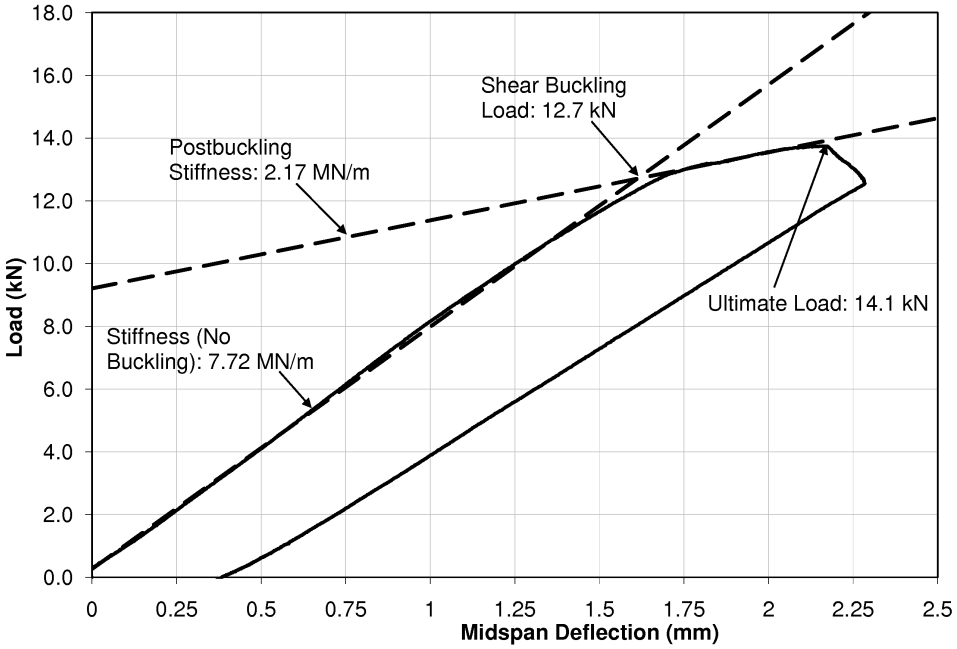

Figure 7.4. Load-deflection data for the shear buckling test

ness (i.e. slope of the load-deflection line) prior to shear buckling is 7.72 MN/m, and the observed postbuckling stiffness is 2.17 MN/m. Following the procedure recommended by Davies and Fragos [110,111], the shear buckling load is determined by the intersection of the two line fits to be 12.7 kN. The ultimate load observed in the test was 14.1 kN. The shear buckling and ultimate loads are indicated on the plot.

Shear buckling failure occurred in the webs between the loads and supports. Amplifications of the initial bowing imperfections (see Section 7.1) were observed early in the test. As the applied load approached the buckling strength, these deformations developed into the diagonal wave pattern characteristic of shear buckling failure, shown in Figure 7.5(a). As the load increased beyond the buckling strength, one buckling peak grew disproportionately larger than the others. Investigation of the failed panel revealed debonding between the web and foam beneath this peak. Foam crushing was observed beneath the largest buckling trough.

Ultimate failure was by fracture of the foam in shear. The fracture pattern, shown in Figure 7.5(b), matches that reported in the literature for the shear failure of foam core sandwich panels (e.g. [38]). The crack initiated near the neutral bending axis and spread downward to the lower (tensile) face sheet, along which it then propagated as a debonding fracture mode.

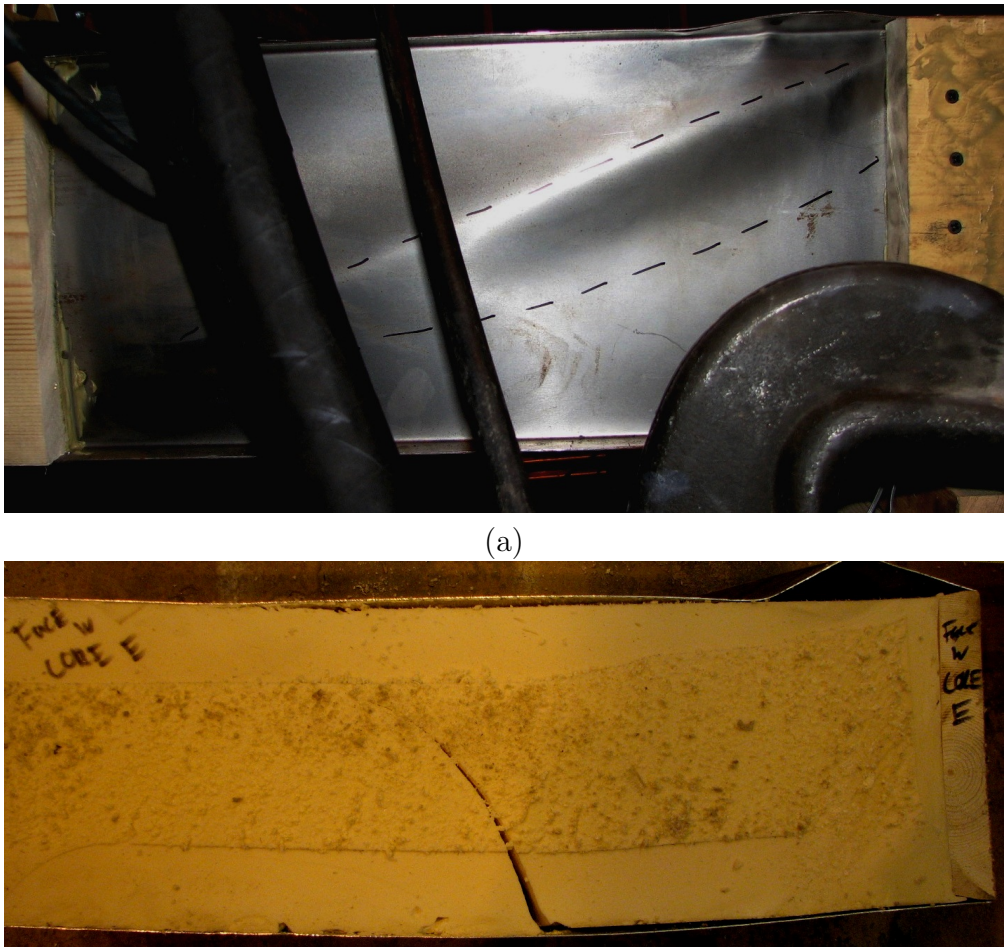

(a)

(b)

Figure 7.5. Observed panel failure modes: (a) web shear buckling, and (b) core shear fracture.

7.2.5 Discussion

The observed behavior of the shear buckling test is compared to the predicted behavior and summarized in Table 7.3. The predicted shear buckling strength (13.2 kN) is about 4% greater than the observed strength of 12.7 kN. The agreement between predicted and observed buckling strengths is reasonable considering the variability that is typical of buckling tests. The observed panel stiffness prior to shear buckling agrees to within 2% of the predicted value of 7.57 MN/m. The observed postbuckling stiffness is about 21% lower than predicted. This difference may be partly attributable to damage in the foam following the initial buckling. In addition to the debonding and crushing at the interface with the webs, some debonding with the face sheet

Table 7.3. Predicted vs. observed shear buckling test behavior

Failure Mode	**Predicted**	**Observed**
Shear buckling	13.2 kN	12.7 kN
Stiffness (no buckling)	7.57 MN/m	7.72 MN/m
Postbuckling stiffness	2.74 MN/m	2.17 MN/m
Ultimate strength	N/A	14.1 kN

was also observed. This debonding may have reduced the panel stiffness enough to account for the difference between predicted and observed values.

7.3 Bearing Strength Model Validation

Validation of the bearing strength model was obtained through non-symmetric three-point bending tests. This configuration allowed for two tests on each panel, one on each end. The support not under test was located at a distance $\approx\lambda$ from the panel edge to avoid supporting the panel (for the second bearing test) over the region damaged by the first test. In this test, the applied load $\mathcal{Q}$ was measured along with actuator displacement, used to determine the onset of bearing failure.

7.3.1 Bearing Failure Test Model

The shear and bending moment diagrams for the bearing failure tests are illustrated in Figure 7.6. Bearing failure occurs at the support closer to the load point ($x = 0$). The load on the web at $x = 0$ is the reaction force V, given by

$$V = \mathcal{Q}\left(1 - \frac{\lambda}{a}\right). \tag{7.6}$$

The applied load $\overline{\mathcal{Q}}$ to cause bearing failure is thus

$$\overline{\mathcal{Q}} = \frac{\overline{Q}}{1 - \frac{\lambda}{a}}, \tag{7.7}$$

with $\overline{Q}$ determined using Equation (5.16). The strength predictions in this chapter are calculated using $F_C = 1$ (i.e. no reduction factor). In Section 7.3.4, a value of F_C for panel design is recommended based on the test results. Bearing failure is accompanied by a partial or complete loss of panel stiffness. This behavior is observed as a change in slope or a limit load, respectively, on a plot of $\mathcal{Q}$ versus actuator displacement.

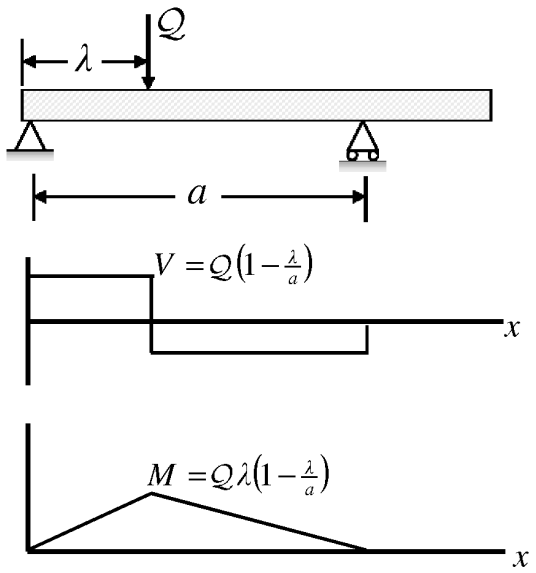

Figure 7.6. Shear and bending moments for the bearing failure tests

Web shear buckling is possible in the region $0 \leq x \leq \lambda$. From the shearing force V in that region, Equation (7.6), the predicted critical shear buckling load $\overline{Q}_w$ is

$$\overline{Q}_w = \chi_\beta \frac{\pi^2 D_w}{h_c \left(1 - \frac{\lambda}{a}\right)}. \tag{7.8}$$

Face sheet buckling is possible near the load point ($x = \lambda$), where the bending moment is greatest. Because of expected postbuckling strength, the onset of buckling does not affect the bearing strength results as long as bearing failure occurs at a distinctively different load than face sheet buckling. Based on the maximum bending moment, the critical load $\overline{Q}_f$ for face sheet buckling is predicted by

$$\overline{Q}_f = \chi_f \frac{\pi^2 d D_f}{p\lambda \left(1 - \frac{\lambda}{a}\right)}. \tag{7.9}$$

The face sheet sections are not long (aspect ratios λ/p and $(a - \lambda)/p$ both less than 4), so Equation (7.9) underestimates the face sheet buckling strength by as much as 50% (due to the non-uniform loading, see Reference [116]). Face sheet buckling is not a concern for the present tests, so the effect of non-uniform loading is neglected.

7.3.2 Bearing Failure Prototypes

Two panels labeled "A" and "B" were tested to validate the bearing strength model. The panels were designed, subject to the constraints in Section 7.1, with bearing failure as the limiting failure mode. A depth of 235 mm was specified for both panels to allow reinforcement of the webs by dimensional lumber during the foaming process. The prototype geometry is detailed in Table 7.4.

The panels were hot-dip galvanized prior to foaming to provide a clean surface for foam adhesion. The galvanizing process for Panel B was not well controlled, however, and the webs had an extremely thick coating layer as a result. Measurements of the base metal and of coating chips revealed a coating thickness of 0.56 mm on each side of the base metal (the standard coating thickness is 4.5 μm [135]). The coating accounted for about half the total thickness of the webs and had a significant effect on material properties. The effective material properties of the web were taken with respect to the total thickness (i.e. including the coating). The elastic modulus and yield strength of zinc are much less than those of steel [136], so the properties of the web are weaker than those of solid steel. The coating on the face sheets was within specified limits, and the face sheet thickness for Panel B matched that of Panel A. The material properties of the face sheets were not appreciably affected by the galvanizing process.

The material properties for the bearing tests are given in Table 7.5. As with the shear buckling test, the foam properties were obtained by BASF. The metal properties were obtained through tensile tests per ASTM A-370 [137]. Test coupons were cut from undamaged portions of each web and from one of the face sheets. The specimens

Table 7.4. Geometry of the bearing failure prototypes

	Panel A	**Panel B**
t_f	1.68 mm	1.68 mm
t_w	0.92 mm	2.26 mm
h_c	235 mm	235 mm
p	610 mm	610 mm
a	1816 mm	1791 mm
λ	546 mm	556 mm
c_e	140 mm	114 mm
c_i	114 mm	184 mm

Table 7.5. Material properties for the bearing failure prototypes

	Panel A	**Panel B**
ρ_c	30.8 kg/m^3	33.6 kg/m^3
E_c	2339 kPa	2413 kPa
G_c	1054 kPa	1160 kPa
σ_{uc}	104 kPa	121 kPa
τ_c	156 kPa	188 kPa
E_w	194 GPa	136 GPa
σ_{yw}	225 MPa	172 MPa
σ_{yf}	286 MPa	286 MPa

Table 7.6. Strength predictions for the bearing failure tests

Model	**Panel A**	**Panel B**
Bearing strength	22.0 kN	34.0 kN
Face sheet buckling	29.4 kN	31.2 kN
Shear buckling	25.2 kN	98.5 kN

from the webs were cut in the (y-) direction of panel depth, and the specimen from the face sheet was cut in the length (x-) direction. The web material properties for Panel A are typical of mild steels [129].

The predicted behavior for the bearing failure prototypes is listed in Table 7.6. In addition to bearing strength, predictions of face sheet buckling and shear buckling strength are also provided. The predicted shear buckling load for both panels is greater than the load for bearing failure. The predicted face sheet buckling strength of Panel B is less than the bearing strength due to the fabricating irregularities discussed above. However, accounting for the considerations in the previous section, face sheet buckling was not expected to occur during the test on Panel B. In fact, careful examination of the panel during and after the test revealed no evidence of face sheet buckling.

7.3.3 Test Procedure

The bearing failure prototypes were tested per the "end one-flange" loading configuration prescribed by steel design codes [102]. The key requirement for this configuration is a minimum clear distance of $1.5h_c$ between the load and support[1]. The tests described in this chapter were performed with a clear distance of $\approx 1.8h_c$. All of the

[1]Accounting for the supports, the clear distance is $\lambda - (c_e + c_i)/2$ for the setup in Figure 7.1

wood reinforcing blocks used for foaming were removed for this test: to provide an undamaged, unstiffened bearing surface, the blocked ends (yz-faces) were cut off.

As with the shear buckling test, spreader blocks were used at both the actuator and the supports to spread the load across the full panel width and over a finite bearing length. The bearing lengths at the load and support points were c_i and c_e respectively, chosen to ensure failure at the support. As with the shear buckling test, neoprene pads were placed between the spreader blocks and the panel. The load was applied by increasing actuator displacement at a rate of 0.38 mm/min (0.015 in./min) until a limit load was observed. Bearing failure was observed visually at the supports and correlated to the load at failure using load-displacement data from the actuator. The actuator displacement includes deformation of the neoprene pads in addition to panel displacement. Due to compression of the neoprene pads, large initial displacements (≈8–10 mm) were observed at low loads. Following this initial displacement, the compressive modulus of the neoprene became nearly constant [138], and the load-displacement behavior of the actuators allowed accurate determination of bearing strength.

7.3.4 Results

With the exception of one test on Panel A, the general behavior was the same for all tests. The panels exhibited linear load-deflection behavior (following the initial non-linearity due to the neoprene pads) up to the onset of end bearing failure. Following end failure, the panels continued to bear load, though with greatly reduced stiffness, until interior bearing failure occurred. The latter mode led to ultimate panel failure in every case. In this section, qualitative descriptions of the bearing failure modes are provided, followed by quantitative descriptions of the individual test results.

The observed end bearing failure mechanism is shown in Figure 7.7. Figure 7.7(a) shows an end view of the webs, and Figure 7.7(b) shows a side view. Together the photographs demonstrate that the failure mode qualitatively matches the expected end failure mechanism (Figure 5.2), i.e. two yield lines meeting at a plastic hinge on the lower face sheet. The bearing length c_e is indicated to show the extent of the damage. The webs lose their bearing capacity following the formation of the hinge, so any residual panel strength comes from the foam. Although the foam crushed

(a)

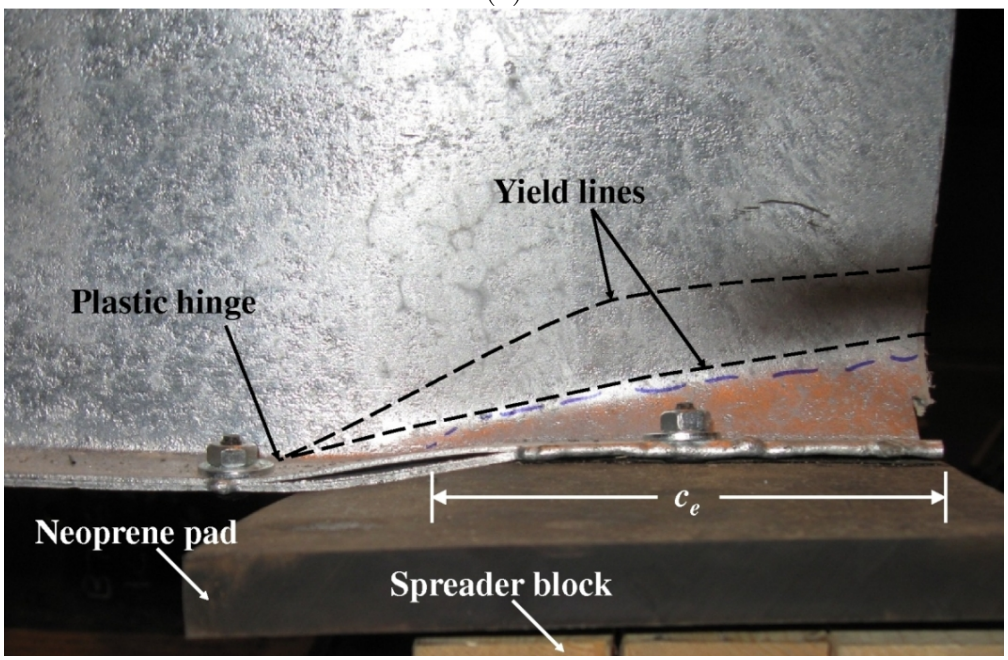

(b)

Figure 7.7. Bearing failure mode: (a) end view, and (b) side view showing the location of yield lines

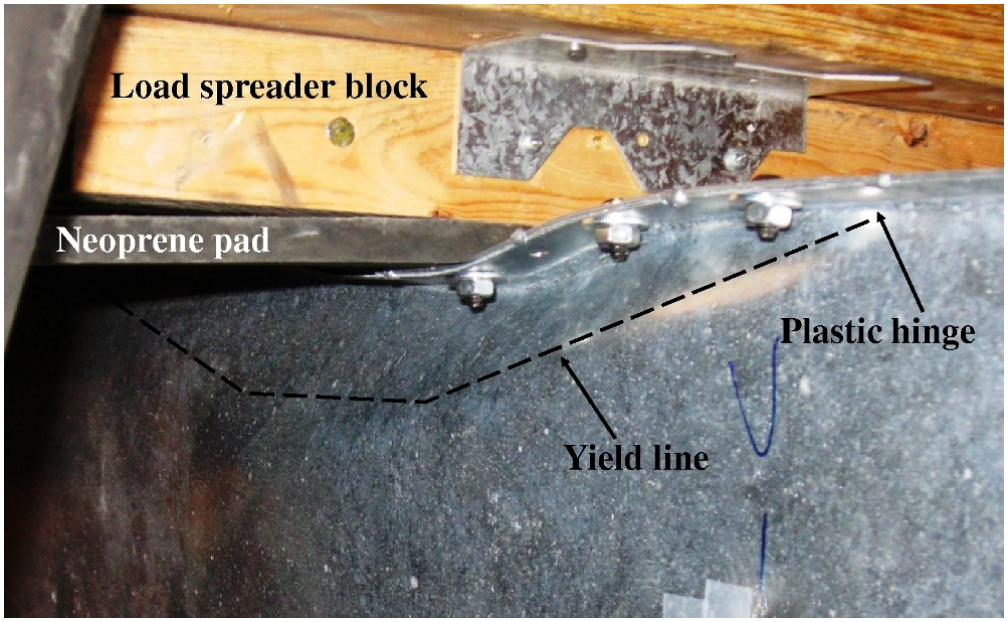

Figure 7.8. Interior bearing failure mode with yield line

in the region near the failed webs, densification and the transfer of stresses into the surrounding material allowed the bulk of the foam to carry additional loads.

The interior bearing failure mode, shown in Figure 7.8, resembled the interior web crippling mode typically reported in the literature (e.g. [100]). As with end bearing failure, it is characterized by the formation of yield lines meeting at plastic hinges. In this case, however, damage to the web was accompanied by yielding of the compressed face sheet, leading to ultimate panel failure. Interior bearing failure is not a concern for simply supported roof panels; therefore, no analysis of the interior bearing failure mode is provided here beyond a reporting of the observed strengths.

The load-deflection data for the bearing tests are plotted in Figure 7.9 for Panel A and in Figure 7.10 for Panel B. Each figure has two plots corresponding to the tests on each end of the panels. The loads corresponding to end and interior bearing failure are indicated on the plots. The end failure load $\overline{\mathcal{Q}}$ was determined by the same procedure used to determine the shear buckling load in Section 7.2 (i.e. intersection of line fits to the behavior before and after failure).

End 1 of Panel A had significant initial debonding between the webs and core material. As a result, the behavior was very different from that observed in the other bearing tests. The load-displacement results, plotted in Figure 7.9(a), indicate the behavior

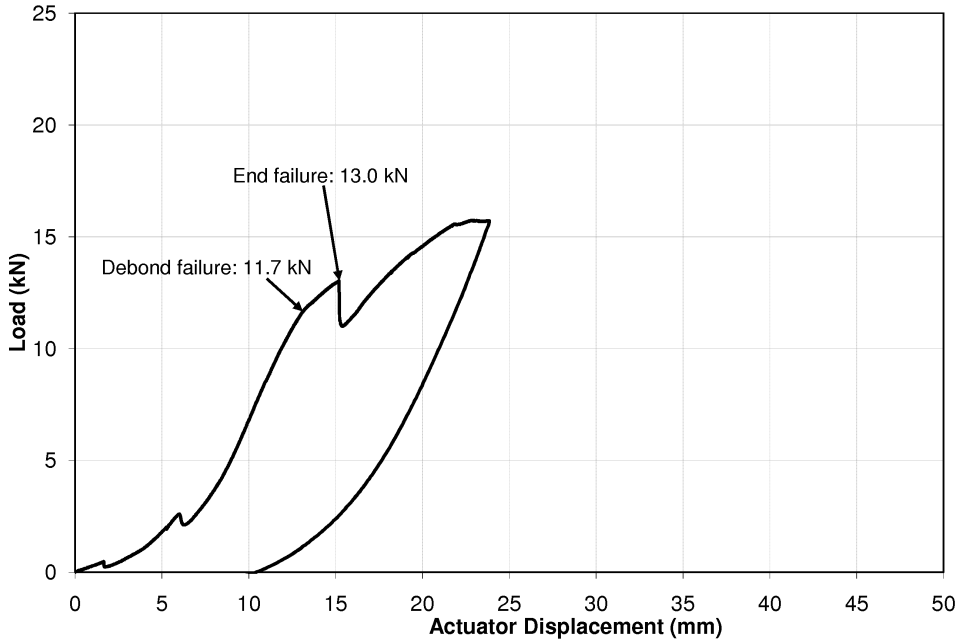

(a)

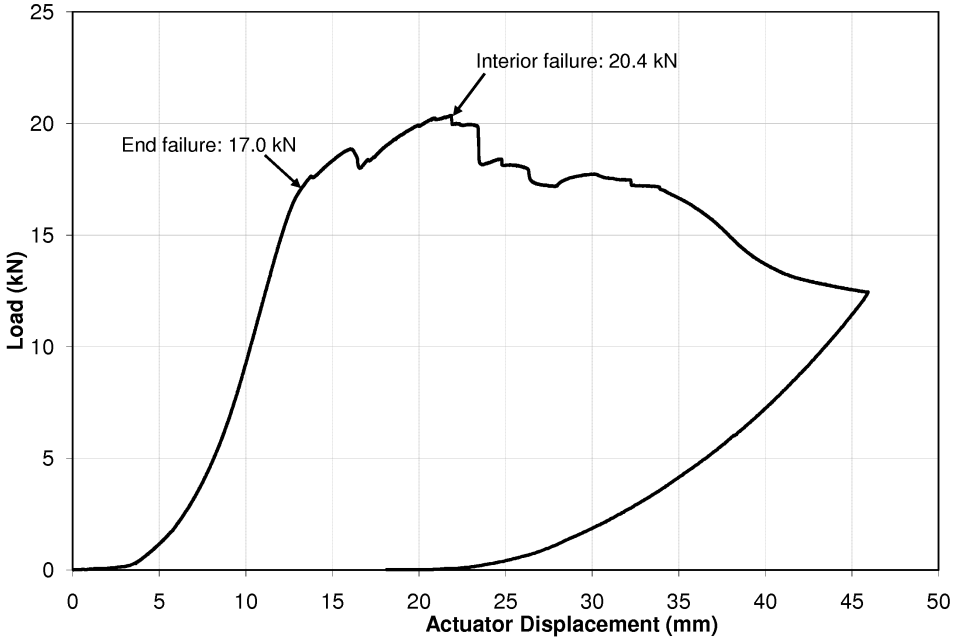

(b)

Figure 7.9. Load vs. displacement for the tests on Panel A: (a) end 1 (containing an initial debonding imperfection), and (b) end 2

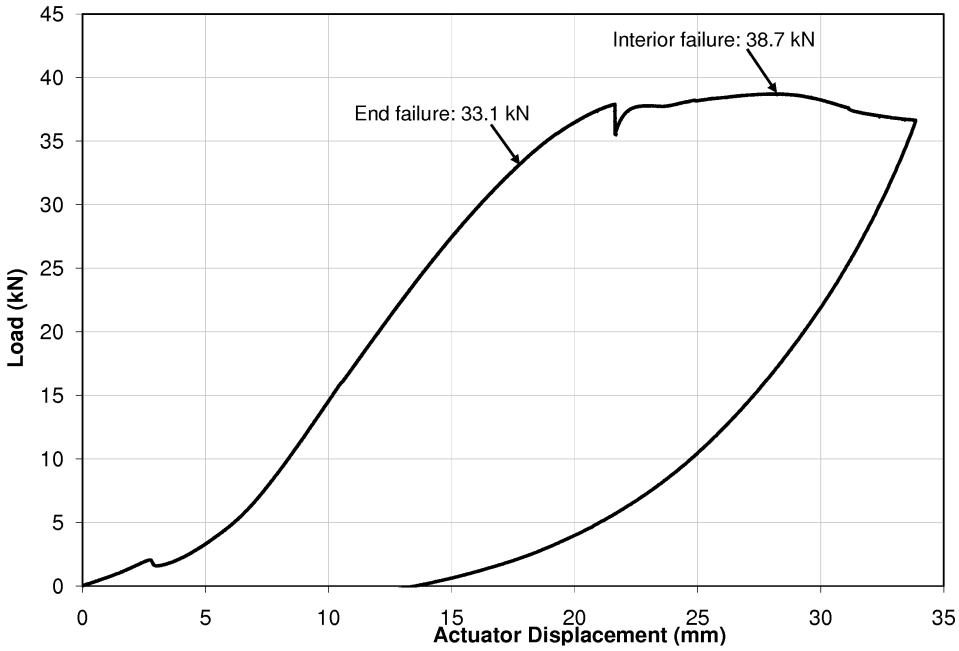

(a)

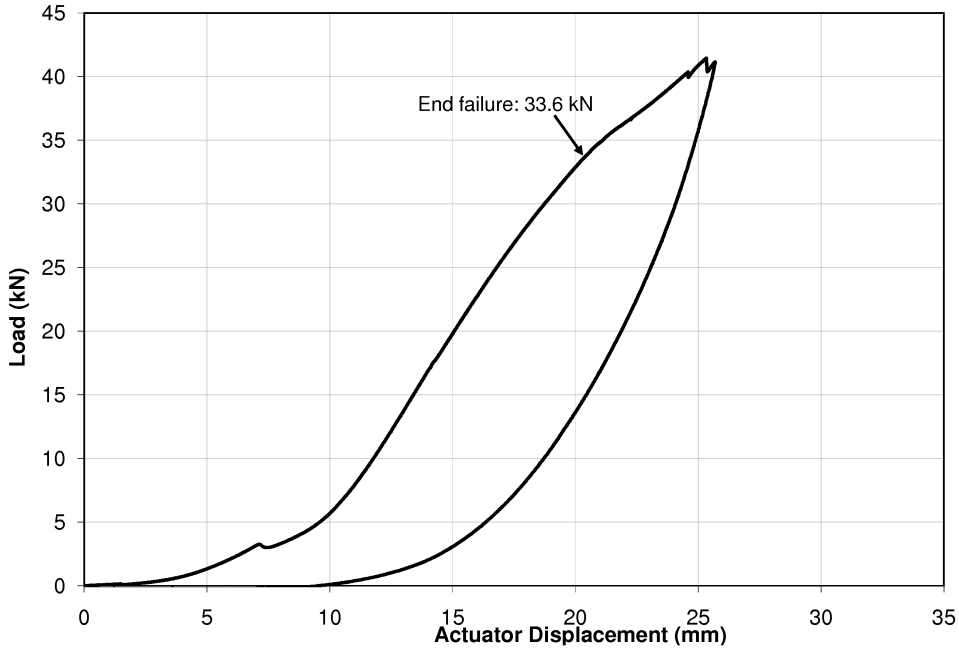

(b)

Figure 7.10. Load vs. displacement for the tests on Panel B: (a) end 1, and (b) end 2

was approximately linear up to a load of 11.7 kN. At this point, the initial debonding suddenly propagated deep in the x-direction. This propagation was accompanied by shear buckling of the newly-debonded web. Bearing failure occurred along yield lines immediately below the debond at a load of 13.0 kN and caused further propagation of the debond, resulting in a sharp decrease in load. Following this behavior, the panel continued to bear load until the test was stopped at a load of 15.7 kN due to the onset of interior bearing failure.

End 2 of Panel A experienced end bearing failure at a load of 17.0 kN. A small limit load occurred at 18.9 kN when the webs creased along the yield lines, leading to a loss of web bearing capacity. Interior bearing failure occurred at 20.4 kN. The decrease in load following the interior failure is non-smooth and non-monotonic because the failure occurred via a series of incremental yielding and propagations of the debonded region. This behavior was not observed in the tests on Panel B because interior bearing failure occurred on that panel without debonding.

The test on end 1 of Panel B was paused for several minutes at a displacement of 21.7 mm for visual inspection. Because end failure of the web had commenced (at a load of 33.1 kN), the damaged region continued to grow (due to foam creep below the crippled web) during this period. The result, as seen in Figure 7.10(a), was a load relaxation of about 2 kN. When the test was resumed, the load ramped quickly back to the previous load ($\approx$37.9 kN). Interior failure occurred at a load of 38.7 kN and was ultimate. End failure occurred on end 2 of Panel B at a load of 33.6 kN. At a load of about 41 kN, the load spreader block failed, and the panel was immediately unloaded. The test was repeated following replacement of the spreader block by a thicker laminated wood beam. Interior failure occurred at a load of 48.2 kN and was ultimate.

7.3.5 Discussion

The observed bearing strengths $\overline{\mathcal{Q}}$ are compared to the predicted strengths $\overline{\mathcal{Q}}_a$ in Table 7.7. The accuracy of the predictions is assessed via the ratio of predicted to observed strength, $\overline{\mathcal{Q}}_a/\overline{\mathcal{Q}}$, also included in the table. The results indicate that the model in this work overpredicts bearing strength by about 11% on average, although the strength of Panel B was predicted more accurately than that of Panel A.

Table 7.7. Predicted ($\overline{\mathcal{Q}}_a$) vs. observed ($\overline{\mathcal{Q}}$) bearing strength results

Test	$\overline{\mathcal{Q}}_a$	$\overline{\mathcal{Q}}$	$\overline{\mathcal{Q}}_a/\overline{\mathcal{Q}}$
Panel A end 2	22.0 kN	17.0 kN	1.29
Panel B end 1	34.0 kN	33.1 kN	1.03
Panel B end 2	34.0 kN	33.6 kN	1.01

To understand the differences between the two prototypes, the results in terms of $\overline{\mathcal{Q}}/\overline{\mathcal{Q}}_a$ are illustrated graphically in Figure 7.11. Multiple columns are given for each panel. The first column shows the breakdown of the web and core contributions to total strength, and the other columns compare test data to the predicted strengths. In Panel A, the core contributes 77% of the predicted bearing strength. In Panel B, the core contribution is 33% of the total strength. If the predicted contribution $\overline{Q}_w$ from web crippling is taken as exact, the results indicate the core contribution is overestimated by about 18%. This result is consistent with that in Reference [100] for web crippling with no foam, i.e. Equation (5.2) overpredicts $\overline{Q}_w$ by 25% on average if no reduction factor F_R is applied.

Although the sample size in this work is limited, the results suggest the foam may reduce the variability in bearing strength compared that of webs with no foam. Roberts and Newark [100] reported a spread of ±45% in observed web crippling strength. The results in this work had a spread of ±14% which appears to be related at least in part to the difference in relative web contribution between the two panels. The foam is less sensitive than the webs to imperfections and is thus expected to provide a more repeatable contribution to bearing strength than that of the webs.

7.4 Conclusions

The prototype tests reported in this chapter validated the models for the effect of core material on the shear buckling and bearing strength of the webs in foam-filled panels. The test described in Section 7.2 validated the deflection and shear buckling models, both of which predicted the observed results to within 4%. The test also showed that the postbuckling stiffness can be predicted with reasonable accuracy by assuming the buckled webs do not contribute to panel stiffness. The latter result is useful as an indication that shear buckling is not an ultimate failure mode in foam-filled panels if the core material has sufficient shear strength. Although designs that exploit the posbuckling capacity are not recommended due to the dependence on the foam, the

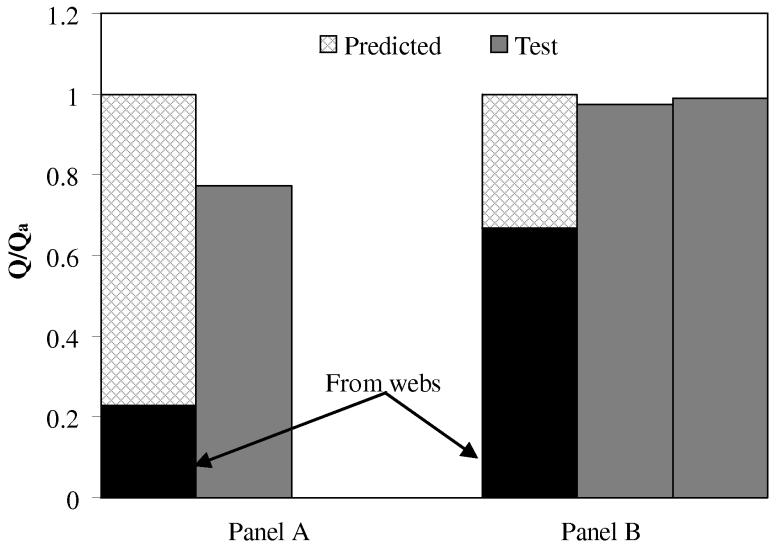

Figure 7.11. Predicted vs. observed bearing strength; the predicted strengths indicate the relative contribution from the webs (dark shading) and the core (hatched)

results suggest shear buckling in foam-filled panels is not as harmful as in empty panels. More thorough investigation of the postbuckling behavior is recommended by this work, as it may be reasonable to reduce the safety factors for shear buckling in panel design.

The bearing strength of foam-filled panels was overestimated somewhat by the mechanism model developed in this work. Based on the breakdown of predicted strength from the webs versus that from the foam, the results suggest the core contribution is overpredicted by about 18%. The observed variability in strength was less than that reported in the literature for webs with no foam. As a result, it may be possible to use reduced safety factors (compared to current design code) in design as long as compensation is made for the overestimation of foam strength. This compensation can be achieved by reducing the calculated core contribution or (for panels with slender webs) by neglecting the contribution from web crippling.

Chapter 8

Design of Two-Layer Web Core Roof Panels

Insulated steel sandwich panels offer several advantages over conventional construction techniques for residential roof design, including improved energy efficiency, durability, decreased construction costs, and amenability to integrated solar panels or other energy-saving technology. Web core panels (foam core panels with internal webs) provide these benefits, but the webs have a substantial impact on thermal insulating performance. The webs create a thermal bridge between the face sheets, resulting in the need to use additional insulation to achieve a desired R-value. An alternative concept investigated in this chapter is the two-layer web core panel, in which thermal performance is provided in part by an additional insulating layer. The impact of the insulating layer on panel performance is provided, as well as an investigation of the substantial tradeoff between total panel depth and weight. Minimum weight designs are developed for three representative load conditions to investigate the impact of the insulating layer on design. The designs are shown to also minimize material cost because cost and weight are both sensitive to face sheet thickness. The results show that, in some cases, two-layer panels allow reductions in weight and material cost compared to panels with no external insulating layer. The reductions are particularly significant when large loads are applied.

8.1 Introduction

Steel sandwich panels offer several advantages over conventional construction techniques for residential roof design. These advantages include improved energy efficiency [3, 5, 8] and durability [13], and decreased construction costs [9]. Foam core panels (SIPs) have been used successfully in residential wall structures, but they are ill-suited to meet the unique challenges of roof applications. Roofs are required to sustain transverse loads over unsupported spans up to 6.8 m while simultaneously providing thermal insulation. Foam core panels rely on the polymer foam core material to provide transverse shear stiffness. Creep in the core material leads to excessive deformations over the lifetime of a roof.

Web core panels, illustrated in Figure 8.1, are a solution to the limitations of foam core roof panels. Web core panels are foam filled panels with thin metal webs connecting the face sheets. The webs provide greater shear stiffness than the core material and are not subject to creep. However, they create a thermal short between the face sheets, leading to reduced thermal insulating performance. Additional insulating material is necessary to compensate for the reduced thermal performance of the webs. The additional material can be added to the core, as in Figure 8.1(a). It can also be added as an external insulating layer, Figure 8.1(b). In the extreme case, Figure 8.1(c), the insulating material is removed from the structural layer entirely. An example of such a two-layer panel with a metal core is the truss core panel, for which roof designs were developed in Reference [27].

The design considerations for web core panels with no external insulating layer, Figure 8.1(a), were investigated in Chapter 6. It was shown that roof panel designs are determined by consideration of four limit states: thermal insulating performance, panel deflection, face sheet buckling, and shear buckling of the webs. The thermal performance and shear buckling strength are particularly limiting because large panel

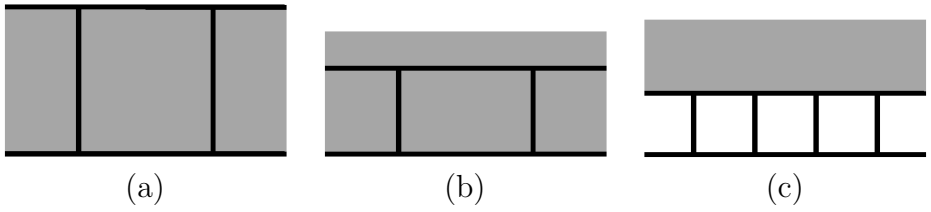

Figure 8.1. Sandwich panel concepts for roofs: (a) web core, (b) two-layer web core, and (c) two-layer metal core

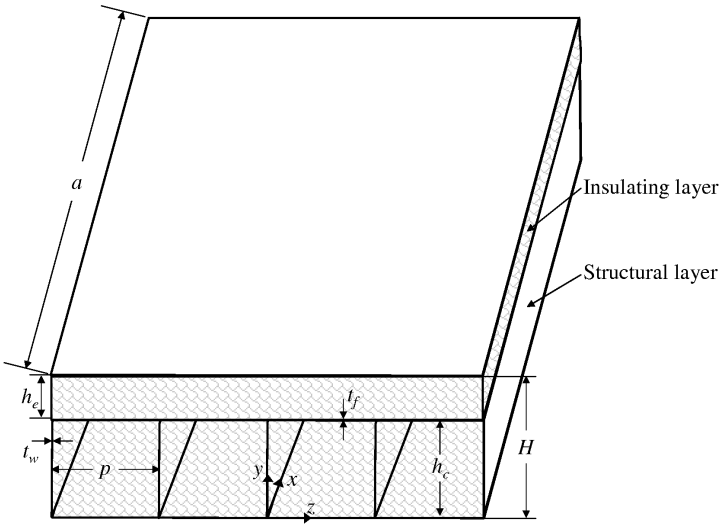

Figure 8.2. Two-layer web core panel geometry and coordinate system; the insulating layer is placed on the exterior or interior face of the structural layer depending on climate

depths are required to meet both requirements simultaneously. One way to reduce the impact of the thermal requirement is to use web materials with low thermal conductivity. For example, stainless steel webs allow reductions in core depth of up to 90 mm compared to panels with carbon steel webs.

A potential drawback to the use of stainless steel webs is cost (the material cost of stainless steel is 3.6 times that of carbon steel [18]). Other materials with low thermal conductivity (e.g. composites) are likely also expensive and tend to have lower stiffness than steel. The two-layer panel, Figure 8.1(b), is proposed in this chapter as an alternative to the concept described in Chapter 6. The structural layer is a foam-filled web core panel with carbon steel webs. The contribution to thermal performance is significant but generally limited by the influence of the webs.

The geometry of two-layer web core panels is illustrated in Figure 8.2. The face sheet and web thicknesses are t_f and t_w, and the web spacing is p. The structural layer has a core depth h_c, and the insulating layer has a depth h_e. The total foam depth is thus $H = h_c + h_e$. The insulating layer can be located on the exterior or interior face of the panel. The choice of location is based on hygrothermal performance and depends on climate [2]. As a rule of thumb, the insulating layer should be located on the colder face to keep the interface between the structural and thermal layers warm and thereby minimize the risk of condensation (leading to corrosion) within the panel [139]. Thus, in warm (dry) climates, the foam is located on the interior

face. In cold climates, the foam is located on the exterior face. Two-layer panels are not recommended for warm climates with high humidity due to the high risk of condensation for either placement of the insulating layer [26].

This chapter is focused on the design of two-layer web core panels for roofs. The influence of the insulating layer on thermal and structural performance is investigated, along with the resulting impact on feasible panel designs. A sensitivity analysis is performed to investigate the tradeoff between panel depth and weight and to determine a suitable approach to design. The approach is demonstrated through the design of web core panels subject to the requirements of typical roofs in three US climate zones. Because of the tradeoff between depth and weight, minimum material cost is proposed as a design objective. Minimum cost designs are shown to match the designs for minimum weight. The results in this chapter demonstrate that, with carbon steel webs, two-layer panels allow reductions in weight, foam use, and material cost compared to panels with no external insulating layer.

8.2 Design of Two-Layer Panels

It was demonstrated in Chapter 6 that roof panel design is dictated by four limit states: thermal performance, panel deflection, face sheet buckling, and shear buckling of the webs. The same considerations are applicable to the design of two-layer panels, but slight modifications to the R-value and deflection models to account for the effect of the insulating layer on the temperature distribution. The considerations related to that effect are discussed in this section, along with validation of the the thermal model and a discussion of the impact of the insulating layer on the feasible panel design space.

8.2.1 Effect of the Insulating Layer on Panel Performance

The thermal insulating performance is evaluated by the R-value, which is a measure of the resistance of the panel assembly to conductive heat transfer. Higher R-values translate to improved energy performance by reducing the heating and cooling loads in the interior space. The R-value is determined in this work using the isothermal planes method for one-dimensional heat transfer [30]. In this method, the panel is approximated as a thermal resistance network, illustrated in Figure 8.3. The temperatures of the interior and exterior faces are T_i and T_e respectively. The temperature

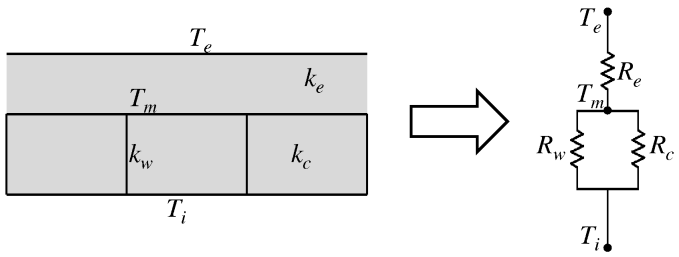

Figure 8.3. Isothermal planes approximation for two-layer web core panels; each component has a thermal conductivity k_i corresponding to a resistance R_i in the circuit diagram

T_m is assumed uniform along the entire interface between the structural and thermal layers. The webs, core, and insulating material have thermal conductivity k_w, k_c, and k_e, respectively.

A key assumption of the present approach is that the interface temperature T_m is uniform across the entire section. In reality, the webs provide a thermal short, and a slight variation in T_m exists across the panel width (< 2°C when the gradient across the panel is 55°C [74]). The implications of this variation for the accuracy of the isothermal planes method are examined in Section 8.2.2.

The assembly in Figure 8.3 shows the webs, core, and insulaing layer have R-values R_w, R_c, and R_e, respectively. These R-values are given by

$$R_w = \frac{h_c}{k_w \frac{t_w}{p}}, \tag{8.1}$$

$$R_c = \frac{h_c}{k_c \left(1 - \frac{t_w}{p}\right)}, \tag{8.2}$$

$$R_e = \frac{h_e}{k_e}. \tag{8.3}$$

The overall R-value of the panel is found by combining the resistances, i.e.

$$R = \left(R_w^{-1} + R_c^{-1}\right)^{-1} + R_e = \frac{h_c}{k_w \frac{t_w}{p} + k_c \left(1 - \frac{t_w}{p}\right)} + \frac{h_e}{k_e}. \tag{8.4}$$

In the present work, the same foam material is used in both the core and the insulating layer, so $k_e = k_c$. Equation (8.4) shows that, in terms of thermal performance, the foam is necessarily more effective in the insulating layer than in the structural layer. The most effective use of foam in a web core panel is therefore one in which

the structural layer is designed independent of the thermal requirements and the insulating layer is used to provide additional R-value as needed.

The analysis of panel deflection in Reference [29] includes a thermal contribution due to the temperature gradient across the face sheets. The use of an insulating layer affects panel deflection by reducing the thermal gradient across the structural layer. Referring to Figure 8.3, the temperature difference across the structural layer is $\Delta T_i = T_i - T_m$, given by

$$\Delta T_i = \Delta T \frac{R_i}{R}, \tag{8.5}$$

where $\Delta T = T_i - T_e$ is the gradient across the whole panel, and $R_i = (R_w^{-1} + R_c^{-1})^{-1}$ is the R-value of the structural layer. As the thickness h_e increases, thermal deflection decreases. The use of an insulating layer does not affect the local buckling strength of the face sheets and webs.

8.2.2 Validation of the Thermal Performance

The equations in the previous section were derived by lumping the panel assembly into a one-dimensional heat transfer model. This approach is effective for determining the R-value of panels with no external insulating layer, but it is not entirely accurate for two-layer panels. The webs create thermal bridges through the structural layer that result in variations in temperature along the interface with the thermal layer. As a result, the problem is inherently two-dimensional, and the present approach underestimates the R-value somewhat [74]. Given the importance of the thermal requirement in determining feasible designs, it is desirable to understand the impact of the temperature variations on the accuracy of the isothermal planes approach. To that end, a finite element study of the thermal performance of two-layer panels was performed.

Note that Equations (8.4) and (8.5) can be rearranged as

$$\frac{R}{R_i} = 1 + \frac{R_e}{R_i}, \tag{8.6}$$

$$\frac{\Delta T_i}{\Delta T} = \frac{R_i}{R}. \tag{8.7}$$

The panel performance is expressed in terms of the structural layer properties to allow for the limiting case of panels with no insulating layer. The work in this section

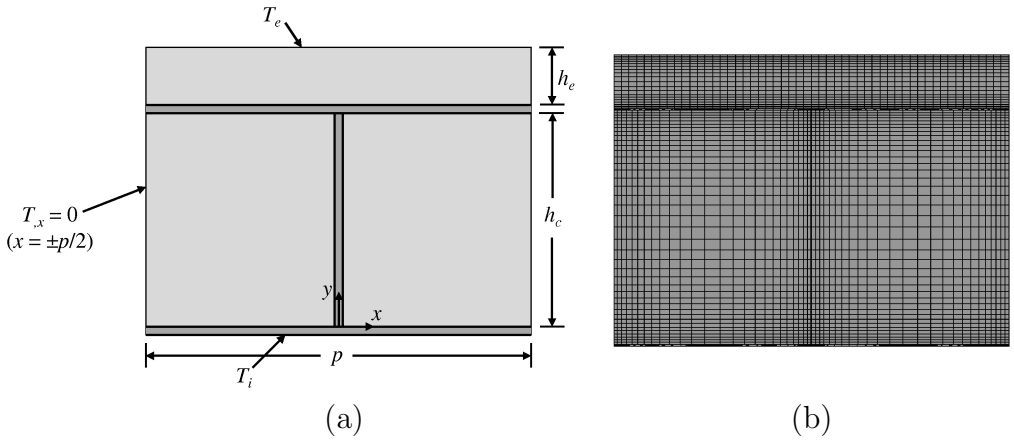

Figure 8.4. Finite element model and boundary conditions for the analysis of thermal performance in two-layer panels: (a) schematic illustration with metal thicknesses exaggerated for clarity, and (b) typical mesh

is performed using carbon and stainless steel webs to illustrate the effect of web properties on the accuracy of the present model.

The finite element model used for the present study is illustrated schematically in Figure 8.4(a). It is a panel cross section of width p, centered in a web. The face sheets, web, and insulating material are all modeled in ANSYS using PLANE77 elements. The PLANE77 a quadrilateral thermal element that uses a quadratic shape function and was chosen to provide accurate modeling of the thin metal sections with only a few elements through the thickness. A uniform temperature T_i is applied on the interior surface and a temperature T_e is applied on the exterior surface. The planes of symmetry ($x = \pm p/2$) are modeled by imposing zero heat flux, i.e. $T_{,x} = 0$. Carbon and stainless steel webs are modeled, and the panel geometry is allowed to vary.

Figure 8.4(b) shows a typical mesh used in the analysis. The face sheets and webs had 2 elements in the direction of thickness, and the rest of the panel was meshed using 50 elements in the x-direction. The core was meshed using 40 elements in the y-direction, and the insulating layer used 25 elements in the y-direction. The mesh density in the core and insulating layer was varied so that the elements near the boundaries were smaller than the elements in the centers. To check for convergence, the analysis was repeated after doubling the mesh density. Both R and T_m changed by 0.1% after refining, so the mesh in Figure 8.4(b) was deemed adequate.

The R-value of the panel assembly is determined from the calculated heat flux $q_y^{'}$ at the exterior surface. Following the circuit analogy for one-dimensional heat transfer, the R-value of the panel assembly (per unit panel length) is

$$R = \frac{\Delta T}{q_y} p, \tag{8.8}$$

where q_y is the total heat transfer across the surface, obtained by numerically integrating $q_y^{'}$ along the panel width.

Equation (8.5) is validated by averaging the temperature along the interface between the structural and thermal panel layers ($y = h_c + t_f$). The averaged interface temperature T_m is

$$T_m = \frac{1}{p} \int_{-p/2}^{p/2} T\Big|_{y=h_c+t_f} dx, \tag{8.9}$$

and $\Delta T_i = T_i - T_m$. Validation of ΔT_i is important because thermal deflection can be an important concern in panel design (Chapter 6).

The R-value ratio R/R_i is plotted as a function of R_e/R_i in Figure 8.5. For reference, Equation (8.6) is plotted as a dashed line. For panels with carbon steel webs, the model in this work predicts panel R-value to within 3%. In panels with stainless steel webs, the model is accurate to within less than 1%. This result makes sense because the thermal bridging effect of stainless steel webs is significantly less than that of carbon steel webs.

The relative temperature drop $\Delta T_i/\Delta T$ across the structural panel layer is plotted as a function of R_i/R in Figure 8.6, with Equation (8.7) included as a dashed line for reference. As with the previous figure, the present model predicts ΔT_i to within about 3% with carbon steel webs and to within less than 1% with stainless steel webs. The temperature varies along the interface by up to 3°C, consistent with the results reported in Reference [74]. The variation in temperature decreases along with R_i/R, reflecting the decreased ability for thermal shorts to affect R-value as the structural layer contributes less to thermal performance. As a consequence, the accuracy in $\Delta T_i/\Delta T$ improves systematically as R_i/R decreases.

The results in this section indicate that the isothermal planes method accurately predicts the thermal performance of two-layer web core panels. Although the interface between the layers allows for two-dimensional heat transfer, the impact on R-value and

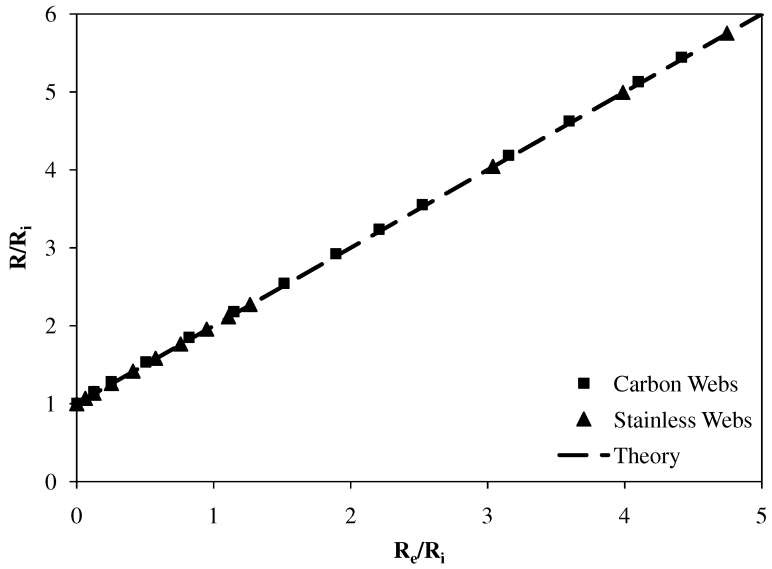

Figure 8.5. Plot of R-value ratio R/R_i vs. R_e/R_i for panels with carbon and stainless steel webs

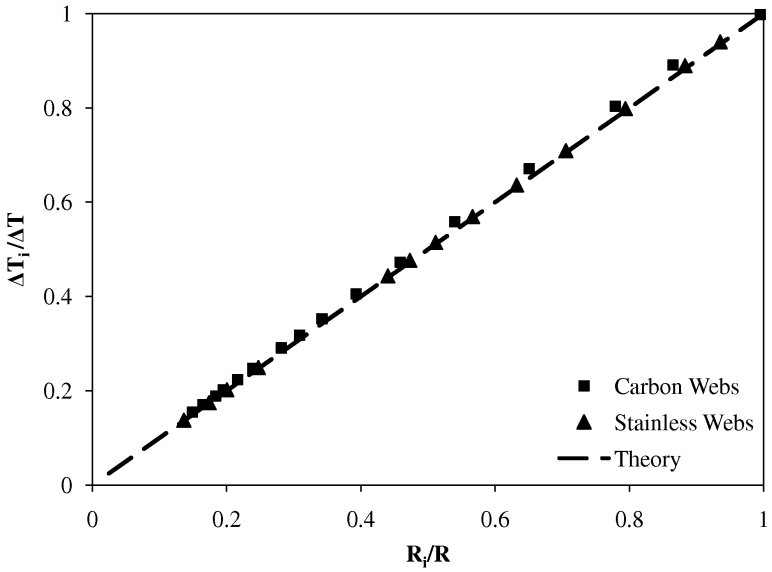

Figure 8.6. Relative temperature gradient $\Delta T_i/\Delta T$ across the structural layer vs. R_i/R for panels with carbon and stainless steel webs

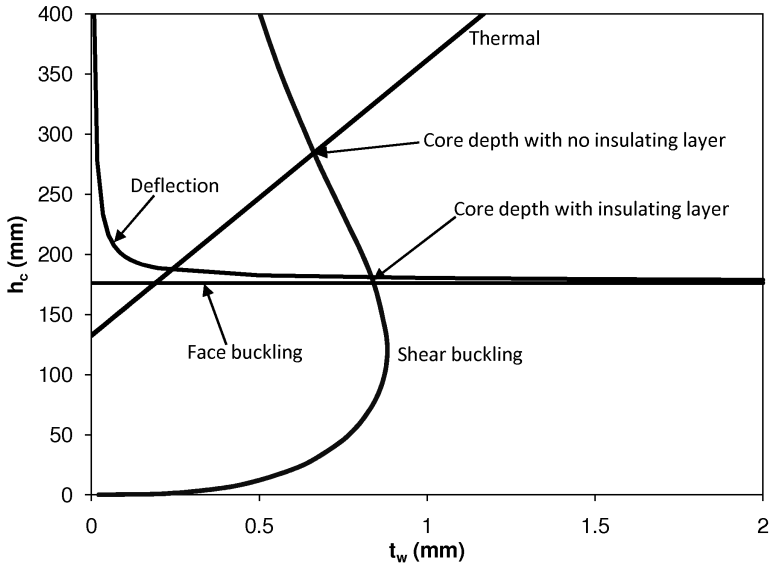

Figure 8.7. Failure mode map for web core panels with $a = 7$ m, $q = 1500$ N/m^2, and $R = 5.3$ m^2-K/W ($p = 1.2$ m, $t_f = 2.0$ mm); minimum depth designs for panels with and without an external insulating layer are indicated

temperature distribution is limited. Equations (8.4) and (8.5) are thus recommended without modification for panel design.

8.2.3 Effect of the Insulating Layer on Feasible Designs

To understand the impact of the insulating layer on panel design, it is useful to examine the influence of the failure modes—especially the R-value requirement—on panel design. This influence is investigated by mapping the effect of each failure mode on the feasible (t_w,h_c) design space (see Section 6.5). An example of a failure mode map is plotted in Figure 8.7 for panels 7 m long, subject to an applied load of 1500 N/m^2 and R-value requirement of 5.3 m^2-K/W[1]. The curves for the minimum web thickness to prevent shear buckling and the minimum core depth to satisfy the other requirements are shown for panels with 2.0 mm face sheets and web spacing 1.2 m.

The minimum required core depths for panels with and without an external insulating layer are indicated in Figure 8.7. For panels with no insulating layer, the core depth is 282 mm. That depth, determined by the thermal requirement, is much greater than would be possible based on structural requirements only. If an external insulating

[1]Figure 8.7 is the same as Figure 6.6(b), but only the curves relevant to the present discussion are included.

layer is assumed, the core depth reduces to 176 mm, determined by the face sheet buckling requirement. The structural layer for that design would have an R-value of 2.87. The required insulating layer depth is then 60 mm, so the total foam depth H is 236 mm—a net reduction of 46 mm compared to the panel with no external insulating layer.

The example in this section illustrates the potential for two-layer panels to reduce the required foam use for a given R-value. This reduction is possible because the insulating layer, which lacks the thermal bridging effect of the webs, is much more efficient thermally than the structural layer. Note that foam is still necessary in the structural layer to avoid designs with thick, closely-spaced webs, but this example demonstrates that the structural layer can be designed without consideration for the thermal requirements.

8.3 Minimum Weight Design

The weight W of two-layer web core panels is given by

$$W(t_f, t_w, h_c, p, h_e) = 2\gamma_f t_f + \gamma_w h_c \frac{t_w}{p} + \gamma_c h_c \left(1 - \frac{t_w}{p}\right) + \gamma_e h_e, \tag{8.10}$$

where $\gamma_i = \rho_i g$ is the specific weight of each component i. The minimum weight optimization problem is given by

$$\begin{aligned} &\text{minimize} \quad && W(t_f, t_w, h_c, p, h_e) \\ &\text{subject to} \quad && F_i \leq \psi_i \overline{F}_i. \end{aligned} \tag{8.11}$$

The constraints, $F_i \leq \psi_i \overline{F}_i$, require the panel geometry to meet all thermal and structural performance criteria with safety factors ψ_i.

The nature of the minimum weight solution can be understood through a sensitivity analysis, temporarily neglecting the constraints. The gradient $\boldsymbol{\nabla} W$ is

$$\boldsymbol{\nabla} W = \begin{pmatrix} 2\gamma_f \\ (\gamma_w - \gamma_c)\,\frac{h_c}{p} \\ \gamma_w \frac{t_w}{p} + \gamma_c \left(1 - \frac{t_w}{p}\right) \\ \frac{h_c}{p}\frac{t_w}{p}\,(-\gamma_w + \gamma_c) \\ \gamma_e \end{pmatrix}. \tag{8.12}$$

An order of magnitude evaluation of Equation (8.12) provides insight into the effect of each geometric variable on panel weight. Assume the face sheet thickness varies by an amount Δt_f. The resulting variation ΔW in panel weight is approximately $W_{,t_f} \Delta t_f$. This process is repeated for each design variable—those that yield the largest values for ΔW have the greatest influence on panel weight.

In steel panels with PUR core, $\rho_f = \rho_w = 7870$ kg/m^3, and $\rho_c = \mathcal{O}(10^1)$ kg/m^3 (e.g. $\rho_c = 36$ kg/m^3 in this work). For typical designs, $h_c/p = \mathcal{O}(10^{-1})$ and $t_w/p = \mathcal{O}(10^{-3})$. Thus,

$$\boldsymbol{\nabla} W \approx \begin{pmatrix} \mathcal{O}(10^5) \\ \mathcal{O}(10^3) \\ \mathcal{O}(10^2) \\ -\mathcal{O}(10^0) \\ \mathcal{O}(10^2) \end{pmatrix} [\mathrm{N/m^3}]. \tag{8.13}$$

The sheet metal thicknesses vary on the order of ± 0.1 mm, and the core and insulating layer depths vary on the order of ± 10 mm. Thus, variations in t_f and H (i.e. $h_c + h_e$) change the panel weight on the order of $\pm 10^1$ and $\pm 10^0$ N/m^2 respectively. Changes in the other variables have smaller effects on weight. The minimum depth required to meet the deflection and face sheet buckling requirements decreases as face sheet thickness increases. Thus, in the constrained optimization problem, Equation (8.11), t_f and H are inversely related. Because the sensitivity of panel weight to t_f is so much greater than the sensitivity to H, any weight reductions from using less foam are more than offset by the corresponding increase due to the face sheets.

A tradeoff thus exists between weight and depth. To meet the deflection and face buckling requirements with thin face sheets requires relatively deep cores. Minimum

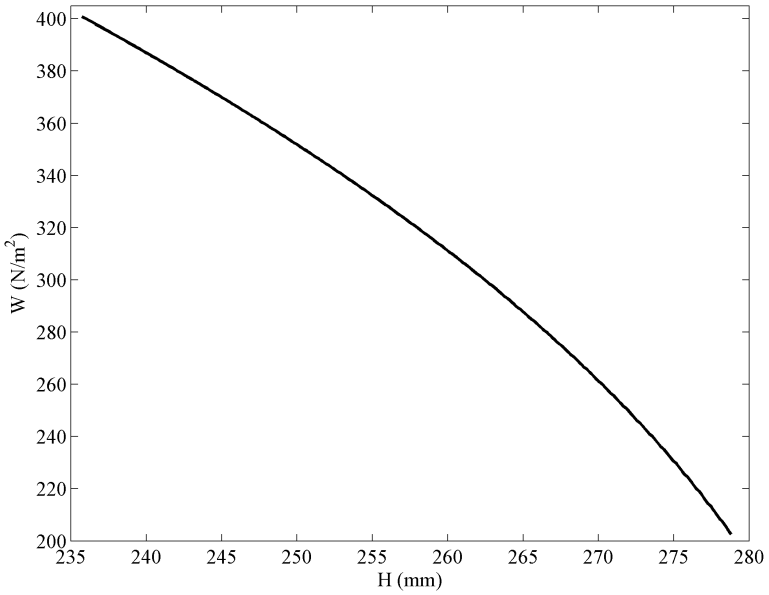

Figure 8.8. Pareto optimal curve (weight W vs. panel depth H) for panels with $a = 7$ m, $q = 1500$ N/m^2, and $R = 5.3$ m^2-K/W ($p = 1.2$ m)

weight design is therefore achieved by using the thinnest allowable face sheets (e.g. 0.6 mm in this work), with h_c as large as necessary to meet the structural requirements. Conversely, core depth can be reduced by increasing face sheet thickness, and minimum core depth is achieved using the maximum allowable face sheet thickness (2.0 mm). Naturally, the minimum depth design comes at a great cost in terms of weight: assuming constant H, for example, an increase in t_f from 0.6 to 2.0 mm causes an increase in panel weight of 216 N/m^2. Minimum depth and minimum weight represent the limits of possible design objectives.

The tradeoff between weight and depth can be visualized by examining the Pareto optimal curve (i.e. the locus of designs for which a reduction in one objective requires an increase in the other) for typical designs. The Pareto curve for the example in Section 8.2.3 is plotted in Figure 8.8. The endpoints of the curve represent designs for minimum weight and minimum depth. The range of depths between those two designs is 236–279 mm. The range of weights is much more dramatic: 203–401 N/m^2. Without a strong motivation for reducing the core depth (e.g. if the foam is much more expensive than the steel), the corresponding weight increases cannot be justified.

A procedure for minimum weight panel design is suggested by the considerations in this chapter. The use of an insulating layer allows the design of the structural layer

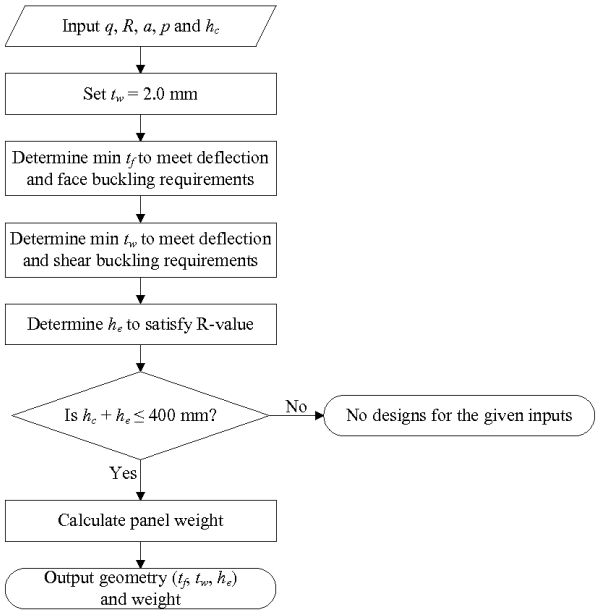

Figure 8.9. Flowchart of the minimum weight design procedure for two-layer web core panels

without imposing R-value requirements. Thus, an effective design strategy is to vary the structural depth h_c and web spacing p and determine the sheet thicknesses based on structural requirements. The insulating layer depth h_e then follows readily from Equation (8.4).

The procedure described above has two independent variables: h_c and p. To allow efficient placement into a roof assembly, the values for p are restricted to integer increments of panel width. Because the minimum weight problem is convex, a convenient strategy is to start with the largest allowable value for p and reduce until the panel weight begins to increase. In each case, the value of h_c is varied using a golden section search to find the minimum weight. The remaining panel geometry is determined for a given (h_c, p) input based on structural and thermal requirements.

The procedure to determine panel geometry for a given (h_c, p) combination is illustrated in Figure 8.9. Other inputs are the applied load, R-value, and panel length. Face sheet thickness t_f is determined from the face sheet buckling and deflection requirements. The deflection is minimized by temporarily setting t_w to the maximum value of 2.0 (to minimize R_i, Equation (8.4)). If the face buckling requirement is more limiting (i.e. requires thicker face sheets) than deflection, the web thickness $t_w < 2.0$ mm is determined from the deflection and shear buckling requirements. The mini-

Table 8.1. Loads and R-values used for panel design

	Load (N/m^2)	**R-value (m^2-K/W)**
Climate I	1576	5.3
Climate II	2173	6.8
Climate III	3322	6.8

mum t_f and t_w to meet the structural requirements in each case are determined using bisection. The thickness h_e of the insulating layer is determined from the structural layer geometry based on the thermal requirement. The total depth H is limited to 400 mm; therefore, a check on H is performed after determining h_e.

8.4 Roof Panel Designs

In this section, the effect of using an external insulating layer on design is illustrated through a case study. Web core designs are developed for roof panels 6.8 m long, subject to three load conditions detailed in Table 8.1. The load conditions—designated Climate I, II, and III—correspond to the loading and R-value requirements for locations in the southern, central, and northern US respectively [26]. The R-value requirements are set by building code [71], and the loads are derived from ground snow loads (958, 1915, and 3352 N/m^2 respectively [43]) per Reference [140], assuming a 6:12 roof pitch. Each load in the table also includes an allowance of 718 N/m^2 for dead loads (panel weight plus finishing layers). A panel width of 2.4 m is assumed.

Several geometric constraints are imposed to improve manufacturability. To ensure that cold-rolled steel can be used, the face sheet and web thicknesses are limited to the range 0.6–2.0 mm. Based on handling and architectural requirements, the panel depth H and weigh W are limited to 400 mm and 500 N/m^2 respectively. Web spacing is limited to integer increments of the total width.

Steel face sheets and webs are assumed, with the material properties given in Table 6.1. The core and insulating layer are assumed to be rigid polyurethane (PUR) foam, with properties reduced to account for creep. The creep reductions depend on duration of load: 2000 hours for live loads and 100,000 hours for dead loads [70]. The nominal properties of the foam are given in Table 6.2 along with reduced properties (based on Reference [34]) for live and dead load creep. Following the recommendations

Table 8.2. Minimum weight panel designs with carbon steel webs (all values in mm unless otherwise noted)

	t_f	t_w	h_c	p (m)	h_e	H	Weight (N/m^2)
No external insulating layer							
Climate I	0.60	0.66	285	1.2	0	285	205
Climate II	0.60	0.71	379	1.2	0	379	243
Climate III	—	—	—	—	—	—	—
With external insulating layer							
Climate I	0.60	0.68	272	1.2	8	280	203
Climate II	0.60	0.79	324	1.2	33	358	235
Climate III	1.32	0.61	339	0.6	61	400	372

in Reference [102] (see Table 6.3), the safety factor for web shear buckling is 1.6, and all other safety factors are set at 1.0.

The geometry of the minimum weight panels is given in Table 8.2 for web core panels with and without an external insulating layer. Two-layer panels are thinner and lighter weight than the corresponding web core designs with no insulating layer. The reductions in W and H become more substantial as load is increased. Thus, while the designs are nearly indistinguishable in Climate I, design for Climate III is possible only with the use of two-layer panels. Correspondingly, the depth h_e of the insulating layer increases with load from 8 mm in Climate I to 61 mm in Climate III. Referring to Equation (8.4), the insulating layer provides 36% of the total R-value of the Climate III design. In contrast, the thin insulating layer in the Climate I design contributes only 6% of the total R-value. The use of such a thin foam layer is impractical from a manufacturing standpoint, so the design with no insulating layer is recommended for Climate I.

It is interesting to compare the minimum weight designs to corresponding designs with minimum panel depth. Minimum depth designs are given in Table 8.3 for panels with and without an external insulating layer. Note that the use of an insulating layer allows considerable reductions in panel depth (64 and 91 mm in Climates I and II) compared to designs with no insulating layer. Corresponding to the discussion in the previous section, however, the two-layer panels are considerably heavier than the panels with no insulating layer. The insulating layer provides most (≈70–80%) of the R-value in the minimum depth designs.

Table 8.3. Minimum depth panel designs with carbon steel webs (all values in mm unless otherwise noted)

	t_f	t_w	h_c	p (m)	h_e	H	Weight (N/m^2)
No external insulating layer							
Climate I	0.60	0.66	285	1.2	0	285	205
Climate II	0.60	0.71	379	1.2	0	379	243
Climate III	—	—	—	—	—	—	—
With external insulating layer							
Climate I	2.00	0.60	116	0.4	104	221	400
Climate II	2.00	0.60	156	0.4	132	288	428
Climate III	2.00	0.60	221	0.4	116	337	453

For panels with no insulating layer, the minimum depth design matches the minimum weight design (compare Tables 8.2 and 8.3). The differences between the minimum weight and minimum depth designs for two-layer panels emphasize the tradeoff between depth and weight. Consistent with the preceding sensitivity analysis, the minimum weight designs use thin (0.6 mm) face sheets (except in Climate III, where thicker face sheets are necessary to meet the structural requirements). The minimum depth designs use thick (2.0 mm) face sheets, which add almost 200 N/m^2 to the panel weight.

8.5 Material Cost

Given the significant tradeoff between depth and weight, it is informative to consider alternative design objectives. A natural choice is cost, which can influence builder acceptance of new roof concepts. A full economic analysis of a related panel concept was recently performed at the University of Minnesota [2]. From this analysis it was found that material costs are by far the most significant contribution, at ≈80% of the total panel cost. Thus, the minimum cost design can reasonably be approximated based on material cost.

The material cost C is determined by a modification of Equation (8.10):

$$C(t_f, t_w, h_c, p, h_e) = 2\kappa_f\gamma_f t_f + \kappa_w\gamma_w h_c\frac{t_w}{p} + \kappa_c\gamma_c h_c\left(1 - \frac{t_w}{p}\right) + \kappa_e\gamma_e h_e, \qquad (8.14)$$

where κ_i is the cost per unit weight of each panel component i. The material costs used in the present analysis are listed in Table 8.4. The cost per unit weight of PUR

Table 8.4. Web core component material costs κ_i per unit weight

Carbon steel [18]	\$0.08/N
Stainless steel [18]	\$0.29/N
PUR [2]	\$0.45/N

is about 5.5 times greater than that of steel, so the most cost-effective designs may involve heavier panels with less foam. As a design objective, Equation (8.14) takes the same form as the minimum weight. Thus, the design for minimum material cost is performed using the procedure described in this work

The designs for minimum material cost are detailed in Table 8.5 for panels with and without an insulating layer. Comparison with Table 8.2 reveals that, in every case, the minimum cost design matches the design for minimum weight. As such, the minimum cost design recommendations match those for minimum weight, i.e. the use of an external insulating layer is recommended for Climates II and III but not for Climate I. An understanding of these results is obtained by sensitivity analysis. The gradient $\boldsymbol{\nabla} C$ of the material cost function is on the order of

$$\boldsymbol{\nabla} C = \begin{pmatrix} 2\kappa_f \gamma_f \\ (\kappa_w \gamma_w - \kappa_c \gamma_c) \frac{h_c}{p} \\ \kappa_w \gamma_w \frac{t_w}{p} + \kappa_c \gamma_c \left(1 - \frac{t_w}{p}\right) \\ \frac{h_c}{p} \frac{t_w}{p} \left(-\kappa_w \gamma_w + \kappa_c \gamma_c\right) \\ \kappa_e \gamma_e \end{pmatrix} \approx \begin{pmatrix} \mathcal{O}(10^4) \\ \mathcal{O}(10^2) \\ \mathcal{O}(10^2) \\ -\mathcal{O}(10^{-1}) \\ \mathcal{O}(10^2) \end{pmatrix} [\$/\mathrm{m}^3]. \tag{8.15}$$

As with weight, material cost is most sensitive to t_f and H. In this case, variations in each parameter change the panel cost on the order of $\pm 10^0$ [\$/m^2]. The two effects are similar due to the high cost of the foam relative to the steel.

8.6 Comparison of Panel Concepts

To provide perspective on the roof panel concepts described in this chapter, minimum cost designs for two-layer panels are compared to web core designs with stainless steel webs with no external insulating layer. Based on these results, conclusions are made regarding the effective use of material in web core roof panels. The designs are also compared to truss core panel designs developed in Reference [27]. This comparison

Table 8.5. Panel designs with carbon steel webs and minimum material cost (all values in mm unless noted)

	t_f	t_w	h_c	p (m)	h_e	H	Cost ($/m^2)
No external insulating layer							
Climate I	0.60	0.66	285	1.2	0	285	53.48
Climate II	0.60	0.71	379	1.2	0	379	68.84
Climate III	—	—	—	—	—	—	—
With external insulating layer							
Climate I	0.60	0.68	272	1.2	8	280	52.78
Climate II	0.60	0.79	324	1.2	33	358	65.45
Climate III	1.32	0.61	339	0.6	61	400	81.94

Table 8.6. Minimum cost designs with stainless steel webs (all values in mm unless noted)

	t_f	t_w	h_c	p (m)	h_e	H	Cost ($/m^2)
Climate I	0.60	0.70	272	1.2	0	272	54.10
Climate II	0.60	0.81	324	1.2	0	324	63.65
Climate III	1.48	0.60	307	0.48	0	307	75.83

allows a first assessment of the cost-effectiveness of web core panels, as well as insight into possible avenues of improvement for future designs.

The minimum cost designs for web core panels with stainless steel webs are given in Table 8.6. All of the designs are developed without an external insulating layer. As with the two-layer designs, the designs for Climates I and II also provide minimum weight. In fact, the geometry of the structural layer is essentially the same for the two concepts in Climates I and II. To understand this result, recall (Table 6.1) that the thermal conductivity of stainless steel is about a third that of carbon steel, while the elastic modulus is nearly the same. As a result, the minimum weight designs have essentially the same structural geometry with either web material. The designs with stainless steel webs meet the R-value requirements without an external insulating layer, unlike the designs with carbon steel webs.

The designs for minimum material cost are summarized and compared in Table 8.7. In addition to the designs from Tables 8.4 and 8.5, truss core panel designs from Reference [27] for the same loading conditions are included. The total depth H, panel weight W, and material cost C are provided. The web core designs for Climates I and II weigh less than the truss core designs. In addition, the panel depths are comparable or smaller for web core versus truss core panels in Climates I and II. These designs

Table 8.7. Summary of minimum material cost designs for each panel type; truss core designs from Reference [27] are included for comparison

	H (mm)	W ($\mathrm{N/m^2}$)	C ($\mathrm{\$/m^2}$)
	Climate I		
Carbon webs	285	205	53.48
Stainless webs	272	201	54.10
Truss Core	272	223	38.61
	Climate II		
Two-layer	358	235	65.45
Stainless webs	324	223	63.65
Truss Core	359	243	46.87
	Climate III		
Two-layer	400	372	81.94
Stainless webs	307	367	75.83
Truss Core	359	298	51.32

illustrate the effectiveness of using core materials in the design of lightweight thin-walled structures.

The web core designs for Climate III weigh more than the truss core designs due to the effect of the thermal requirement. The designs for Climates I and II use thin (0.6 mm) face sheets, which keep the designs lightweight. In Climate III, however, the core depths h_c up to 398 mm are necessary with such thin face sheets, and it is impossible to meet the thermal requirement with $H \leq 400$. Thicker face sheets are necessary, and the panel weights are correspondingly higher.

An obvious result in Table 8.7 is the high cost of web core panels compared to truss core panels. The material costs of the truss core designs are $\approx\$14$–$25/\mathrm{m^2}$ less than those of the corresponding web core designs. Insight into this result is gained by examining the breakdown of material cost among the panel components. The contributions of the face sheets, core, webs, and insulating layer for each minimum cost design, including panels with carbon steel webs and no external insulating layer, are plotted in Figure 8.10[2]. In the web core designs, the foam is by far the most expensive panel component, contributing 60–90% of the total material cost. Truss core panels, in contrast, use almost 50% less foam than web core panels.

[2]For the truss core designs, the costs are given only in terms of the structural layer and the insulating layer

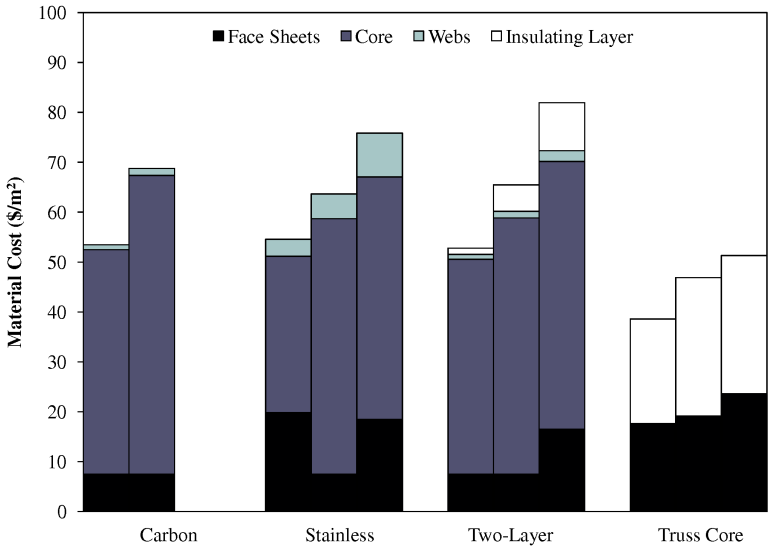

Figure 8.10. Material cost for each panel concept; the three columns correspond to Climates I, II, and III respectively

An important caveat must be noted in the comparison of material costs between truss core and web core panels. The truss core designs use V-shaped channel webs, with a spacing of 0.4 m [27]. The V-channels require three welds per web (compared to two welds per web core web), and more webs per panel compared to any of the minimum cost web core designs. These differences have a large potential impact on manufacturing costs. To achieve a production volume of 50,000 truss core panels/year requires seven welding machines [2]. Applying the same capacity assumptions to web core panels with $p = 1.2$ m, the same production volume is achieved using two machines. The five extra machines for truss core panels require significant capital investment, as well as additional workers and operating expenses. Furthermore, as noted in Chapter 1, the wide web spacing allows the possibility of simplified production processes. It may be economical, for example, to produce foam core panels 1.2 m wide and use webs as panel-to-panel joints. The impact of these manufacturing scenarios has not been studied in the present work, but they create a real possibility that the final cost of web core panels may be competitive with that of truss core panels.

Focusing on web core designs, Figure 8.10 suggests recommendations for material use in roof panels. Compared to designs with carbon steel webs and no external insulating layer, stainless steel webs and two-layer designs allow reduced material cost for Climates II and III. The designs with stainless steel webs have the lowest cost in these cases. For Climate I, the lowest-cost option is the panel with carbon

steel webs and no insulating layer. These results lead to the conclusion that the use of an insulating layer does not reduce the material cost of web core panels. The difference in cost between the face sheets and core material is not great enough to justify the use of thicker face sheets in place of a thick core. The use of stainless steel webs, even at a cost of 3.6 times greater than carbon steel, is more effective in reducing cost.

Reduction in foam cost is a clear avenue for future improvements to web core panel design. The cost could be reduced either through the development of new, lower-cost foam materials, or through the use of denser foam in the structural layer. The latter possibility is of particular interest because the cost per unit weight of foam is essentially independent of density. The stiffness and strength properties, however, increase in a nonlinear way (see Equation 2.1). The potential thus exists to achieve net reductions in weight and material cost by increasing core density, particularly if low-density (i.e. low thermal conductivity) foam is used in the insulating layer. The technology to foam higher-density PUR *in-situ* is not currently available, so it has not been considered in the present work[3].

8.7 Conclusions

Steel web core sandwich panels offer several benefits over conventional construction methods for residential roofs. A challenge to the design of roof panels, however, is the impact of the webs on thermal insulating performance. Traditional web core panels compensate for this impact by increasing the core depth h_c. This chapter proposes an alternate approach, two-layer panels, to satisfying the thermal requirement while exploiting the core material to achieve lightweight design.

The influence of the insulating layer on thermal and structural performance of web core panels was investigated, along with the resulting impact on feasible panel designs. The use of an insulating layer allows net reductions in panel depth by providing thermal performance more efficiently than in the structural layer. Corresponding reductions in panel weight are possible as a result. These reductions become more significant as the applied load is increased. The effect of the insulating layer on minimum depth design was also investigated. Two-layer panels achieve net reductions

[3]The comments about cost and *in-situ* foaming capability are from conversations with Michael Krupa of BASF

of up to 91 mm in panel depth compared to designs with no insulating layer. A significant tradeoff exists between depth and weight, however, and the minimum depth designs are heavier than the minimum weight designs by up to ≈200 mm.

Minimum weight designs were developed for panels made of carbon steel and PUR, subject to typical load conditions for the continental US. Two-layer panels provide reductions in weight and depth compared to panels with no insulating layer. The advantage of two-layer designs is particularly notable in Climate III, where designs are not possible without the use of an insulating layer. In contrast, the benefit of two-layer panels in Climate I is negligibly small. Based on these results, two-layer panels are not recommended for Climate I, but they are recommended for Climates II and III.

Designs for minimum material cost were also investigated in this chapter. The material cost for each panel component is proportional to weight, so the resulting design problem is solved in the same manner as with minimum weight. The minimum cost design matches the minimum weight design. Even though the core material is by far the most expensive panel component, it is not sufficiently expensive (compared to the face sheets) to justify the use of thicker face sheets. Web core panels with stainless steel webs are thinner and lighter weight than the corresponding two-layer panel designs. In Climates II and III, they are also lower cost. In all three climates, however, truss core designs have lower material cost than the web core designs. The extra cost of the web core panels is due to the added foam use.

This chapter has demonstrated that web core panels are a viable option for residential roofs. Two methods to compensate for the effect of the webs on thermal performance—the use of stainless steel webs and the use of an external insulating layer—were proven viable. Based on material cost, two-layer panels are not recommended for roofs. For Climate I, the recommended panel design uses carbon steel webs, and for Climates II and III stainless steel webs should be used. The web core panel designs for Climates I and II are thin and lightweight compared to the corresponding truss core designs. The drawback to the web core designs is the high material cost associated with the use of added foam to achieve the required thermal insulating performance. Reductions in foam cost are identified as a research area that could potentially improve the cost competitiveness of web core designs.

Chapter 9

Conclusions

This work has examined the structural and thermal considerations for residential roof design using steel web core sandwich panels. Steel panels offer several benefits over conventional construction techniques, including improved energy efficiency, reduced construction costs, increased durability, and architectural benefits. Web core panels meet the structural and thermal requirements for roofs using steel webs and a polymer foam core. Compensation for the effect of the webs on thermal performance is achieved through increased core depth or by adding an external insulating layer. Thermoset polymer foams are an ideal core material for roof panels because they provide good thermal insulating performance as well as stiffness to improve the performance of the webs. Rigid polyurethane has the additional benefit that it can be foamed *in-situ*, bonding directly to the panel structure without the need for additional adhesives.

The webs must be thin and widely-spaced to minimize the detrimental effect on thermal performance. Thin webs are subject to a variety of local failure modes, and efficient panel design is possible only by understanding and exploiting the interaction between the webs and core material to prevent these failure modes. To that end, this work has focused on the development and validation of models for the strength of thin webs in foam-filled panels. Two models were developed: an elastic foundation model suitable to the analysis of local buckling modes (particularly shear buckling), and a bearing strength model, for which the failure mechanism is primarily local crushing of the core material. Approaches to the design of web core roof panels, with and without an external insulating layer, were also developed.

9.1 Conclusions

The shear buckling strength of the webs is successfully predicted by treating the webs as plates on a Pasternak elastic foundation. The Pasternak foundation model is especially suitable for panels with wide web spacing because the influence of shear stiffness is significant in deep foundations. In addition to the analytical buckling solution, which was previously not available in the literature, closed-form approximations were developed for square and infinitely long plates. These approximations match the analytical solutions with very good accuracy and can be used to find upper and lower bounds on buckling strength. The approximation for long plates is useful for design because the buckling strength converges quickly to that of infinitely long plates in webs with aspect ratio $a/h_c \geq 4$. Roof panel webs exceed this aspect ratio in practice ($a/h_c \geq 8$ for all designs in this work), so the webs can reasonably be treated as infinitely long.

Another key element of the shear buckling model is the determination of suitable foundation parameters based on the properties of the core material. A model was developed in this work using energy methods and validated using finite element analysis. Applying the resulting foundation constants to the analytical shear buckling solution results in very accurate strength predictions for plates resting on sufficiently deep ($Hk \geq 2$, see Chapter 4) foundations. The effectiveness of the plate buckling model for web core panels was also investigated. The webs are slightly stronger than predicted by the model. This difference is attributable to the assumption of simply supported webs at the interface with the face sheets. In practice, the face sheets provide some rotational restraint, thus strengthening the webs. The difference in strength is small (less than 25%) and, given the large safety factors typically prescribed for shear buckling [102], can reasonably be neglected for design.

A mechanism model for bearing strength was developed that accounts for the interactions between the face sheets, webs, and core material, thus providing insight into the influence of each material on bearing strength. A particularly interesting result is the contribution of core crushing strength, which accounts for up to 80% of the total bearing strength in panels with thin webs. The form of the model also suggests a straightforward modification of existing empirical design code equations to account for the core material. The modified AISI model predicts bearing strength within about 15% of that predicted by the hinge model. The difference between the models

is primarily due to the assumptions about core crushing strength: the core crushing prediction in the hinge model is based in part on the length of the damaged region in the web after failure, while in the modified AISI model it is based on bearing length only.

The shear buckling, deflection, and bearing failure models were validated through prototype testing. The shear buckling strength was predicted by the present model to within 4%. The deflection model in this work accurately predicted the panel stiffness before and after the onset of shear buckling. The model overpredicted bearing strength by up to 29% for the tests reported in this work. Based on the breakdown of expected contributions from the webs and core material, the results suggest the model in this work overestimates the foam crushing strength by about 18%. The variability in strength is reduced, however, suggesting it may be possible to achieve greater reliability in bearing strength compared to current practice by using a foam in-fill.

Design procedures were developed for web core panels by examining the factors that limit the range of feasible designs. For web core panels with no external insulating layer, the thermal and shear buckling requirements limit the designs. These two requirements have opposing effects on panel design—increasing web thickness causes an increase in shear buckling strength and a decrease in thermal performance. As a result, the core depth is sensitive to the choice of web material: panels with carbon steel webs are typically about 100 mm deeper than panels with stainless steel webs.

The structural and thermal insulating layers of two-layer web core panels are designed independently, thus allowing more design flexibility compared to panels with no external insulating layer. A consequence of this increased flexibility is a substantial tradeoff between total panel depth and weight. A wide variety of Pareto optimal designs for depth and weight are possible, and selection of an appropriate single objective function is useful for design. Minimum material cost was investigated in this work as a reasonable approximation to minimizing the total panel cost. Given the materials used in this work (steel, stainless steel, and 36 kg/m^3 PUR foam), designs for minimum material cost were developed for three US climate zones and a panel length of 6.8 m (corresponding to a span of 6.1 m (20 ft) and 6:12 roof pitch).

The lowest-cost designs are the ones that also minimize panel weight. This result can be understood through sensitivity analysis of the weight and cost objective functions.

The panel weight is much more sensitive to face sheet thickness than to the other geometric variables, so minimum weight is achieved using thin face sheets and large core depth (to meet the thermal requirement). Minimum core depth, in contrast, is achieved using thick face sheets, resulting in high panel weight. The material cost of each component is proportional to its weight. Although the cost of carbon steel used for the face sheets is about a fifth that of the core material, the total material cost is slightly more sensitive to face sheet thickness than to foam depth when carbon steel webs are used.

The minimum cost designs with carbon steel webs are two-layer panels. As the applied load or R-value requirement increases, the reduction in cost by using two-layer panels increases. The minimum cost design with stainless steel webs in Climates I and II have the same structural layer geometry as the two-layer designs with carbon steel webs. The thermal conductivity of stainless steel is about a third that of carbon steel, however, with the result that the stainless steel designs meet the R-value requirement without an external insulating layer. The panels with stainless steel webs are thinner and lighter-weight than the panels with carbon steel webs. In Climates II and III, the designs with stainless steel webs have lower material cost as well.

The minimum cost designs were compared to truss core designs developed in Reference [27] for the same loading conditions. Web core panels use more foam than truss core panels and have 40–60% greater material costs as a result. The web core designs for Climates I and II have weight and depth that are comparable to or lower than those of the corresponding truss core designs. Thus, if considerations other than material cost play a role in design, web core panels may become preferable for those climates. In particular, it can be noted that the fabrication of the web core designs requires substantially less welding (i.e. lower fabrication costs) than the truss core designs. Thus, while material cost is a useful objective function for web core design, it may not be suitable for comparing web core to truss core designs.

9.2 Recommendations for Future Work

The work described in this thesis suggests several avenues for future research. A key area of improvement is the development of advanced foam technologies. In particular, higher-density foams that can be formed *in-situ* are needed. The design space for roof panels is limited by a combination of the thermal requirement, shear buckling, and

face sheet buckling. The use of higher-density foam cores provides increased buckling resistance that can potentially more than offset the effect on thermal performance. As a result, it may be possible to use less foam, especially for panels with carbon steel webs. The development of stiffer or higher density *in-situ* foams would allow a broader range of panel designs.

Another approach that should be investigated for roof panels is functionally graded foams (i.e. foams with material properties that vary with location in the panel). In web core panels, the foam has a structural role only in localized regions of the panel—near the supports, for example. Reductions in total foam use may be possible by using dense foam in locations to prevent buckling failure and low-density (optimized for thermal conductivity) foam everywhere else. The technology to produce structurally graded foams is currently very preliminary; however, the development of new processing techniques (e.g. variation of foaming agent ratio and ultrasonic irradiation [141]) could make the technology more amenable to mass production.

The test results reported in Chapter 7 suggest the possibility of residual postbuckling capacity in shear and at the bearings. The bearing test results further suggest the foam may reduce imperfection sensitivity in the webs, which may in turn allow the use of smaller safety factors compared to current design practice. A complete study of postbuckling behavior should thus be performed to gain understanding of these two effects. The study should focus on the relationships of several variables to postbuckling strength, including foam and web material properties, initial imperfections, and localized damage (e.g. foam crushing and debonding). In addition, long-term testing should be performed to characterize the effects of creep deflection and rupture on postbuckling strength.

References

[1] US Department of Energy 2009 Buildings Energy Data Book. http://buildingsdatabook.eere.energy.gov, Accessed November 15, 2009.

[2] J. H. Davidson, S. C. Mantell, G. L. Di Muoio, G. Mittelman, C. Briscoe, B. Schoenbauer, D. Huang, T. Okazaki, C. K. Shield, B. J. Siljenberg, J. C. Carmody, G. E. Mosiman, D. H. MacDonald, and P. Kalish. Advanced energy efficient roof system: DE-FC26-04NT42114 final report. Project report, available online at www.osti.gov/servlets/purl/947089-XhPfAF, 2008.

[3] R. Hedrick. Costs & savings for houses built with ducts in conditioned space: Technical information report. Technical Report 500-03-082-A-31, New Buildings Institute, 2003.

[4] A. O. Desjarlais, T. W. Petrie, and T. Stovall. Comparison of cathedralized attics to conventional attics: Where and when do cathedralized attics save energy and operating costs? In *Performance of Exterior Envelopes of Whole Buildings IX International Conference*, pages 1–15, Clearwater Beach, FL, 2004.

[5] A. Rudd. Field performance of unvented cathedralized (UC) attics in the USA. *Journal of Building Physics*, 29(2):145–169, 2005.

[6] A. Rudd and S. Chandra. Side-by-side evaluation of a stressed-skin insulated-core panel house and a conventional stud-frame house. Technical Report FSEC-CR-664-93, Florida Solar Energy Center, 1994.

[7] J. Christian. Ultra-low energy residences. *ASHRAE Journal*, 47(1):20–27, 2005.

[8] J. E. Christian, J. Atchley, L. Richards, H. Moon, and P. Childs. Energy efficiency, SIPS, geothermal, and solar PV used in near zero-energy house. *ASHRAE Transactions*, 112(2):275–284, 2006.

[9] M. A. Mullens and M. Arif. Structural insulated panels: Impact on the residential construction process. *Journal of Construction Engineering and Management*, 132(7):786–794, 2006.

[10] Manufactured Housing Research Alliance. Design for a cold-formed steel framed manufactured home. Technical report, Partnership for Advancing Technology in Housing, 2002.

[11] M. Nowak, L. Bowles, J. Lyons, and C. Barbour. Research agenda: Advanced residential roof systems. Project report, Partnership for Advancing Technology in Housing, 2005.

[12] J. Nieminen and M. Salonvaara. Hygrothermal performance of light steel-framed walls. Technical report, VTT Technical Research Centre of Finland, 2000.

[13] S. A. Chini and K. Gupta. A comparison between steel and wood residential framing systems. *Journal of Construction Education*, 2(2):133–145, 1997.

[14] T. Höglund and H. Burstrand. Slotted steel studs to reduce thermal bridges in insulated walls. *Thin-Walled Structures*, 32:81–109, 1998.

[15] T. Blomberg and J. Claesson. Heat transmission through walls with slotted steel U-girders. In *International Conference on Steel in Green Building Construction*, Orlando, USA, 1998.

[16] G. Gedge. Structural uses of stainless steel—buildings and civil engineering. *Journal of Constructional Steel Research*, 64(11):1194–1198, 2008.

[17] N. R. Baddoo. Stainless steel in construction: A review of research, applications, challenges, and opportunities. *Journal of Constructional Steel Research*, 64(11):1199–1206, 2008.

[18] MEPS world steel prices. http://www.meps.co.uk/world-price.htm, Accessed December 20, 2009.

[19] M. J. Kucirka. *Analysis and design of sandwich panel residential roof systems.* M.S. thesis, Massachusetts Institute of Technology, 1989.

[20] J. Crowley, L. Morse-Fortier, J. Dentz, M. Parent, L. J. Gibson, T. Tonyan, and L. Glicksman. Innovative materials and construction systems for energy-efficient building envelopes. In *Thermal Performance of the Exterior Envelopes of Buildings*, volume 12, pages 105–113, 1995.

[21] M. A. Dweib, B. Hu, A. O'Donnell, H. W. Shenton, and R. P. Wool. All natural composite sandwich beams for structural applications. *Composite Structures*, 63:147–157, 2004.

[22] M. A. Dweib, B. Hu, H. W. Shenton, and R. P. Wool. Bio-based composite roof structure: Manufacturing and processing issues. *Composite Structures*, 74:379–388, 2006.

[23] D. E. Thomas. *Structural Analysis of Sandwich Panels for Residential Roof Construction.* M.S. thesis, University of Minnesota, 2005.

[24] D. E. Thomas, S. C. Mantell, J. H. Davidson, L. F. Goldberg, and J. Carmody. Analysis of sandwich panels for an energy efficient and self-supporting residential roof. *Journal of Solar Energy Engineering*, 128(3):338–348, 2006.

[25] J. H. Davidson, S. C. Mantell, C. Briscoe, B. Schoenbauer, D. Huang, and J. Carmody. Options for an energy efficient panelized residential roof. In *Solar 2007*, pages 623–630, Cleveland, OH, 2007. American Solar Energy Society.

[26] S. C. Mantell, J. H. Davidson, G. L. Di Muoio, G. Mittelman, T. Okazaki, B. J. Siljenberg, C. K. Shield, G. E. Mosiman, J. C. Carmody, and D. H. MacDonald. Manufactured panelized roof system for residential buildings. In *Scaling Up: Building Tomorrow's Solutions, 2009 ACEEE Summer Study on Energy Efficiency in Buildings*, Pacific Grove, CA, 2008.

[27] G. L. Di Muoio. *Investigation of a Light Gage Steel Panelized Roof System for Residential Applications*. M.S. thesis, University of Minnesota, 2008.

[28] C. R. Briscoe, S. C. Mantell, and J. H. Davidson. Shear buckling in foam-filled web core sandwich panels using a pasternak foundation model. *Thin-Walled Structures*, 48(10):460–468, 2010.

[29] C. R. Briscoe, S. C. Mantell, J. H. Davidson, and T. Okazaki. Design procedure for web core sandwich panels for residential roofs. *Journal of Sandwich Structures and Materials*, In press doi: 10.1177/1099636210365441.

[30] *ASHRAE Fundamentals*. American Society of Heating, Refrigerating, and Air-Conditioning Engineers, Atlanta, GA, 2005.

[31] N. C. Hilyard, editor. *Mechanics of Cellular Plastics*. Macmillan, New York, 1982.

[32] N. C. Hilyard and A. Cunningham, editors. *Low Density Cellular Plastics: Physical Basis of Behaviour*. Chapman & Hall, London, 1994.

[33] L. J. Gibson and M. F. Ashby. *Cellular Solids: Structure and Properties*. Cambridge University Press, New York, second edition, 1997.

[34] J.-S. Huang and L. J Gibson. Creep of polymer foams. *Journal of Materials Science*, 26:637–647, 1991.

[35] T. Kilpeläinen and P. Hassinen. Long-term behaviour and strength of EPS foam sandwich panels. In *Nordic Steel Construction Conference*, volume 2, pages 645–652, Malmö, Sweden, 1995. Swedish Institute of Steel Construction.

[36] M. Just. Ergebnisse experimenteller untersuchungen zum langzeitverhalten von purhartschaumstoff-stutzkernbauteilen und schlussfolgerungen fur die anwendung (the results of an experimental investigation of the long-term behavior of building elements utilizing a rigid plastic foam core and conclusions regarding their use). *IfL-Mitteilungen*, 22(3):95–104, 1983.

[37] D. Zenkert, editor. *The Handbook of Sandwich Construction*. North European Engineering and Science Conference Series. EMAS, Cradley Heath, UK, 1997.

[38] D. Zenkert, A. Shipsha, and M. Burman. Fatigue of closed cell foams. *Journal of Sandwich Structures and Materials*, 8:517–522, 2006.

[39] S. Abrate. Criteria for yielding or failure of cellular materials. *Journal of Sandwich Structures and Materials*, 10(1):5–51, 2008.

[40] D. Benderly and S. Putter. Characterization of the shear/compression failure envelope of rohacell foam. *Polymer Testing*, 23(1):51–57, 2004.

[41] J. M. Davies. Design criteria for sandwich panels for building construction. In *Proceedings of the ASME Aerospace Division*, pages 273–284, 1997.

[42] J. M. Davies, editor. *Lightweight Sandwich Construction*. Blackwell, Oxford, UK, 2001.

[43] *2003 International Residential Code for One- and Two-Family Dwellings*. International Code Council, Country Club Hills, IL.

[44] *ASTM E 84-05: Standard Test Method for Surface Burning Characteristics of Building Materials*. ASTM International, West Conshohocken, PA, 2005.

[45] J. G. Abbott. Standard laboratory tests: How meaningful are they in assessing fire performance of insulation materials? In *Conference on Fire and Cellular Polymers*, pages 199–218, 1986.

[46] J. M. Davies. Performance of sandwich panels in fire 1. onshore applications. In *Sandwich Construction 3*, University of Southampton, 1996.

[47] J. Rakic. Fire rated insulated (sandwich) panels. *Fire Australia*, pages 33–37, May 2003.

[48] J. Zicherman. Fire performance of foam-plastic building insulation. *Journal of Architectural Engineering*, 9(3):97–101, 2003.

[49] A. H. Landrock, editor. *Handbook of Plastic Foams: Types, Properties, Manufacture and Applications*. Noyes, Park Ridge, NJ, 1995.

[50] J. M. Davies. Core materials for sandwich cladding panels. In *International Conference on Building Envelope Systems and Technology*, pages 299–306, Singapore, 1994.

[51] S. T. Lee and N. S. Ramesh, editors. *Polymeric Foams: Mechanisms and Materials*. CRC Press, Boca Raton, FL, 2004.

[52] D. Randall and S. Lee, editors. *The Polyurethanes Book*. Wiley, New York, 2002.

[53] General Plastics. Nominal physical property data for LAST-A-FOAM® FR-7100 rigid foam. Online datasheets, www.generalplastics.com, 2008.

[54] R. J. Booth, C. DeRushie, and K. Liu. Protection of foam plastic thermal insulation in low sloped roofing systems. *Journal of Thermal Envelope and Building Science*, 25(4):255–274, 2002.

[55] R. C. Wool and X. S. Sun. *Bio-Based Polymers and Composites*. Elsevier, London, 2005.

[56] S. S. Narine, X. Kong, L. Bouzidi, and P Sporns. Physical properties of polyurethanes produced from polyols from seed oils: II. foams. *Journal of the American Oil Chemists' Society*, 84:65–72, 2007.

[57] A. Azim, A. M. Atta, and R. A El-Ghazawy. Synthesis of rigid polyurethane foams from recycled poly(ethylene terephthalate) waste. *Cellular Polymers*, 25(1):35–48, 2006.

[58] K. Ashida. *Polyurethane and Related Foams: Chemistry and Technology*. Taylor & Francis, Boca Raton, FL, 2007.

[59] N. Mills. *Polymer Foams Handbook: Engineering and Biomechanics Applications and Design Guide*. Elsevier, Burlington, MA, 2007.

[60] S. T. Lee and D. Scholz. *Polymeric Foams: Technology and Developments in Regulation, Process, and Products*. Taylor & Francis, Boca Raton, FL, 2009.

[61] *ASTM C-578-08: Standard Specification for Rigid, Cellular Polystyrene Thermal Insulation*. ASTM International, West Conshohocken, PA, 2008.

[62] *ASTM E 1730-04: Standard Specification for Rigid Foam for Use in Structural Sandwich Panel Cores*. ASTM International, West Conshohocken, PA, 2004.

[63] *ASTM C-591-08: Standard Specification for Unfaced Preformed Rigid Cellular Polyisocyanurate Thermal Insulation*. ASTM International, West Conshohocken, PA, 2008.

[64] Diversifoam. Physical properties of RayLite EPS insulation. Online datasheet, www.diversifoam.com, 2008.

[65] Owens Corning. FOAMULAR© 400/600/1000 high compressive strength rigid foam insulation product data sheet. Online Datasheet 58307-D, www.owenscorning.com, 2008.

[66] BASF Chemical Company. ELASTOPOR® P17226R resin/ELASTOPOR® P1046U isocyanate rigid urethane foam system. Data sheet, 2006.

[67] BASF Chemical Company. University of Minnesota panel results: Physical testing results of panel made at BASF in May, 2008. Data sheet, 2008.

[68] Elliott Company. ELFOAM® polyisocyanurate foam. Online datasheets, www.elliottfoam.com, 2008.

[69] D. Klempner and K. C. Frisch, editors. *Handbook of Polymeric Foams and Foam Technology*. Hanser, New York, 1991.

[70] ECCS. European recommendations for sandwich panels: Part I Design. volume TC 7. European Convention for Constructional Steelwork, 1991.

[71] *2003 International Energy Conservation Code*. International Code Council, Country Club Hills, IL.

[72] A. C. Ugural and S. K. Fenster. *Advanced Strength and Applied Elasticity*. Prentice Hall, Upper Saddle River, NJ, fourth edition, 2003.

[73] J. Kosny and J. E. Christian. Thermal performance and wall ratings. *ASHRAE Journal*, 38(3):1–8, 1996.

[74] B. H. Schoenbauer. *Thermal Analysis of Panels for Residential Roof Constructions*. M.S. thesis, University of Minnesota, 2007.

[75] R. I. Kliger and P. J. Pellicane. Prediction of creep properties of chipboard used in stressed-skin panels. *Journal of Testing and Evaluation*, 23(6):408–414, 1995.

[76] R. I. Kliger and P. J. Pellicane. Time-dependent bending properties of lumber. *Journal of Testing and Evaluation*, 24(3):187–193, 1996.

[77] S. Thelandersson and H. J. Larsen, editors. *Timber Engineering*. John Wiley & Sons, West Sussex, UK, 2003.

[78] J. A. Hartsock. Thermal warp of composite panels. *Journal of Cellular Plastics*, 1(2):291–295, 1965.

[79] C. Libove and S. B. Batdorf. A general small-deflection theory for flat sandwich plates. NACA TR 899, 1948.

[80] N. J. Hoff. Bending and buckling of rectangular sandwich plates. NACA TN 2225, 1948.

[81] J. R. Robinson. The buckling and bending of orthotropic sandwich panels with all edges simply-supported. *Aeronautical Quarterly*, 6(2):125–148, 1955.

[82] T. S. Lok and Q. H. Cheng. Elastic deflection of thin-walled sandwich panel. *Journal of Sandwich Structures and Materials*, 1(4):279–298, 1999.

[83] T. S. Lok and Q. H. Cheng. Elastic stiffness properties and behavior of truss-core sandwich panel. *Journal of Structural Engineering*, 126(5):552–559, 2000.

[84] A. Klanac. Bending of steel sandwich panels under lateral loading. Report M-285, Helsinki University of Technology Ship Laboratory, 2004.

[85] T. C. Fung, K. H. Tan, and T. S. Lok. Analysis of C-core sandwich plate decking. In *Third International Offshore and Polar Engineering Conference*, pages 244–249, Singapore, 1993. International Society of Offshore and Polar Engineers.

[86] T. C. Fung, K. H. Tan, and T. S. Lok. Shear stiffness D_{Qy} for C-core sandwich panels. *Journal of Structural Engineering*, 122(8):958–966, 1996.

[87] T. C. Fung, K. H. Tan, and T. S. Lok. Elastic constants for Z-core sandwich panels. *Journal of Structural Engineering*, 120(10):3046–3055, 1994.

[88] T. C. Fung and K. H. Tan. Shear stiffness for Z-core sandwich panels. *Journal of Structural Engineering*, 124(7):809–816, 1998.

[89] H. Kolsters. *Structural Design of Laser-Welded Sandwich Panels for Marine Applications*. Doctoral thesis, Royal Institute of Technology, 2004.

[90] G. Winter. Stress distribution in and equivalent width of flanges of wide, thin-wall steel beams. NACA TN 784, 1940.

[91] F. B. Hildebrand and E. Reissner. Least-work analysis of the problem of shear lag in box beams. NACA TN 893, 1943.

[92] C. Lertsima, T. Chaisomphob, E. Yamaguchi, and J. Sa-nguanmanasak. Deflection of simply supported box girder including effect of shear lag. *Computers and Structures*, 84(1):11–18, 2005.

[93] S. P. Timoshenko and J. M. Gere. *Theory of Elastic Stability*. McGraw-Hill, New York, second edition, 1961.

[94] N. Pokharel and M. Mahendran. Experimental investigation and design of sandwich panels subject to local buckling effects. *Journal of Constructional Steel Research*, 59(12):1533–1552, 2003.

[95] N. J. Hoff and S. E. Mautner. The buckling of sandwich-type panels. *Journal of the Aeronautical Sciences*, 12:285–297, 1945.

[96] F. J. Plantema. *Sandwich Construction: The Bending and Buckling of Sandwich Beams*. Wiley, New York, 1966.

[97] H. G. Allen. *Analysis and Design of Structural Sandwich Panels*. Pergamon Press, Oxford, UK, 1969.

[98] S. Aimmanee and J. R. Vinson. Analysis and optimization of foam-reinforced web core composite sandwich panels under in-plane compressive loads. *Journal of Sandwich Structures and Materials*, 4:115–139, 2002.

[99] W. Yu. *Cold-Formed Steel Design*. Wiley, New York, third edition, 2000.

[100] T. M. Roberts and A. C. B. Newark. Strength of webs subjected to compressive edge loading. *Journal of Structural Engineering*, 123(2):176–183, 1997.

[101] J. Romanoff. Täyteaineen vaikutus teräksisen kerroslevypaneelin paikalliseen äärilujuuteen (The effect of a filling material on the local ultimate strength of an all steel sandwich panel). Report M-256, Helsinki University of Technology Ship Laboratory, 2000. In Finnish.

[102] *North American Specification for the Design of Cold-Formed Steel Structural Members*. American Iron and Steel Institute, Washington, DC, 2001.

[103] T. Okazaki, B. J. Siljenberg, C. K. Shield, and S. C. Mantell. Web crippling strength of a steel sandwich panel with V-shaped webs. *Journal of Constructional Steel Research*, 65(8-9):1721–1730, 2009.

[104] C. G. Salmon and J. E. Johnson. *Steel Structures: Design and Behavior*. Harper Collins, New York, fourth edition, 1996.

[105] R. V. Southwell and S. W. Skan. On the stability under shearing forces of a flat elastic strip. *Proceedings of the Royal Society A*, 105(733):582–607, 1924.

[106] M. Stein and J. Neff. Buckling stresses of simply supported rectangular flat plates in shear. NACA TN 1222, 1947.

[107] B. Budiansky and R. W. Connor. Buckling stresses of clamped rectangular flat plates in shear. NACA TN 1559, 1948.

[108] I. T. Cook and K. C. Rockey. Shear buckling of rectangular plates with mixed boundary conditions. *Aeronautical Quarterly*, 14(4):349–356, 1963.

[109] D. J. Johns. Shear buckling of isotropic and orthotropic plates: A review. ARC R&M 3677, 1971.

[110] A. S. Davies, J. M.and Fragos. Shear strength of empty and infilled cassettes. *Thin-Walled Structures*, 41:109–125, 2004.

[111] A. S. Davies, J. M.and Fragos. The local shear buckling of thin-walled cassettes infilled by rigid insulation. *Journal of Constructional Steel Research*, 60(3-5):581–599, 2004.

[112] E. Reissner. Note on the formulation of the problem of the plate on an elastic foundation. *Acta Mechanica*, 4:88–91, 1967.

[113] A. D. Kerr. On the determination of foundation model parameters. *Journal of Geotechnical Engineering*, 111(11):1334–1340, 1985.

[114] L. Sironic, N. W. Murray, and R. H. Grzebieta. Buckling of wide struts/plates resting on isotropic foundations. *Thin-Walled Structures*, 35(3):153–166, 1999.

[115] C. J. Wiernicki, F. Liem, G. D. Woods, and A. J. Furio. Structural analysis methods for lightweight metallic corrugated core sandwich panels subjected to blast loads. *Naval Engineers Journal*, 103(3):192–203, 1991.

[116] C. Libove, S. Ferdman, and J. J. Reusch. Elastic buckling of a simply supported plate under a compressive stress that varies linearly in the direction of loading. NACA TN 1891, 1949.

[117] J. Zaraś, J. Rhodes, and M. Królak. Buckling and post-buckling of rectangular plates under linearly varying compression and shear: Part 1 - theoretical analysis. *Thin-Walled Structures*, 14(1):59–87, 1992.

[118] G. Fauconneau and R. D. Marangoni. Natural frequencies and elastic stability of a simply-supported rectangular plate under linearly varying compressive loads. *International Journal of Solids and Structures*, 7:473–493, 1971.

[119] H. Hu, A. Badir, and A. Abatan. Buckling behavior of a graphite/epoxy composite plate under parabolic variation of axial loads. *International Journal of Mechanical Sciences*, 45:1135–1147, 2003.

[120] X. Chu, Z. Ye, R. Kettle, and L. Li. Buckling behaviour of cold-formed channel sections under uniformly distributed loads. *Thin-Walled Structures*, 43(4):531–542, 2005.

[121] H. C. Bui. Buckling analysis of thin-walled sections under general loading conditions. *Thin-Walled Structures*, 47(6-7):730–739, 2009.

[122] A. D. Kerr. Elastic and viscoelastic foundation models. *Journal of Applied Mechanics*, 31:491–498, 1964.

[123] K. Y. Lam, C. M. Wang, and X. Q. He. Canonical exact solutions for levy-plates on two-parameter foundation using Green's functions. *Engineering Structures*, 22:364–378, 2000.

[124] J. Romanoff. The effect of a filling material on the local ultimate strength of an all steel sandwich panel. *Journal of Structural Mechanics*, 35(1):19–39, 2001.

[125] M. Z. Khan and A. C. Walker. Buckling of plates subjected to localized edge loading. *The Structural Engineer*, 50(6), 1972.

[126] K. C. Rockey and D. K. Bagchi. Buckling of plate girder webs under partial edge loadings. *International Journal of Mechanical Sciences*, 12(1):61–76, 1970.

[127] M. Elgaaly. Web design under compressive edge loads. *AISC Engineering Journal*, 20(4):153–171, 1983.

[128] *Commentary on North American Specification for the Design of Cold-Formed Steel Structural Members*. American Iron and Steel Institute, Washington, DC, 2001.

[129] AISI 1020 steel, cold rolled. MatWeb.com online materials database, October 16, 2007.

[130] AISI type 317 stainless steel, annealed sheet. MatWeb.com online materials database, October 16, 2007.

[131] R. Loov and N. Parthasarathi. Study of shear provisions for stiffened plate girders. *Canadian Journal of Civil Engineering*, 31(1):160–167, 2004.

[132] T. V. Galambos. *Guide to Stability Design Criteria for Metal Structures*. Wiley, New York, fifth edition, 1998.

[133] *ASTM C-393-06: Standard Test Method for Core Shear Properties by Beam Flexure*. ASTM International, West Conshohocken, PA, 2006.

[134] A. D. Lanzo, G. Garcea, and R. Casciaro. Asymptotic post-buckling analysis of rectangular plates by HC finite elements. *International Journal for Numerical Methods in Engineering*, 38(14):2325–2345, 2005.

[135] *ASTM A-123: Standard Specification for Zinc (Hot-Dip Galvanized) Coatings on Iron and Steel Products*. ASTM International, West Conshohocken, PA, 2009.

[136] Zinc, Zn. MatWeb.com online materials database, October 27, 2009.

[137] *ASTM A-370-09: Standard Test Methods and Definitions for Mechanical Testing of Steel Products*. ASTM International, West Conshohocken, PA, 2009.

[138] L. Fan, J. Rondal, and S. Cescotto. Finite element modelling of single lap screw connections in steel sheeting under static shear. *Thin-Walled Structures*, 27(2):165–185, 1997.

[139] H. R. Trechsel. *Moisture Analysis and Condensation Control in Building Envelopes*. ASTM International, West Conshohocken, PA, 2001.

[140] *ASCE/SEI 7-05, Minimum Design Loads for Buildings and Other Structures*. American Society of Civil Engineers, 2005.

[141] C. Torres-Sanchez and J. R. Corney. Toward functionally graded cellular microstructures. *Journal of Mechanical Design*, 131(9), 2009.

Appendix A

Loads and R-Value Requirements

Design loads and R-value requirements for residential roofs are specified by building codes. The specifications from the International Residential Code [43] and ASCE-7 [140] are used in the present work to determine load requirements. The R-value requirement is determined according to the International Energy Conservation Code [71]. A full analysis of the live and dead load calculations is provided in Reference [2]. The results are summarized in this appendix.

A.1 Roof Loads

The roof load consists of two contributions: a live load due to snow and wind loading, and a dead load due to the weight of the panel and any attached roofing and fixtures. The snow, wind, and dead loads are combined in several manners as defined by code [140], and the load combination with the highest resultant load is used. Provisions for wind uplift resistance are also provided by the design code. The net wind uplift loads are smaller than the live and dead loads, however. The strength of symmetric web core panels is the same under snow and uplift loads, so the latter are not considered in the present work.

The continental United States has been divided in the present project into three climate zones based on snow loads, as illustrated in Figure 3.1. Climate I consists of areas for which the ground snow load is less than 958 N/m^2 (20 psf), Climate II consists of areas with ground snow loads up to 1915 N/m^2 (40 psf), and Climate III consists of areas with ground snow loads up to 3352 N/m^2 (70 psf). Two other regions

of interest are included in Figure 3.1. The areas colored white (mainly located in the Rocky Mountain region) have large local variability in the snow loading and cannot be readily lumped into any climate region. The hatched regions (mainly the gulf and east coasts) are subjected to large wind uplift loads. Loading in this region is also site-dependent, but the net loads are comparable to the live loads for Climate II [2].

The dead load includes the panel self weight (assumed to be less than 500 N/m^2, 10.4 psf), plus exterior roofing, felt vapor barrier, and an interior gypsum board (required for fire protection [43]) and fasteners. The weight of the components is assumed to be 218 N/m^2 (4.6 psf), so the total assumed dead load is 718 N/m^2 (15.0 psf) in all three climates. To ensure that designs do not fail as a result of underestimating the panel weight, the assumed maximum weight of 500 N/m^2 has been set as a design constraint throughout this work.

The design load for Climate I is based on the combination of dead plus 75% of the snow and wind loads [2, 140]; the design load for Climates II and III is based on the dead and snow load. The snow and dead loads are assumed to act due to gravity, i.e. perpendicular to the ground. They are resolved into the component acting perpendicular to the roof, which has a 6:12 pitch for all of the designs in this work. The maximum wind load is 479 N/m^2 (10.0 psf) throughout the US (excepting the hatched regions in Figure 3.1), so the design loads for Climates I, II, and III are 1576, 2173, and 3322 N/m^2 (32.9, 45.4, and 69.4 psf) respectively.

A.2 Thermal Requirement

The R-value requirement for insulated residential roofs is specified by building code and is determined by the average heating degree days (HDD) at the building site [71]. Heating degree days are defined relative to a base temperature (usually 65°F, 18°C)and are a way to quantify the coldness of a climate. The relationship between R-value requirement and HDD is plotted in Figure A.1. The R-value requirement ranges from 3.5 m^2-K/W in regions with no HDD up to 7.0 m^2-K/W in extreme cold climates.

The heating degree days in the continental US vary from zero in the deep south up to about 10,500. The R-value requirement corresponding to 10,500 HDD is 6.8 m^2-K/W. The thermal requirements in the present work are developed by dividing the

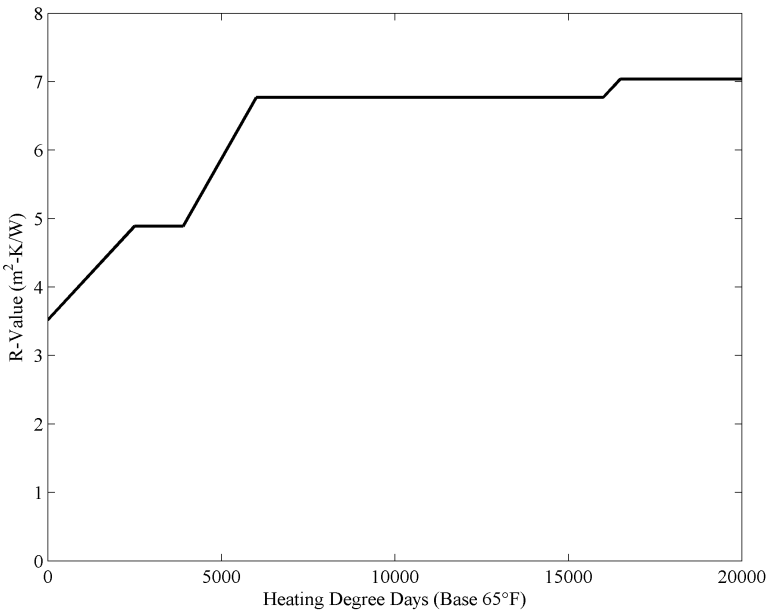

Figure A.1. R-value requirement vs. heating degree days (HDD), as specified by building code [71]

Table A.1. Loads and R-value requirements for panels with a 6:12 roof pitch

	Load (N/m^2)	**R-value (m^2-K/W)**
Climate I	1576	5.3
Climate II	2173	6.8
Climate III	3322	6.8

country into two regions: areas with less than 4400 HDD, which require R-5.3, and areas with more HDD, which require R-6.8. The boundary between these regions roughly corresponds with the boundary between Climates I and II. Based on the considerations given in this appendix, the load and R-value requirements for web core roof panels are given in Table A.1.

Appendix B

Non-Limiting Failure Mode Models

As noted in Chapter 3, two potential failure modes—flexural web buckling, and buckling of the face sheet into the webs—were ruled out as limiting factors for web core panel design. Models for these failure modes and the resulting implications on panel design are presented in this appendix.

B.1 Flexural Buckling

The curvature of a loaded panel imposes a bending moment distribution on the webs. The bending moment in turn causes a load distribution N_x along the transverse edges, as illustrated in Figure B.1. The load distribution is described by

$$N_x = -N_0 \left(1 - \alpha \frac{y}{b}\right), \tag{B.1}$$

where N_0 is the maximum compressive load (located at $y = 0$) and α is a parameter that defines the position of the neutral axis. The case $\alpha = 0$ represents pure compression, and $\alpha \geq 1$ represents bending, with the neutral bending axis located at a distance b/α from the top edge ($y = 0$). For symmetric web core panels, the neutral axis is at the midplane $y = b/2$, i.e. $\alpha = 2$. As with the shear and face sheet buckling models, the core material is modeled as a Pasternak elastic foundation.

Timoshenko [93] found the critical buckling load for simply supported plates (with no foundation) under in-plane bending using the principle of minimum potential energy. His approach is modified here to include the influence of a Pasternak foundation on

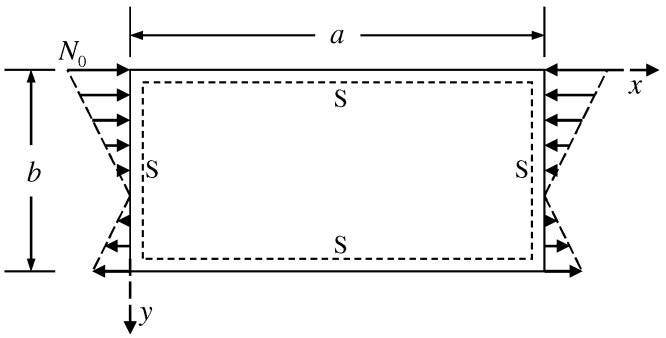

Figure B.1. Model used for determination of the web flexural buckling load

buckling strength. The von Kármán governing equation in this case is

$$D\nabla^4 w = -\left(K_W w - K_P \nabla^2 w\right) + N_x w_{,xx}. \tag{B.2}$$

The buckling strength is characterized by the critical load $\overline{N}_0$, given by [93]

$$\overline{N}_0 = \chi_{fb} \frac{\pi^2 D}{b^2}, \tag{B.3}$$

where χ_{fb} is the flexural web buckling coefficient. Unless otherwise noted, all other variables in this section are as defined in Chapter 4.

The minimum potential energy approach requires that $\delta U - \delta V = 0$ (Equation (4.5)). Approximating w by the double sine series, Equation (4.6), the strain energy U is given by Equation (4.8). The work V is

$$V = \frac{1}{2} \int_0^b \int_0^a \left[N_0 \left(1 - \alpha \frac{y}{b}\right) w_{,x}^2 - K_W w^2 - K_P \left(w_{,x}^2 + w_{,y}^2\right) \right] dxdy. \tag{B.4}$$

Evaluation of the integral in Equation (B.4) yields

$$\begin{aligned} V = \frac{ab}{8} \Bigg[& N_0 \sum_{m=1}^{\infty} \sum_{n=1}^{\infty} A_{mn}^2 \frac{m^2 \pi^2}{a^2} - K_W \sum_{m=1}^{\infty} \sum_{n=1}^{\infty} A_{mn}^2 \\ & - K_P \pi^2 \left(\sum_{m=1}^{\infty} \sum_{n=1}^{\infty} \left(\frac{m}{a}\right)^2 A_{mn}^2 + \sum_{m=1}^{\infty} \sum_{n=1}^{\infty} \left(\frac{n}{b}\right)^2 A_{mn}^2 \right) \Bigg] \\ & - \frac{N_0 \alpha a}{4b} \sum_{m=1}^{\infty} \frac{m^2 \pi^2}{a^2} \left[\frac{b^2}{4} \sum_{n=1}^{\infty} A_{mn}^2 - \frac{8b^2}{\pi^2} \sum_{n=1}^{\infty} \sum_{i}^{\infty} \frac{A_{mn} A_{mi} ni}{(n^2 - i^2)^2} \right]. \end{aligned} \tag{B.5}$$

The final summation is taken only over values of i such that $n \pm i$ is odd. Substitution of the terms into the minimum potential energy expression (4.5) yields a set of equations of the form

$$\left[\left(m^2 + n^2\beta^2\right)^2 + f_W\beta^4 + f_P\beta^2\left(m^2 + n^2\beta^2\right) - \chi_{fb}\left(1 - \frac{\alpha}{2}\right)m^2\beta^2 \right] A_{mn} - \frac{8\alpha}{\pi^2} m^2\beta^2\chi_{fb} \sum_i^\infty \frac{A_{mi} ni}{\left(n^2 - i^2\right)^2} = 0. \tag{B.6}$$

As with shear buckling, the buckling coefficient is approximated by taking a subset of these equations and solving for the minimum value of χ_{fb} to make the system indefinite. Note that each of the Equations (B.6) contains terms relating to only one value for m. The system can thus be divided into sub-groups of equations, each containing a single value of m. If any sub-group is indefinite, the entire system is indefinite [93]. As a result, the plate will buckle into m_c repeating units in the x-direction, i.e.

$$A_{mn} = 0, \forall m \neq m_c. \tag{B.7}$$

The value of m_c is a function of β, f_W, and f_P and cannot be known *a priori*. A useful implication of this property is the ability to determine the buckling coefficient $\chi_{fb,\infty}$ for long plates by minimizing χ_{fb} with respect to β using an arbitrary value of m. The results reported here for $\chi_{fb,\infty}$ are obtained in this manner.

Plots of the flexural buckling mode shape are provided in Figure B.2 for plates with $\beta = 2$ and varying values of α and the foundation constants. The values of $\alpha \in \{0, 1.5, 2, 3\}$ represent pure compression and bending located at depths $b/3$, $b/2$, and $2b/3$ from the top of the plate respectively (illustrated in the second column for clarity). The foundation parameters used in Chapter 4 are used. The elastic foundation decreases the buckling wavelength in both the x- and y-directions. For the same reasons discussed in Chapter 4, stiffer foundations result in smaller buckling wavelengths. The figure also shows that increasing α leads to increased buckling strength (along with smaller wavelengths in the y-direction). This result occurs because increasing α means a smaller portion of the plate is loaded in compression and a larger portion is loaded in tension, both of which effects have a stabilizing effect on the plate as a whole.

α	Load	$f_W = 0,\ f_P = 0$	$f_W = 300,\ f_P = 20$
0	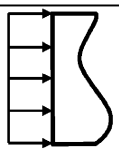	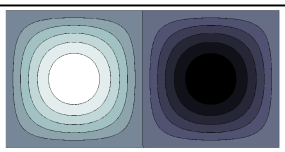 $\chi = 4.0$	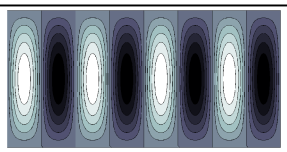 $\chi = 58.1$
1.5	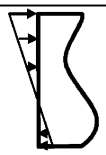	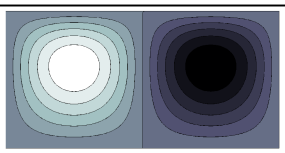 $\chi = 13.5$	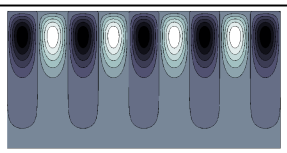 $\chi = 101.8$
2	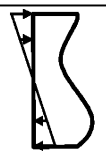	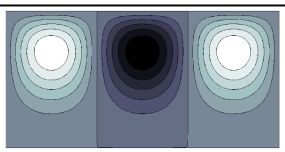 $\chi = 23.9$	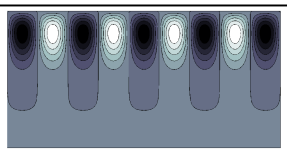 $\chi = 118.3$
3	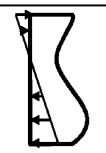	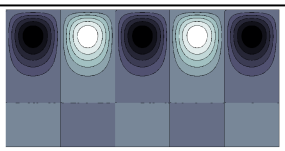 $\chi = 54.3$	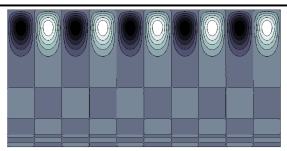 $\chi = 156.3$

Figure B.2. Buckling mode shapes with varying elastic foundation stiffness and α ($\beta = 2$)

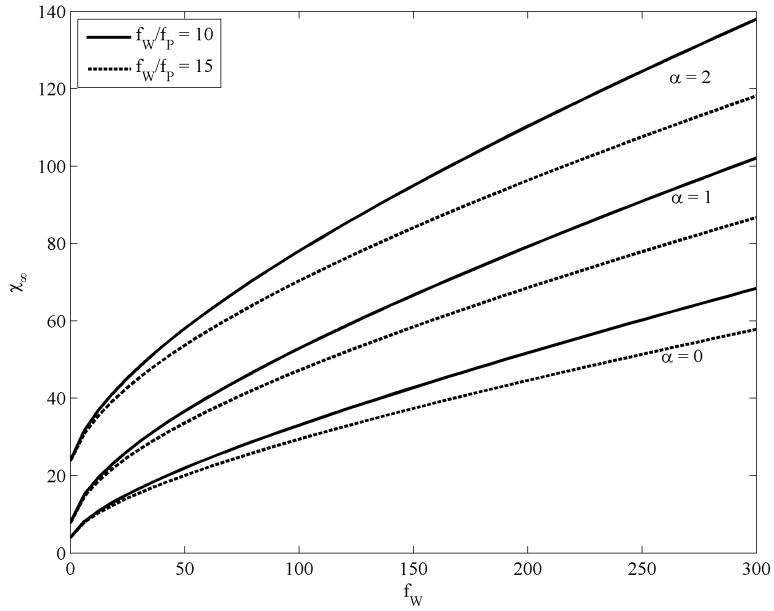

Figure B.3. Long plate flexural buckling coefficient $\chi_{fb,\infty}$ vs. f_W for $f_W/f_P = 10$ and 15; $\alpha = 0$, 1, and 2

The long plate flexural buckling coefficient $\chi_{fb,\infty}$ is a function of α, f_W, and f_P. No attempt was made in the present work to develop a general closed-form equation for this relationship.

A plot of $\chi_{fb,\infty}$ versus f_W is given in Figure B.3 for $\alpha \in \{0, 1, 2\}$ and two values of f_W/f_P: $f_W/f_P = 10$ (typical of slender plates on an isotropic foundation), and $f_W/f_P = 15$ (typical of slender plates and the PUR foam used throughout this work). From the plot it can be seen that $\chi_{fb,\infty}$ is a function of α in addition to f_W and f_P. No attempt was made in the present work to develop a general closed-form equation for this relationship.

The applied load N_0 on the web is obtained from the maximum bending moment on the web. The web and face sheets act in parallel to resist panel bending, so N_0 can be approximated by

$$N_0 = \frac{D_{x,w}}{D_{x,f}} \sigma_f t_w \approx \frac{q a^2 t_w^2}{48 p t_f^2}, \tag{B.8}$$

where $D_{x,f}$ and $D_{x,w}$ are the first and second terms on the right hand side of Equation (6.5). The fraction in Equation (B.8) is thus the ratio of web stiffness to face sheet stiffness in bending. For the designs presented in this work, the face sheets contribute 20–30 times as much as the webs to the total bending stiffness. Combining Equations (B.3) and (B.8), the load $\overline{q}$ to cause flexural buckling failure is

$$\overline{q} = \frac{48 \pi^2 D_w t_f^2 p}{a^2 t_w^2 h_c^2} \chi_{fb}, \tag{B.9}$$

with χ_{fb} evaluated using the foundation parameters given by Equations (4.26) and (4.27).

In the designs presented throughout this work, web thickness is consistently determined by the shear buckling requirement. Flexural and shear buckling affect the web in different locations for panels under distributed load and can be considered independent. Based on these considerations, flexural buckling is a concern only for designs for which the shear buckling load is greater than the flexural buckling load. Thus, it is possible to develop a sufficient condition for which the flexural buckling strength is greater than the shear buckling strength. Comparing Equation (B.9) to

Equation (4.29), it can be seen that shear buckling will limit the design if

$$\frac{\chi_{fb}}{\chi_\infty} > \frac{t_w^2 a h_c}{24 p^2 t_f^2}. \tag{B.10}$$

Consider a panel with $t_f = t_w$, $a = 6.8$ m, $p = 0.6$ m, and $h_c = 400$ mm. This geometry represents the design which is least likely to satisfy Equation (B.10). This geometry requires $\chi_{fb}/\chi_\infty > 0.3$, which is easily satisfied for roof panel designs ($\chi_{fb}/\chi_\infty > 1.5$ for cores with $f_W/f_P = 15$).

B.2 Buckling of the Face Sheet into the Webs

Salmon and Johnson [104] describe the analysis of web buckling under the action of face sheet stresses, as well as methods for dealing with it according to prescriptive steel design codes. The analysis is adapted here to account for the effect of the foam in a web-core panel. The model for face sheet induced web buckling is illustrated in Figure B.4. Figure B.4(a) shows the development of face sheet stresses due to panel curvature. The stresses act at an angle $d\theta$ with respect to the web. As shown in Figure B.4(b), the face sheet bending stress σ_f induces a compressive normal stress σ_w in the webs acting over an area $t_w dx$. The longitudinal strain ϵ_f on the face sheets is

$$\epsilon_f = \frac{h_c}{2}\frac{d\theta}{dx}, \tag{B.11}$$

so that, under small rotations $d\theta$, the stress σ_w on the webs can be expressed as

$$\sigma_w = \frac{\sigma_f A_f d\theta}{t_w dx} = \frac{2\sigma_f A_f}{t_w h_c}\epsilon_f. \tag{B.12}$$

The webs are modeled as simply supported columns, and the core is modeled as an elastic foundation. Neglecting the the shearing contribution K_P[1], the buckling stress $\overline{\sigma}_w$ is

$$\overline{\sigma}_w t_w = \frac{\pi^2 E_w t_w^3}{12 h_c^2} n^2 + K_W \frac{h_c^2}{n^2 \pi^2}, \tag{B.13}$$

where h_c/n is the buckling half-wavelength, and n is the integer that minimizes $\overline{\sigma}_w$. The foundation constant K_W is given by Equation (4.23). Analogous to the plate

[1]Inclusion of the K_P term increases the right hand side of Equation (B.15) by a factor $1 + t_w/2$, i.e. the effect on accuracy is negligible.

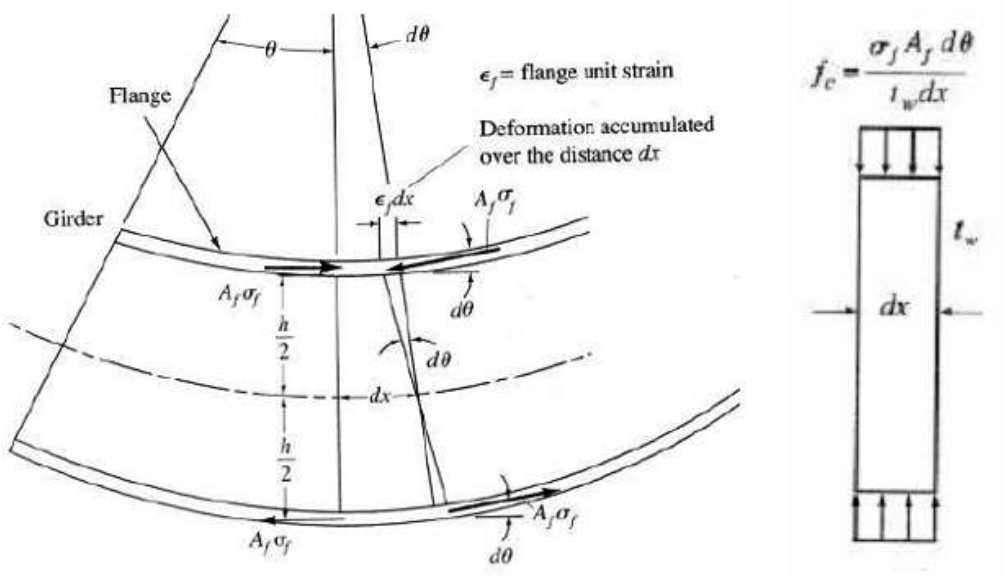

(a) (b)

Figure B.4. Buckling of the face sheet into the webs: (a) curvature of the web due to panel bending, and (b) distribution of compressive stress (denoted f_c in the figure) on a web element (Figures are from Reference [104])

buckling analyses in this work, the critical stress for infinitely long beams is found by minimizing σ_w with respect to h_c. The result is

$$\overline{\sigma}_w = \sqrt{\frac{E_w t_w K_W}{3}} = \left(\frac{E_w E_c G_c}{6}\right)^{\frac{1}{3}}. \tag{B.14}$$

Buckling of the face sheets into the webs is prevented if $\sigma_w \leq \overline{\sigma}_w$. If the bending stress is less than the proportional limit of the face sheet material, $\epsilon_f = \sigma_f / E_f$, and the web buckling requirement is expressed as

$$\frac{2\sigma_f^2 A_f}{E_f t_w h_c} \leq \left(\frac{E_w E_c G_c}{6}\right)^{\frac{1}{3}}. \tag{B.15}$$

A conservative estimate of the buckling requirement is obtained by setting the face sheet stress equal to the yield strength σ_{yf}. Then, noting that $A_f = t_f p$, Equation (B.15) is restated as

$$\frac{t_w h_c}{t_f p} \geq \frac{2\sigma_{yf}^2}{E_f}\left(\frac{6}{E_w E_c G_c}\right)^{\frac{1}{3}}. \tag{B.16}$$

Equation (B.16) can be used to rule out buckling of the face sheets into the webs as a potential failure mode for web core panels based on material properties and the limits of allowable geometry. If the condition imposed by Equation (B.16) is satisfied, this failure mode cannot occur. If the condition is not satisfied, Equation (B.15) should be used (with σ_f from Equation (6.13)) to ensure the design is safe.

Consider a panel with $t_w = 0.6$ mm, $t_f = 2.0$ mm, $h_c = 250$ mm (the thinnest panels likely to occur in practice), and $p = 1.2$ m. Assume steel face sheets and webs with $\sigma_{yf} = 225$ MPa and PUR core with properties reduced to account for creep. Then Equation (B.16) evaluates to $0.069 \geq 0.015$, i.e. the condition is satisfied. Buckling of the face sheets into the webs is not a concern for web core roof panels.

Appendix C

Modeling of Shallow Foundations

The elastic foundation model in Section 4.3 is applicable to relatively deep or stiff foundations, e.g. Equation (6.24). Although this condition is satisfied for all roof panel designs in practice, it is interesting to note that the approach in Section C can also be used to model shallow foundations. This appendix follows the approach used in Section 4.3 to develop Pasternak foundation constants applicable to close web spacing and compares the results to those obtained through finite element analysis.

The model for shallow foundations is illustrated in Figure C.1. This model matches the one used for deep foundations (Figure 4.5), except the buckling deformation is assumed to decay linearly with distance from the plate. In general, the deformation will decay over a depth $h \leq H$, where H is the total foundation depth as used in Section 4.3. For convenience, the coordinate system is redefined so that the origin is at the plane of zero deformation.

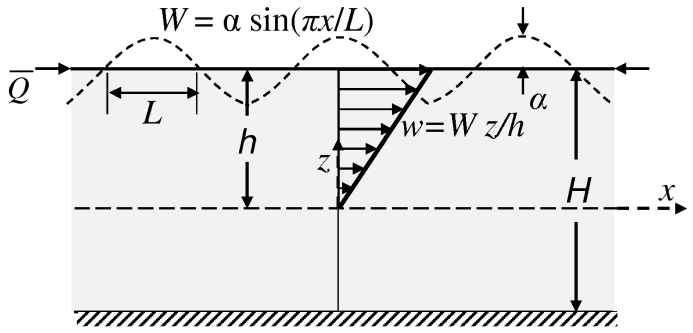

Figure C.1. Model for the determination of shallow foundation stiffness constants

Foundation constants are developed from this model using the principle of minimum potential energy. The three strain energy components are given by

$$U_\epsilon = \frac{E_c}{2}\int_0^L\int_0^h w_{,z}^2\, dzdx = \frac{\alpha^2 E_c L}{4h}, \tag{C.1}$$

$$U_\gamma = \frac{G_c}{2}\int_0^L\int_0^h w_{,x}^2\, dzdx = \frac{\pi^2\alpha^2 G_c h}{12L}, \tag{C.2}$$

$$U_f = \frac{E}{2}\frac{t_w^3}{12}\int_0^L w_{,xx}^2\Big|_{z=h}\, dx = \frac{\pi^4\alpha^2 E t^3}{48L^3}. \tag{C.3}$$

The work W done by the applied force $\overline{Q}$ is

$$W = \frac{\overline{Q}}{2}\int_0^L w_{,x}^2\Big|_{z=h}\, dx = \frac{\pi^2\alpha^2}{4L}\overline{Q}. \tag{C.4}$$

Setting $W = U_\epsilon + U_\gamma + U_f$ and solving for $\overline{Q}$ yields

$$\overline{Q} = \frac{\pi^2 E t^3}{12L^2} + \frac{E_c}{h}\frac{L^2}{\pi^2} + \frac{G_c h}{3}, \tag{C.5}$$

from which the foundation constants are (see Equation (4.22))

$$K_W = \frac{E_c}{h}, \qquad K_P = \frac{G_c h}{3}. \tag{C.6}$$

The depth h is found by minimizing Equation (C.5) with respect to h and L, yielding

$$\frac{h}{t} = \sqrt[3]{\frac{3E_c E}{4G_c^2}} \le \frac{H}{t}. \tag{C.7}$$

The inequality is used to emphasize that sufficiently shallow foundations have $h = H$.

The foundation model in Section 4.3 was validated using a finite element study. The results of that study can also be used to validate the model in this appendix. Recall that the finite element analysis yielded a set of buckling coefficients χ_β as a function of non-dimensional depth Hk, with k defined by Equation (4.25). Using the shallow foundation model in this section, the ratio χ/χ_β is plotted as a function of Hk in Figure C.2. For comparison, the results from the deep foundation model (Figure 4.8 are included using a dashed line.

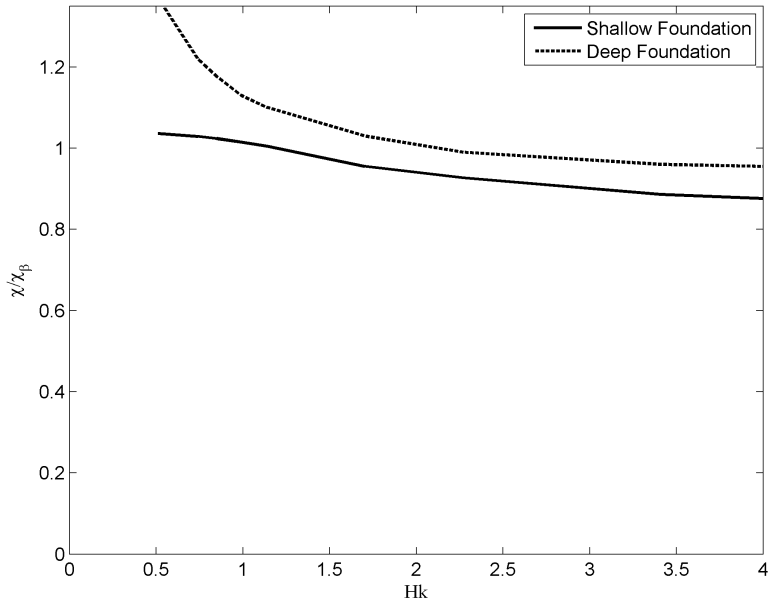

Figure C.2. Comparison of the shallow and deep foundation models vs. non-dimensional foundation depth Hk

For deep foundations, $Hk > 2$, the model in this appendix overestimates buckling strength by about 16%. As described in Section 4.3, the decay of buckling deformation in the core is more accurately modeled by the exponential model. For shallow foundations, the model predicts buckling strength to within 5%. The difference in accuracy between the deep and shallow foundation models is striking, especially for $Hk \leq 1$.

Note that the two models never intersect in the figure: the deep foundation model always predicts higher buckling strength than the shallow foundation model. Recall that the linear and exponential models for decay of buckling deformation are limits to the exact behavior, Equation (4.15). The decay function is not well approximated by either simplification for foundation depths approximately in the range $1 \leq Hk \leq 2$. It is nonetheless interesting to note that the models in this work provide reasonable accuracy for most purposes. For example, if the cutoff between the deep and shallow foundation models is set at $Hk = 2$, the models predict buckling strength to within 5% over the full range of foundation depths.

Appendix D

Rigid Polyurethane Foam Data Sheets

The following pages contain data sheets on all of the foams used in the present work. The first sheet (pg. 180) is from the vendor's nominal property data [66] (the full data sheet contains several pages of processing data unrelated to the present work, therefore not included here). The second data sheet (pp. 181–182) contains test data from the foam sample taken from the shear buckling test. The last data sheet (pp. 183–184) contains test data from the foam samples taken from the bearing failure tests. On this data sheet, the foam from Panel A is labeled "#1" (with density 1.92 pcf), and the foam from Panel B is labeled "#2" (density 2.10 pcf).

Designs presented throughout this work are based on the material properties of the foam from the shear buckling test (pp. 181–182). The compressive modulus was not obtained by the vendors in that test, so the nominal value is used for design.

BASF
The Chemical Company

Technical Product Data

Urethane Specialties

ELASTOPOR® P 17226R RESIN/ELASTOPOR® P 1046U ISOCYANATE RIGID URETHANE FOAM SYSTEM

TYPICAL PHYSICAL PROPERTIES

Molded Panel, pcf	2.25
Core Density, pcf	2.00
Skin Temperature, (F)	105-115
Perpendicular Compressive Strength @10% deflection, psi	16
Perpendicular Compressive Modulus, psi	433
Parallel Compressive Strength @10% deflection, psi	31
Parallel Compressive Modulus, psi	721
Substrate Adhesion, psi	18
k factor, BTU-IN/HR-FT2-°F Initial	0.150
Porosity (%Closed Cells)	92
Friability (% Weight Loss)	1.8
Water Absorption (%)	1.6
Butler Chimney (% Weight Retained)	92
NBS Smoke Density	220
U.L. Subject 723 (File #R5692 - 6" Core Panels)/ASTM E-84	
Flame Spread*	20
E-84 Smoke	450
Minimum Self-Ignition Temperature	430°C (806°F)
Minimum Flash-Ignition Temperature	445°C (833°F)
Dimensional Stability, % Volume Change at 28 days	
100°F/100% RH	0.1
158°F/100% RH	0.4
158°F	0.0
200°F	0.1
-20°F @ 7 Days	0.3

*This numerical flame spread rating is not intended to reflect hazards presented by this or any other material under actual fire conditions.

BASF Corporation
1419 Biddle Avenue
Wyandotte, Michigan 48192-3799
(734) 324-6100
(734) 324-6482 (Fax)

Revision Date:07/28/2006

BASF
The Chemical Company

Technical Product Data

Urethane Specialties

UNIVERSITY OF MINNESOTA PANEL RESULTS
Physical Testing results of panel made at BASF in May, 2008.

TEST	UNITS	VALUE	VALUE
Core Density (ASTM D-1622)	Lbs./cu.ft.	2.23	
K-factor, initial (ASTM C-518)	Btu-in/hr-ft²-°F	0.149	
Compressive Strength (ASTM-D-1621)	**Psi**	**Parallel** 23	**Perpendicular** 20
Flexural Strength (ASTM D790)	**Psi**	37.8	28.2
Flexural Modulus (ASTM D790)	**Psi**	960.67	606.47
Shear Modulus (ASTM C273)	**Psi**	229.53	187.6
Tensile Strength-Young's Modulus (ASTM D-1623)	**Psi**	750.07	605.07
Tensile Strength (ASTM D-1623)	**Psi**	42.8	33.4
Shear Substrate Adhesion (ASTM C273)	**Psi**	32.4	25.07
Tensile Substrate Adhesion (ASTM D-1623)	**Psi**	NT	15.4
Dimensional Stability (ASTM D2126)	**%Volume Change @14 Days @ 158F/100%RH**	0.4	
Dimensional Stability (ASTM D2126)	**%Volume Change @14 Days @ 100F/100%RH**	0.1	
Dimensional Stability (ASTM D2126)	**%Volume Change @14 Days @ 158F**	0.0	

BASF Corporation
1419 Biddle Avenue
Wyandotte, Michigan 48192-3799
(734) 324-6100
(734) 324-6482 (Fax)

Revision Date:7/10/2008

Dimensional Stability (ASTM D2126)	**%Volume Change @14 Days @ -20F**	1.4	
Dimensional Stability (ASTM D2126)	**%Volume Change @14 Days @ 200F**	-0.8	

BASF Corporation
1419 Biddle Avenue
Wyandotte, Michigan 48192-3799
(734) 324-6100
(734) 324-6482 (Fax)

Revision Date:7/10/2008

BASF
The Chemical Company

Technical Product Data

Urethane Specialties

University of Minnesota Panel Physicals

TEST	ASTM	#1	#2
Core Density (pcf)	D-1622	1.92	2.10
Parallel	D-1621		
Compressive Strength (psi)			
Strength @ 10% Deflection (psi)		21.2	21.7
Modulus (psi)		558.3	577.7
Perpendicular	D-1621		
Compressive Strength (psi)			
Strength @ 10% Deflection (psi)		15.1	17.6
Modulus (psi)		339.3	350.0
Flexural Strength	D-790		
Parallel (psi)		24.43	43.53
Perpendicular (psi)		25.03	32.20
Flexural Modulus (Young's Modulus)	D-790		
Parallel (psi)		677.17	1148.93
Perpendicular (psi)		621.67	805.23
K-factor, initial (ASTM C-518) Btu-in/hr-ft^2-°F	C-518	0.149	0.144
Shear Strength	C-273		
Parallel (psi)		28.1	33.0
Perpendicular (psi)		22.6	27.3
Shear Strength (Young's Modulus)	C-273		
Parallel (psi)		187.8	219.8
Perpendicular (psi)		152.8	168.3
Tensile Strength	D-1623		
Parallel (psi)		43.6	44.2
Perpendicular (psi)		29.1	30.9
Tensile Strength (Young's Modulus)	D-1623		
Parallel (psi)		847.3	915.2
Perpendicular (psi)		477.5	568.7
Water Absorption	C-272		
lbs/sq. ft.		0.029	0.031
Percent		1.61	1.73

BASF Corporation
1419 Biddle Avenue
Wyandotte, Michigan 48192
(734) 324-6100
1-800-521-9100

4/2/09

BASF

Water Vapor Transmission (Perm-in)		E-96	2.58	1.88
Porosity (% closed cell)		D-6226	87.17	87.59
Dimensional Stability (% Volume Change)		D-2126		
158°F & 100% R.H.	28 Days		-1.1	2.1
158°F	28 Days		0.6	-1.5
200°F	28 Days		-1.5	0.7
100°F & 100% R.H.	28 Days		-13.0	-1.1
-20°F	28 Days		-0.4	-1.5

BASF Corporation
1419 Biddle Avenue
Wyandotte, Michigan 48192
(734) 324-6100
1-800-521-9100

4/2/09

BASF